

ADA103090

LEVEL

12

NO PRINT



INVESTIGATION OF THE CIRCULATION CONTROL WING/  
UPPER SURFACE BLOWING HIGH-LIFT SYSTEM ON  
A LOW ASPECT RATIO SEMISSPAN MODEL

by

Michael J. Harris

APPROVED FOR PUBLIC RELEASE:  
DISTRIBUTION UNLIMITED

AVIATION AND SURFACE EFFECTS DEPARTMENT

DTNSRDC/ASED-81/10

May 1981

DAVID  
W.  
TAYLOR  
NAVAL  
SHIP  
RESEARCH  
AND  
DEVELOPMENT  
CENTER

BETHESDA  
MARYLAND  
20084

DTIC

AD-A103090

copy

## UNCLASSIFIED

SECURITY CLASSIFICATION OF THIS PAGE (When Data Entered)

REPORT DOCUMENTATION PAGE		READ INSTRUCTIONS BEFORE COMPLETING FORM
1. REPORT NUMBER <i>(X)</i> DTNSRDC/ASED-81/10	2. GOVT ACCESSION NO. <i>AD-A103 090</i>	3. RECIPIENT'S CATALOG NUMBER
4. TITLE (and subtitle) <i>INVESTIGATION OF THE CIRCULATION CONTROL WING/UPPER SURFACE BLOWING HIGH-LIFT SYSTEM ON A LOW ASPECT RATIO SEMISPAN MODEL</i>	5. TYPE OF REPORT & PERIOD COVERED <i>Final Report, August - September 1980.</i>	
7. AUTHOR(s) <i>Michael J. Harris</i>	8. CONTRACT OR GRANT NUMBER(s)	
9. PERFORMING ORGANIZATION NAME AND ADDRESS <i>David Taylor Naval Ship R&amp;D Center Aviation and Surface Effects Department Bethesda, Maryland 20084</i>	10. PROGRAM ELEMENT, PROJECT, TASK AREA & WORK UNIT NUMBERS <i>Program Element 62241N Task Area WF41421000 Work Unit 1600-079</i>	
11. CONTROLLING OFFICE NAME AND ADDRESS <i>Naval Air Systems Command AIR 320D Washington, D.C. 20360</i>	12. REPORT DATE <i>May 1981</i>	
14. MONITORING AGENCY NAME & ADDRESS (if different from Controlling Office) <i>WF41421000</i>	13. NUMBER OF PAGES <i>90</i>	
16. DISTRIBUTION STATEMENT (of this Report) <i>WF41421000</i>	15. SECURITY CLASS. (of this report) <i>UNCLASSIFIED</i>	
17. DISTRIBUTION STATEMENT (of the abstract entered in Block 20, if different from Report)	18. DECLASSIFICATION/DOWNGRADING SCHEDULE	
18. SUPPLEMENTARY NOTES <i>81 8 19 102</i>		
19. KEY WORDS (Continue on reverse side if necessary and identify by block number) <i>Circulation Control Wing STOL Aerodynamics Upper Surface Blowing Wind Tunnel Test High-Lift System Low Aspect Ratio Powered Lift System</i>		
20. ABSTRACT (Continue on reverse side if necessary and identify by block number) <i>The results from one in a series of investigations undertaken to develop the Circulation Control Wing/Upper Surface Blowing (CCW/USB) high-lift concept are presented. Included are: isolation of propulsion jet turning, effects of tip devices, and thrust reversing. As evaluated, the concept employs a modified supercritical wing with a 3.6-percent chord circular trailing edge and tangential blowing from a thin, full-span slot over this.</i>	(Continued on reverse side)	

**UNCLASSIFIED**

**SECURITY CLASSIFICATION OF THIS PAGE (When Data Entered)**

(Block 20 continued)

trailing edge. In addition, turbofans are mounted over the wing so that the exhaust scrubs the upper surface of the wing and is turned by the trailing edge. Unlike other upper surface blowing concepts, thrust deflection is accomplished by entraining the propulsive jet with tangential blowing around the trailing edge. The propulsive-induced lift enhances the proven high lift of the circulation control wing. For a thrust coefficient of 3.76, a tangential blowing coefficient of 0.24, and an angle of attack of 16 deg, the low aspect ratio model produced an untrimmed lift coefficient of 6.5. The system also demonstrated the capability to be used as an effective thrust reverser for deceleration during the landing ground roll.

Accession For	
NTIS	CFM&I
DTIC TAB	<input checked="" type="checkbox"/>
Unannounced	<input type="checkbox"/>
Justification _____	
By _____	
Distribution/	
Availability Code:	
Avail	Major
List	Special
A	

**UNCLASSIFIED**

**SECURITY CLASSIFICATION OF THIS PAGE (When Data Entered)**

## TABLE OF CONTENTS

	Page
LIST OF FIGURES . . . . .	iii
NOTATION . . . . .	iv
ABSTRACT . . . . .	1
ADMINISTRATIVE INFORMATION . . . . .	1
INTRODUCTION . . . . .	1
MODEL AND TEST DESCRIPTION . . . . .	2
DISCUSSION OF THE RESULTS . . . . .	6
STATIC TURNING . . . . .	6
LONGITUDINAL AERODYNAMIC CHARACTERISTICS . . . . .	9
TIP DEVICES . . . . .	11
SIMULATED THRUST REVERSING . . . . .	12
SUMMARY OF RESULTS . . . . .	14
CONCLUSION . . . . .	14
REFERENCES . . . . .	17

## LIST OF FIGURES

1 - Circulation Control Wing/Upper Surface Blowing STOL Aircraft Configuration . . . . .	19
2 - Aspect Ratio 4 Circulation Control Wing/Upper Surface Blowing Semispan Model Planform . . . . .	20
3 - Model Sections . . . . .	21
4 - Turbofan Simulator Nozzle Geometry . . . . .	24
5 - Model Installation on Splitter Plat in DTNSRDC 8- by 10-Foot North Wind Tunnel . . . . .	27
6 - Optional Fences . . . . .	29
7 - Tip Devices . . . . .	32

	Page
8 - Static Turning Employing the Nozzle with an Internal Flap and Partial Span Tangential Blowing . . . . .	36
9 - Effect of Isolating the Propulsive Jet with a Partial Chord Wing Fence . . . . .	38
10 - Static Turning Employing the D-Nozzle and Partial Span Tangential Blowing . . . . .	40
11 - Static Turning Employing the D-Nozzle and Full Span Tangential Blowing . . . . .	42
12 - Flow Visualization of Static Turning Employing the D-Nozzle and Full Span Tangential Blowing . . . . .	45
13 - Effect of Variation in Partial Span Tangential Blowing on the Longitudinal Aerodynamics Associated with Thrust Turning . . . . .	49
14 - Effect of Variation in Angle of Attack on the Longitudinal Aerodynamics Associated with Thrust Turning . . . . .	52
15 - Effect of Variation in Full Span Tangential Blowing on the Longitudinal Aerodynamics . . . . .	55
16 - Effect of Variation in Angle of Attack on the Longitudinal Aerodynamics . . . . .	58
17 - Configuration Build-Up . . . . .	61
18 - Flow Visualization of Inflight Turning Employing the D-Nozzle and Full Span Tangential Blowing . . . . .	65
19 - Partial Chord Tip Fence Influence on Lift and Drag . . . . .	69
20 - Tip Sails and Cascades Influence on Lift and Drag. . . . .	71
21 - Winglet Influence on Lift and Drag . . . . .	73
22 - Effect of Upper Surface Winglet and Variation in Full Span Tangential Blowing on Lift and Drag. . . . .	75
23 - Effect of Upper Surface Winglet and Variation in Angle of Attack on Lift and Drag. . . . .	76
24 - Simulated Thrust Reversing During the Landing Ground Roll. . . . .	78
25 - Effect of Percent of Span Employing Tangential Blowing on Simulated Thrust Reversing . . . . .	80

Page

26 - Simulated Thrust Reversing Employing the Nozzle with an Internal Flap and Partial Span Tangential Blowing . . . . .	82
--	----

## NOTATION

AR	Wing aspect ratio
C	Local wing chord, in.
$C_D$	Measured drag (total horizontal force) coefficient, $F_H/qS$
$C_L$	Measured lift (total vertical force) coefficient, $F_V/qS$
$C_M$	Quarter chord pitching moment coefficient
$C_T$	Thrust coefficient, $T_S/qS$
$C_\mu$	Tangential blowing jet momentum coefficient, $\dot{m}V_j/qS$
$F_H$	Measured horizontal force, drag minus horizontal thrust, lb
$F_T$	Total recoverable force, $T_S + \dot{m}V_j$ , lb
$F_V$	Measured vertical force, lift plus vertical thrust, lb
h	Tangential blowing slot height, in.
$h_N$	Engine nozzle height, in.
$\dot{m}$	Tangential blowing mass flow, slugs/sec
$P_d$	Tangential blowing plenum total pressure, psfa
$P_{T_d}$	Tangential blowing plenum total pressure, psig
$P_\infty$	Tunnel static pressure, psfa
q	Corrected tunnel dynamic pressure, $lb/ft^2$
$q_u$	Uncorrected tunnel dynamic pressure, $lb/ft^2$
R	Gas constant, 1715, ft-lb slug $^{\circ}R$
r	Radius of circulation control trailing edge, in.
S	Wing reference area, $ft^2$

$T_d$	Tangential blowing plenum temperature, °R
$T_s$	Calibrated static thrust, lb
$V_j$	Calculated tangential blowing isentropic jet velocity, ft/sec
$W_N$	Engine nozzle width, in.
$\alpha$	Corrected angle of attack, deg
$\alpha_g$	Geometric angle of attack, deg
$\gamma$	Ratio of specific heats, 1.4
$\epsilon$	Solid blockage factor
$\theta$	Computed static turning angle, 180 deg minus arctan ( $F_V/F_H$ )

## ABSTRACT

The results from one in a series of investigations undertaken to develop the Circulation Control Wing/Upper Surface Blowing (CCW/USB) high-lift concept are presented. Included are: isolation of propulsion jet turning, effects of tip devices, and thrust reversing. As evaluated, the concept employs a modified supercritical wing with a 3.6-percent chord circular trailing edge and tangential blowing from a thin, full-span slot over this trailing edge. In addition, turbofans are mounted over the wing so that the exhaust scrubs the upper surface of the wing and is turned by the trailing edge. Unlike other upper surface blowing concepts, thrust deflection is accomplished by entraining the propulsive jet with tangential blowing around the trailing edge. The propulsive-induced lift enhances the proven high lift of the circulation control wing. For a thrust coefficient of 3.76, a tangential blowing coefficient of 0.24, and an angle of attack of 16 deg, the low aspect ratio model produced an untrimmed lift coefficient of 6.5. The system also demonstrated the capability to be used as an effective thrust reverser for deceleration during the landing ground roll.

## ADMINISTRATIVE INFORMATION

The investigation of the circulation control wing/upper surface blowing high-lift system was funded by the Naval Air Systems Command (AIR 320D) under Program Element 62241N, Task Area WF 41.421.000, and David W. Taylor Naval Ship Research and Development Center (DTNSRDC) Work Unit 1600-079-30. The investigation was conducted during August and September 1980. Acknowledgment is extended to Messrs. R.J. Englar and W.H. Eilertson for their assistance in conducting this investigation.

## INTRODUCTION

High-lift coefficients generated by the Circulation Control Wing (CCW) high-lift system will permit short takeoff and landing (STOL) operation or increase the current lifting capability of high performance naval aircraft. This capability was confirmed in flight by the A-6/CCW demonstrator aircraft.<sup>1,2\*</sup> This system employs tangential blowing from the aft upper surface of the airfoil over a small

---

\*A complete listing of references is given on page 17.

radius trailing edge. Due to the Coanda effect, this thin jet sheet remains attached to the round trailing edge. This effect provides boundary layer control and increases the effective wing camber by controlling the locations of the airfoil stagnation points. In the A-6/CCW aircraft, engine bleed air provides the mass flow and jet momentum required for blowing. This aircraft produced a  $C_L$  of  $C_{L_{max}}$  3.9 at a  $C_\mu$  of 0.3 with an aspect ratio 5.3 and an airfoil section about 8.5-percent thick at the mean aerodynamic chord. This is an 85-percent increase in  $C_L$  over a conventional A-6 with a flap deflection of 30 deg. Also demonstrated were flight speeds as low as 67 knots.

Another proven high-lift concept based on the Coanda effect is Upper Surface Blowing (USB), as demonstrated by the YC-14 and QSRA aircraft. Wing lift is enhanced in the USB system by the use of large radius Coanda flaps which turn the propulsive jet down at the trailing edge of the wing. A typical high aspect ratio (AR=8.2), twin engine configuration produced an untrimmed  $C_L$  of 9.2 at an  $\alpha$  of 30 deg for a  $C_T$  of 3.6.<sup>3</sup> This lift was produced with a 60-deg flap deflection on a 12-percent thick airfoil and boundary layer control blowing on both the leading edge and the drooped ailerons. This system, however, is rather complex and heavy, with double-slotted flaps, large radius Coanda flaps, the associated support structure, and actuators.

The Circulation Control Wing/Upper Surface Blowing (CCW/USB) concept utilizes both propulsive-induced lift due to thrust turning and increased circulation lift provided by circulation control (CC). Additionally, by turning the propulsive jet with the CC trailing edge, instead of with a mechanical flap, the system can be mechanically simple and lightweight. Thrust turning is pneumatically controlled by varying the tangential blowing jet momentum. This arrangement produces static turning angles unachievable in other USB systems, and allows the CCW/USB system to be used as a thrust reverser for deceleration during the landing ground roll. The sketch in Figure 1 represents a proposed advanced STOL aircraft employing the CCW/USB high-lift system. This high-lift system is being developed by DTNSRDC. Initial confirmation of the STOL potential of this system has been reported by Nichols and Englar.<sup>4,5</sup>

#### MODEL AND TEST DESCRIPTION

A generic, semispan model previously evaluated in separate CCW and USB configurations<sup>6,7</sup> was modified to combine CCW and USB. This model, however, does not represent a desired CCW/USB configuration, due to the low aspect ratio. As shown in Figures 2 and 3, the basic wing is a 14-percent thick supercritical airfoil with an aspect ratio 4.0 planform and a half-span area of 2.125 ft<sup>2</sup> (0.197 m<sup>2</sup>). The sweep of the quarter chord is 19.7 deg, with no sweep at the trailing edge. A Krueger leading edge flap protects against leading edge flow separation. This flap is 15 percent of the chord and is fixed at 40 deg. The modified supercritical section accommodates a full-span CC trailing edge and the associated plenum as shown in Figure 3. The trailing edge parameters in this test are based on the parameters used during development of the A-6/CCW aircraft. A radius-to-chord ratio of 0.036 was used with a tangential blowing slot height-to-radius of 0.031.<sup>7</sup> A smaller trailing edge with a radius-to-chord ratio of 0.0094 is under development concurrently.<sup>5</sup> The plenum that supplies air for tangential blowing runs the full wing span. To investigate the effects of turning the propulsive jet without tangential blowing outboard, a plenum separator was inserted within the plenum during portions of this test at a point 59.7 percent out the span.

A turbofan simulator employing tandem 5.5-in. (0.14-m) tip-turbine fans mounted above the wing. Driven by compressed air at 200 lb/in<sup>2</sup> (1380 KN/m<sup>2</sup>), the simulator produced a maximum of 80 lb (356 N) of static thrust. Physically the simulator is oversize for the wing span and, therefore, a greater percent of the span is immersed in the exhaust. Two different nozzles were used with the simulator in this test. The geometry of these nozzles is found in Figure 4.

The wing-engine arrangement is shown in Figure 5 mounted vertically on the balance frame in the DTNSRDC 8- by 10-ft north subsonic wind tunnel. A splitter plate was used to isolate the wing from the tunnel boundary layer, and a body-of-revolution simulated fuselage was mounted on this plate. With the splitter plate and fuselage isolated from the balance frame, only forces on the wing and engine were measured.

In previous testing with this model, an interaction was found between the flow around the wing root and air in the balance frame cavity emerging through the gap between the wing and fuselage. As in the previous test, a thin flow fence

(Figures 2 and 3) was mounted on the wing near the wing-fuselage junction. The fence minimized this flow interaction, but also diminished normal wing-fuselage interaction.

For portions of the test, a fence was mounted on the wing outboard of the turbofan simulator at the plenum division. This fence (Figure 6) was used to isolate the portion of the wing scrubbed by the exhaust from the outer wing (CCW) section. Tip fences were also mounted during a portion of the test. Two different size fences were evaluated for preventing the tangential blowing from separating near the tip. (The geometry of the fences is given in Figure 6.) Several other tip devices were employed to improve the span loading and reduce drag on this low aspect ratio wing.

Testing was conducted in four phases. First, the installed static thrust  $T_S$  produced by the turbofan simulator was measured for each nozzle configuration. This thrust was calibrated against the engine drive air pressure. In the second phase, the static turning angle  $\theta$  and the efficiency with which this turning was achieved were resolved from force data for several configurations. The aerodynamics of the low aspect ratio, CCW/USB configuration in the presence of a free stream were determined in the third phase. The final phase determined maximum thrust deflection available during approach and simulated thrust reversing during the landing ground roll. This was accomplished by maintaining constant engine drive air pressure and tangential blowing supply air pressure while force data were taken at discrete dynamic pressures as the wind velocity was reduced from 130 ft/sec (40 m/s) to tunnel idle.

Where thrust  $T_S$  or thrust coefficient  $C_T$  are noted, the thrust is based on the static calibration in phase 1 with no correction for ram drag, although the correction would be small at these low dynamic pressures ( $q$ ). Additionally, the drag  $C_D$  and lift coefficient  $C_L$  include the horizontal and vertical thrust components. All forces and moments are resolved about the quarter chord of the mean aerodynamic chord (MAC).

Static weight tares recorded over the angle-of-attack range, were used to correct the balance data. Also accounted for were the effects of pressurizing the air supply lines. Static pressure tares were recorded independently for engine drive air supply lines and the tangential blowing air supply line at several angles of attack over the range of air pressures. These values, though small, were

subtracted from the measured data. Corrections for tunnel wall effects were also applied to all nonstatic runs. The angle of attack was corrected by an increment defined by:

$$\Delta\alpha(\text{deg}) = 0.2031 C_L$$

The increment applied to the drag coefficient was:

$$\Delta C_D = 0.003552 C_L^2$$

These values were derived by Englar.<sup>8</sup>

The tunnel dynamic pressure was measured with a calibrated pitot static tube and corrected for solid blockage by:

$$q = q_{\mu} (1 + 2\varepsilon)$$

where  $(1 + 2\varepsilon) = 1.0024533$ .<sup>9</sup>

Data were also recorded to determine the tangential blowing coefficient  $C_\nu$ , defined as:

$$C_\nu = \frac{\dot{m}V_j}{qS}$$

where  $\dot{m}$  was measured with a venturi meter in the blowing air supply line, and  $V_j$  was calculated by measuring total conditions in the blowing plenum, assuming isentropic expansion to free stream conditions:

$$V_j = \left\{ 2RT_d \left( \frac{\gamma}{\gamma-1} \right) \left[ 1 - \left( \frac{P_x}{P_d} \right)^{\frac{\gamma-1}{\gamma}} \right] \right\}^{1/2}$$

## DISCUSSION OF RESULTS

### STATIC TURNING

The capability of CCW/USB to produce the high lift required for STOL operation or increased lifting capability of an aircraft is dependent on how efficiently the propulsive jet can be turned. An indication of this efficiency is the static turning capability. Several exhaust nozzle shapes, ranging from round to higher aspect ratio D-nozzles, have been evaluated previously on the CCW/USB model to determine those parameters that effect static turning. Static turning improves when either the propulsive jet is spread wider and closer to the wing surface, or the height of the propulsive jet is reduced relative to the average height of the tangential blowing slot. The best static turning performance (Figure 8) is achieved employing the nozzle with an internal flap and partial span blowing. (A description of this nozzle is given in Figure 4a.) To investigate the static forces produced by turning the propulsive jet alone, only the inboard section of the wing scrubbed by the engine exhaust was blown. The outboard portion of the plenum was sealed off with minimal leakage to this section. In the proposed aircraft design (Figure 1), the tangential blowing associated with turning the engine exhaust would be provided from core bleed air. Air diverted from the fan would provide blowing outboard.

With no tangential blowing, the propulsive jet was statically turned 29 deg due to the nozzle geometry and the effects of scrubbing the upper surface of the wing. The unblown thrust deflection is shown in Figure 8a where at  $\alpha_g = 0$  deg the static turning angle ( $\theta$ ) is plotted against both the total pressure in the tangential blowing plenum ( $P_T$ ), and the tangential blowing momentum is divided by the wing reference area ( $\bar{m}V_j/S$ ). The latter parameter is equivalent to the tangential blowing coefficient  $C_u$ , (used in all nonstatic figures) with the dynamic pressure  $q$  set nominally to 1. Resolving the static turning of the tangential blowing without engine thrust, shown as the dashed curve, yields  $\theta$  greater than 160 deg over the blowing range. The dashed curve represents the upper limit of achievable static turning.

The lower three curves in Figure 8a representing thrust levels above 40 lb (178 N) show that  $\theta$  increases parabolically with increasing tangential blowing. For comparison, the scaled installed thrust of a TF-34 turbofan engine at 60 knots, sea level tropical day, would be 56.7 lb (252.2 N). With 10-percent core bleed,

this value drops to 46.2 lb (205.5 N). Typical STOL approaches require a  $\theta$  of about 60 deg. This level of turning is easily obtained at low blowing levels over the entire thrust range and is controllable by varying the blowing level. As the thrust level decreases, the maximum turning angle increases. The upper two curves representing thrust levels below 40 lb (178 N) initially show a parabolic increase in  $\theta$  with blowing; however, as  $\theta$  reaches 100 deg, the curves diverge. Small increases in blowing produce large changes in  $\theta$ . This results in a maximum turning angle for the 23.3-lb (103.6-N) thrust level equal to the turning produced by tangential blowing alone.

The efficiency with which turning is achieved is shown in Figure 8b. Nearly 100 percent of the combined thrust and blowing momentum is recovered statically for  $\theta$  through 55 deg. Beyond 55 deg, the efficiency is less, particularly at high thrust levels. However, for the thrust setting of 23.3 lb (103.6 N), over 60 percent of the thrust and blowing momentum is recovered for  $\theta$  up to 110 deg; over 50 percent is recovered for  $\theta$  up to 160 deg. This thrust is essentially recovered as a rearward horizontal force and can provide deceleration during the landing ground roll.

A fence was added to the configuration at the wing station where the blowing plenum is divided. This fence was intended to isolate the propulsive jet from the unblown wing section to improve the static turning. For thrust levels above 40 lb, however, the static turning performed is unaffected by the installation of the fence. Furthermore, the fence actually degraded the maximum turning performance at thrust levels below 40 lb (178 N). This degraded performance is illustrated by comparing the results obtained with the fence installed (Figure 7) with the previous results obtained without this fence. The curves of  $\theta$  versus blowing momentum for the lower thrust levels (Figure 7a) do not diverge from a parabolic shape, as happened without the fence installed; see Figure 8a. Therefore, the maximum achieved turning angle with the fence installed is 25 percent lower than the maximum turning angle achieved without this fence. The position of this fence was not optimum, and the propulsive jet spread beyond the fence at higher thrust levels. Generally, isolating the propulsive jet and eliminating the lateral (or spanwise) inflow into this jet were detrimental with respect to static turning.

Although the nozzle with an internal flap provided excellent static turning, some mechanization would be required to retract the internal flap during cruise flight. Furthermore, unblown thrust turning due to wing and nozzle shape should be

minimized in cruise flight, as should be cruise drag due to external nozzle shape. A D-shaped nozzle representing such a design compromise is shown in Figure 4b.

The static turning performance produced with the D-nozzle and partial span blowing is presented in Figure 10. The unblown static turning due to the geometry of the D-nozzle and the scrubbing effects is 25 deg compared to 29 deg for the nozzle with an internal flap. A better integration of the engine and wing would result in a further reduction in this unblown thrust turning.

As with the nozzle with an internal flap, static turning increases parabolically with increased blowing at higher thrust levels, and a divergence from parabolic occurs at lower thrust levels. Due to a higher nozzle-height-to-slot-height ratio, the maximum  $\theta$  produced with this D-nozzle drops to about 130 deg for a thrust level of 26.31 lb (117.0 N). Lower maximum  $\theta$  reduces the effectiveness of thrust reversal. For approach conditions where  $\theta$  is less than 60 deg, the turning efficiency is comparable to that achieved with the use of the internal flap.

The static turning results employing full span tangential blowing and the D-nozzle are presented in Figure 11. This turning is also documented through flow visualization in Figure 12. Statically, interaction between the propulsive jet and the blowing outboard is minimal. For partial span blowing, shown in Figure 10a, the 49-lb thrust level is turned statically 67 deg for a total pressure in the tangential blowing plenum of 15 psig ( $103 \text{ KN/m}^2$ ). This corresponds to an  $\dot{m}V_j/S$  value of  $2.25 \text{ lb/ft}^2$  ( $107.73 \text{ N/m}^2$ ). At this pressure, the value increases to  $3.25 \text{ lb/ft}^2$  ( $155.61 \text{ N/m}^2$ ) with full-span blowing (Figure 11a); the resulting  $\theta$  is 73 deg. Forces generated by the increased blowing are mainly responsible for the increase in  $\theta$ . By comparing these curves at constant blowing levels, it can be seen that the static turning becomes less effective as the blowing is spread over a greater portion of the span.

The series of photographs in Figure 12 illustrate the capability of the CC trailing edge to pneumatically deflect the propulsive jet by varying the blowing level while holding the thrust constant at 24.5 lb (109.0 N). In Figure 12a, thrust behavior is shown without tangential blowing ( $P_{T_D} = 0$ ). The tuft attached to the nozzle centerbody follows the propulsive jet which is turned only by nozzle geometry and scrubbing effects. The tuft outboard on the wing also shows the influence of the propulsive jet over this wing section. Conditions shown in Figure 12b were produced with a blowing plenum pressure of 10 psig ( $69 \text{ KN/m}^2$ ). Here, the

outboard tuft is turned nearly around the trailing edge. Increased turning of the propulsive jet due to the tangential blowing is also apparent. When the plenum pressure is increased to 20 psig ( $138 \text{ KN/m}^2$ ), the propulsive jet is turned nearly 90 deg (Figure 12c); for a plenum pressure of 40 psig ( $276 \text{ KN/m}^2$ ), the turning is greater than 90 deg (Figure 12d).

#### LONGITUDINAL AERODYNAMIC CHARACTERISTICS

The longitudinal aerodynamic characteristics of the low aspect ratio, CCW/USB semispan model employing the D-nozzle are presented in Figure 13 through 16. Results associated with turning the propulsive jet with blowing on the inboard section are presented in Figures 13 and 14. Full-span blowing results are presented in Figures 15 and 16. The effects of varying blowing while holding the thrust constant at  $\alpha_g = 0 \text{ deg}$  are shown in Figures 13 and 15. The effects of varying the angle of attack while holding thrust and blowing constant are shown in Figures 14 and 16.

The zero thrust data is distorted due to a loss in local  $q$  behind the windmilling turbofan simulator. In Figure 13, dashed curves approximate the results had this blockage not occurred. Because this condition of blowing on the inboard section of the wing without thrust would not occur in normal operation, the dashed curves are intended only as a reference when noting the effect produced by increasing thrust.

The lift produced with thrust, but without tangential blowing ( $C_u = 0$ ), combines circulation lift due to wing camber with the unblown thrust deflection. Previously, this unblown deflection was shown to be 25 deg statically. This deflection results in a substantial vertical thrust component. Increasing the tangential blowing momentum increases the thrust deflection and, therefore, the lift due to vertical thrust. There is also a corresponding decrease in the recovered horizontal thrust, indicated by a more positive value of drag. Tangential blowing also increases the circulation lift by increasing the effective wing camber.

Trends typical of powered lift systems are shown in Figure 15. Boundary layer control is dominant at lower blowing levels. At higher blowing levels, the increase in effective wing camber becomes more dominant.

An airspeed of approximately 55 knots is anticipated for the advanced CCW/USB STOL aircraft (Figure 1) at takeoff and during the landing approach. This velocity

is approximately equal to a dynamic pressure of  $10 \text{ lb}/\text{ft}^2$  ( $479 \text{ N}/\text{m}^2$ ). Because the capability of the CC trailing edge to deflect the propulsive jet diminishes somewhat with increasing aircraft velocity, most of the data were taken at  $10 \text{ lb}/\text{ft}^2$  ( $479 \text{ N}/\text{m}^2$ ). The effect of dynamic pressure variation is shown in Figure 15. Data taken at a  $q$  of  $10 \text{ lb}/\text{ft}^2$  ( $479 \text{ N}/\text{m}^2$ ) are presented as dashed curves; the solid curves represent data taken at  $20 \text{ lb}/\text{ft}^2$  ( $958 \text{ N}/\text{m}^2$ ). As  $q$  increases, higher thrust and blowing momentum are required to maintain a constant thrust or blowing coefficient.

Typically, the coefficients of lift, drag, and pitching moment are unchanged when  $q$  varies, and the coefficients are compared for constant value of  $C_T$  and  $C_\mu$ . This is demonstrated by the curves for a  $C_T$  of 1.23 in Figure 15. However, the curve for a  $C_T$  of 1.86 at  $20 \text{ lb}/\text{ft}^2$  ( $958 \text{ N}/\text{m}^2$ ) shows a degraded performance as  $C_\mu$  increases. This degraded performance results from premature separation of the tangential blowing jet from the trailing edge due to local conditions influenced by the propulsive jet, dynamic pressure, and trailing edge geometry. No separation is indicated at the same thrust and blowing momentum at  $10 \text{ lb}/\text{ft}^2$  ( $479 \text{ N}/\text{m}^2$ ), which is represented by the curve for a  $C_T$  of 3.75.

The capability of the CCW/USB system to produce the high-lift coefficients required for STOL operation, or to increase the lifting capability of an aircraft, is demonstrated in Figures 14 and 16. These results are also presented for a  $C_T$  of 3.75 in Figure 17 in the form of a configuration buildup. The contribution to the total system lift provided by turning the propulsive jet with the CC trailing edge is a  $C_L$  of 5.75 at an  $\alpha$  of 23 deg for a  $C_\mu$  of 0.16; see Figure 17. The drag produced at these conditions is equal to the recovered horizontal thrust as shown by the zero value of  $C_D$ . One of the benefits of the CCW/USB system is the capability to balance these components at very low velocities and at high-lift coefficients. The high thrust recovery of similar powered lift systems permits equilibrium flight only at higher velocities unless mechanical drag generators are employed.

Applying tangential blowing outboard at the same pressure as applied inboard increases the blowing coefficient to 0.25. This increase in  $C_\mu$  results in a  $C_L$  of 6.95 and a  $C_D$  of 0.7, which is a net drag. Reducing  $\alpha$  to 16 deg again produces a  $C_D$  of zero; but with full span blowing, the  $C_L$  is 6.5. Further reducing

the angle of attack to 9 deg results in a  $C_L$  of 5.75, which was the  $C_L$  achieved at an  $\alpha$  of 23 deg with partial span blowing. The value of  $C_D$  at these conditions and full span blowing is a negative 0.78, which is a net thrust. This demonstrates this system's capability to provide a wide range of flight conditions necessary for STOL operation.

Pitching moment coefficients are also presented in Figures 14 through 17. As with most other powered lift systems, a large nose-down moment is produced at high-lift conditions. One possible approach to trimming this moment is to arrange for an inverse camber of the horizontal tail as was done in the A-6/CCW program.

The series of photographs in Figure 18 illustrate the deflection of the propulsive jet in flight. These photographs were taken at a  $q$  of  $10 \text{ lb}/\text{ft}^2$  ( $479 \text{ N}/\text{m}^2$ ). As in the static flow visualization (Figure 12), a thrust of 24.5 lb was maintained as the tangential blowing was increased. The plenum pressure in Figure 18a is zero psig. This pressure rises to 10 and 20 psig ( $69$  and  $138 \text{ KN}/\text{m}^2$ ) in Figures 18b and 18c with 40 psig ( $276 \text{ KN}/\text{m}^2$ ) in the plenum in Figure 18d.

#### TIP DEVICES

The large span required by aircraft employing a high aspect ratio wing tends to be incompatible with operation aboard naval ships. Tip sails, cascades, and winglets have demonstrated the capability to improve the cruise performance of an aircraft without increasing the wing span. By interacting with the tip vortex, these devices generate a forward axial force, thereby reducing the net wing drag. Such devices, designed to improve cruise performance, could also be beneficial at STOL flight speeds.<sup>6</sup>

A large tip fence used to improve the performance of the low AR, CCW semispan model is described in Reference 7. By reducing the spanwise flow entrainment near the wing-tip blowing slot, this fence prevented premature separation of the tangential blowing jet. The fence also prevented the unloading of the wing tip due to the tip vortex. However, tip fences (endplates) do not necessarily provide cruise performance improvements. Thus, several other tip devices were investigated to determine if the improvements provided by the large tip fence could also be provided by these tip devices without compromising the known cruise performance benefits.

Two small partial wing tip fences (Figure 6) were used to evaluate the possible performance improvement. Modest improvement in lift and drag at higher blowing levels and at low angles of attack are shown in Figure 19. The tip sails and cascades also provide a modest improvement in lift; however, at low angles of attack this increase in lift is offset by an increase in drag, as shown in Figure 20.

The best cruise performance improvement is provided by employing the winglets shown in Figure 7. The winglet with a small lower surface, and the winglet with equal upper and lower surface areas were designed using information provided by NASA Langley.<sup>10,11,12</sup> The performance produced with these winglets is illustrated in Figure 21. By using tufts mounted on the wing and winglet to visualize flow, the lower surface of both winglets was seen to be stalled throughout the range of conditions tested. This condition was not improved with spanwise blowing on the winglet. Additionally, the interaction between the winglet and the tip vortex caused a disturbance in the flow over a portion of the wing leading edge. A third winglet configuration used only the upper surface from that winglet having equal upper and lower surface areas. The improvement in the ratio of lift-to-drag gained by employing this winglet is presented in Figures 22 and 23. Because these tip devices were designed for improved cruise performance, further improvement in high-lift enhancement and drag reduction may be obtained if a design compromised for both high lift and cruise were employed.

#### SIMULATED THRUST REVERSING

During landing approach, the capability of the CCW/USB system to provide high-lift coefficients without excess thrust recovery permits low approach velocities. With less kinetic energy to dissipate after touchdown, shorter ground rolls are possible. Employing the CCW/USB system as a thrust reverser further reduces the landing ground roll. This reduction is accomplished without the penalty of increased weight and mechanical complexity of conventional thrust reversers. Increasing the tangential blowing momentum is the only requirement.

To investigate the thrust reversing capability, the ground roll was simulated by recording data for steady state conditions at discrete velocities, as tunnel  $q$  was reduced from 20 lb/ft<sup>2</sup> (958 N/m<sup>2</sup>) or 130 ft/sec (40 m/s) to tunnel idle (30 ft/sec; 9 m/s). The model was set at 5 deg incidence to account for wing and fuselage incidence with weight on the landing gear. Constant values of thrust and

blowing momentum were maintained, resulting in increasing values of  $C_T$  and  $C_D$  as  $q$  decreased. These data are presented in Figures 24 through 26 in the form of measured horizontal and vertical forces. The vertical force, shown as a dashed curve, combines lift with the recovered vertical thrust. The horizontal force, shown as a solid curve, combines drag with the recovered horizontal thrust. The horizontal force is positive for positive values of drag minus the horizontal thrust component; that is, decelerating, or thrust reversing capability is indicated by a positive horizontal force.

The thrust reversing capability of the CCW/USB configuration with the D-nozzle for tangential blowing at  $P_{T_D}$  of 20 psig ( $138 \text{ KN/m}^2$ ) is presented in Figure 24.

The results with partial span blowing are shown in Figure 24a; the results with full-span blowing are presented in Figure 24b. Using this plenum pressure with partial span blowing produces a value of  $\dot{m}V_j/S$  of  $2.6 \text{ lb/ft}^2$  ( $124.5 \text{ N/m}^2$ ).

Employing full-span blowing at this plenum pressure results in a value of  $\dot{m}V_j/S$  of  $4.2 \text{ lb/ft}^2$  ( $201.1 \text{ N/m}^2$ ). At the scaled maximum thrust of the TF-34 turbofan with 10-percent core bleed of 46.2 lb (205.5 N), Figure 24a shows a near zero horizontal force. Additional blowing outboard produces additional drag as well as enhances thrust turning, and thereby results in a decelerating force as shown in Figure 24b. Reducing the thrust produces an even greater decelerating force since thrust turning increases. At 24.6 lb (109.4 N) of thrust, or 50 percent of the scaled TF-34 thrust, with full-span blowing the decelerating force at 55 knots is nearly equal to the input engine thrust.

Static turning data suggest that concentrating the tangential blowing inboard to deflect the propulsive jet would provide better thrust recovery. However, during the landing ground roll near the touchdown velocity, similar results are obtained with the blowing either concentrated inboard or over the full span; see Figure 26. This operation must be investigated on high aspect ratio wings to determine the best combination of blowing.

Statically, the nozzle with an internal flap provided greater thrust turning capability due to a lower ratio of nozzle-height-to-slot-height improving the propulsive jet spreading. This is also beneficial in the operation as a thrust reverser. Results with partial span blowing for 24.6 and 47.4 lb (109.4 and 210.8 N) of thrust employing the nozzle with an internal flap are presented in

Figure 26. This represents the possible improvement in thrust reversing that could be obtained with improved nozzle geometry.

#### SUMMARY OF RESULTS

Analysis of the data presented indicates:

1. The propulsive jet can be turned and its deflection can be controlled pneumatically by employing a circulation control trailing edge.
2. The lift and drag produced by deflecting the propulsive jet are enhanced by operating the outboard circulation control wing. This enhancement diminishes as aircraft velocity decreases.
3. Nearly 100 percent of the thrust and tangential blowing momentum is recovered for static turning angles ( $\theta$ ) through 55 deg.
4. About 80 percent of the thrust and blowing momentum is recovered at static turning angles near 90 deg.
5. The maximum static turning angle achieved was on the order of 165 deg at a medium thrust level, with about 60 percent of the thrust and blowing momentum recovered.
6. Lift coefficients typically required for STOL operation were achieved employing an aspect ratio 4 wing. For a  $C_T$  of 3.76, a  $C_\mu$  of 0.24, and an  $\alpha$  of 16 deg, a  $C_L$  of 6.5 was produced with the horizontal thrust component and drag in balance ( $C_D = 0$ ).
7. The single, upper winglet improved the blown lift-to-drag ratio of the low aspect ratio CCW/USB configuration.
8. The CCW/USB system demonstrated an effective thrust reversing capability during the simulated landing ground roll.

#### CONCLUSIONS

Wind tunnel results indicate that the CCW/USB high-lift system can provide the necessary high-lift coefficients required for either STOL operation or increased useful payload. This is achieved by combining the propulsive induced lift due to thrust turning, with increased circulation lift produced by the circulation control wing. With the CCW/USB system, deflection of the propulsive jet and the effective wing camber are controlled pneumatically, thereby reducing the mechanical complexity and weight as compared with high-lift systems employing flaps. Further, the landing ground roll can be reduced by employing the CCW/USB system as a thrust

reverser without the penalty of additional weight and mechanical complexity required for conventional thrust reversers.

When combined with a moderate aspect ratio supercritical wing, this system would enable such an aircraft to operate from naval ships without the presence of either catapulting or arresting gear. With the availability of this equipment, the increased lifting capability would provide greater useful payload and improved safety margins.

#### REFERENCES

1. Pugliese, A.J. and R.J. Englar, "Flight Testing the Circulation Control Wing," AIAA Paper No. 79-1791 presented at the AIAA Aircraft Systems and Technology Meeting, New York (Aug 1979).
2. "A-6A Circulation Control Wing Flight Test Final Report," Grumman Aerospace Corporation Report No. FTD-128-55-3.55, (Apr 1979).
3. Phelps, A.E. III, "Wind-Tunnel Investigation of a Twin-Engine Straight-Wing Upper-Surface Blown Jet-Flap Configuration," NASA Technical Note D-7778, Figure 8, p. 30 (Jan 1975).
4. Nichols, J.H. Jr., and R.J. Englar, "Advanced Circulation Control Wing System for Navy STOL Aircraft," AIAA Paper No. 80-1825 presented at the AIAA Aircraft Systems Meeting, Anaheim, California (4-6 Nov 1980).
5. Nichols, J.H. Jr., et al., "Experimental Development of an Advanced Circulation Control Wing System for Navy STOL Aircraft," AIAA paper No. 81-0151 presented at the AIAA 19th Aerospace Sciences Meeting, St. Louis, Missouri (12-15 Jan 1981).
6. Nichols, James H., Jr., "Development of High Lift Devices for Application to Advanced Navy Aircraft," DTNSRDC-80/058 (Apr 1980).
7. Trobaugh, L.A. et al., "Low Speed Aerodynamic Characteristics of Wings of Aspect Ratio 3 and 4 Equipped with High Lift Systems," DTNSRDC Report ASE-80/09 (May 1980).
8. Englar, R.J., "Development of the A-6/Circulation Control Wing Flight Demonstrator Configuration," DTNSRDC Report ASE-79/01 (Jan 1979).
9. Pope, A., "Wind-Tunnel Testing," John Wiley and Sons, Inc., New York, pp. 268-342 (Apr 1964).
10. Whitcomb, R.T., "A Design Approach and Selected Wind-Tunnel Results at High Subsonic Speeds for Wing-Tip Mounted Winglets," NASA Technical Note D-8260 (Jul 1976).

11. Jacobs, P.F. et al., "Effect of Winglets on a First-Generation Jet Transport Wing," NASA Technical Note D-8473 (Jun 1977).

12. Flechner, S.G. and P.F. Jacobs, "Experimental Results of Winglets on First, Second, and Third Generation Jet Transports," NASA Technical Memorandum 22674 (May 1978).

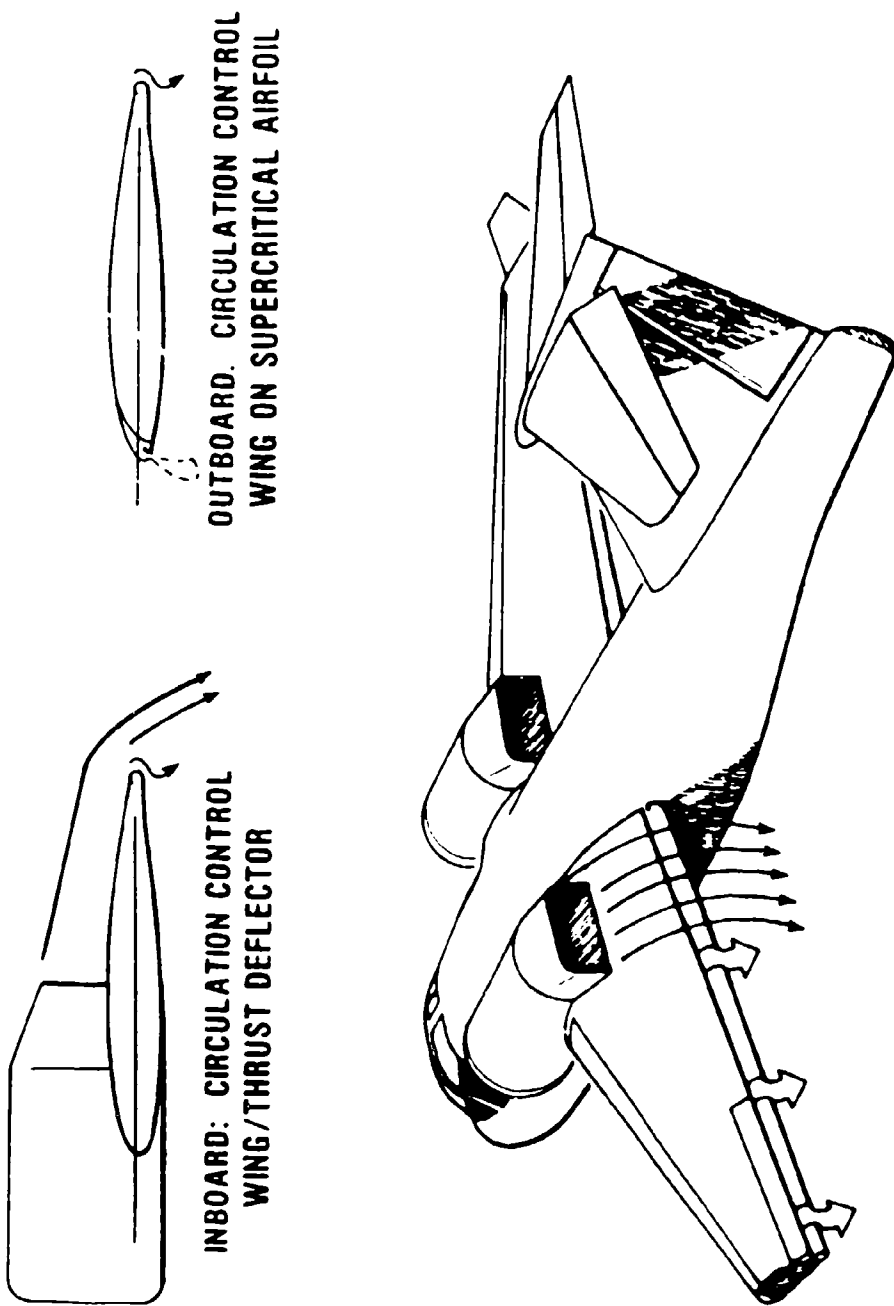


Figure 1 - Circulation Control Wing/Upper Surface Blowing STOL Aircraft Configuration

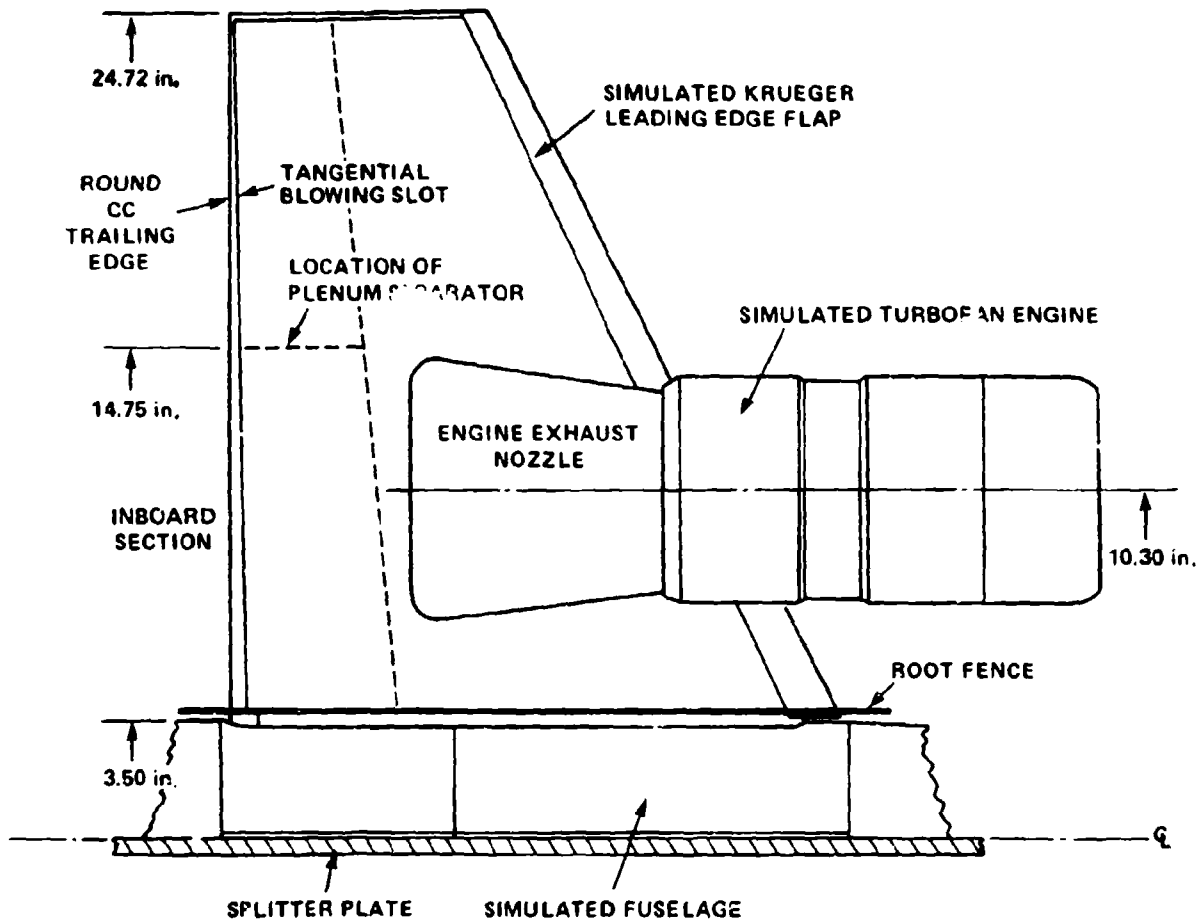


Figure 2 - Aspect Ratio 4 Circulation Control Wing/Upper Surface  
Blowing Semispan Model Planform

Figure 3 - Model Sections

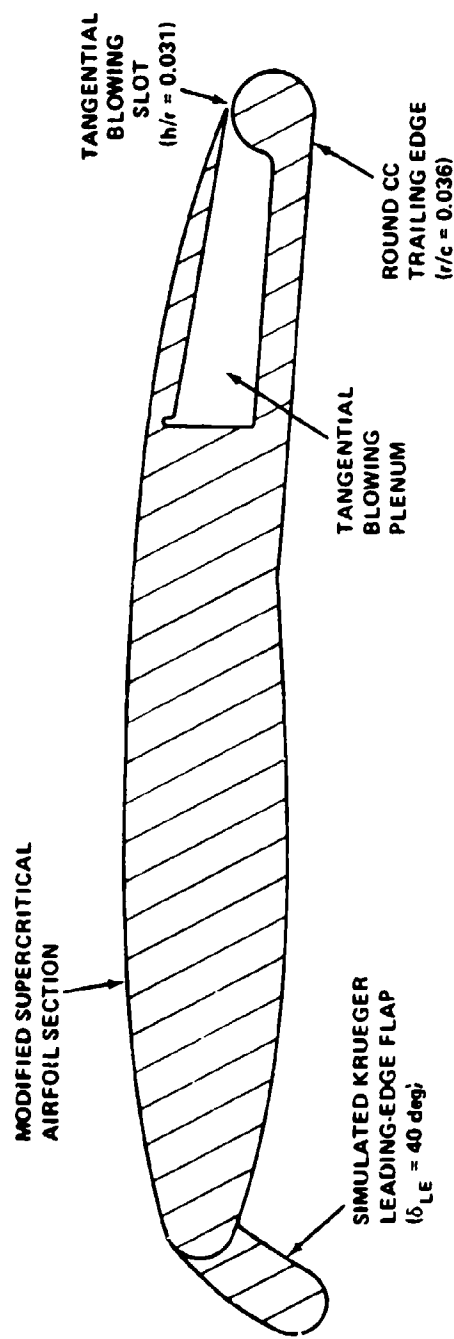


Figure 3a - Wing Section

Figure 3 (Continued)

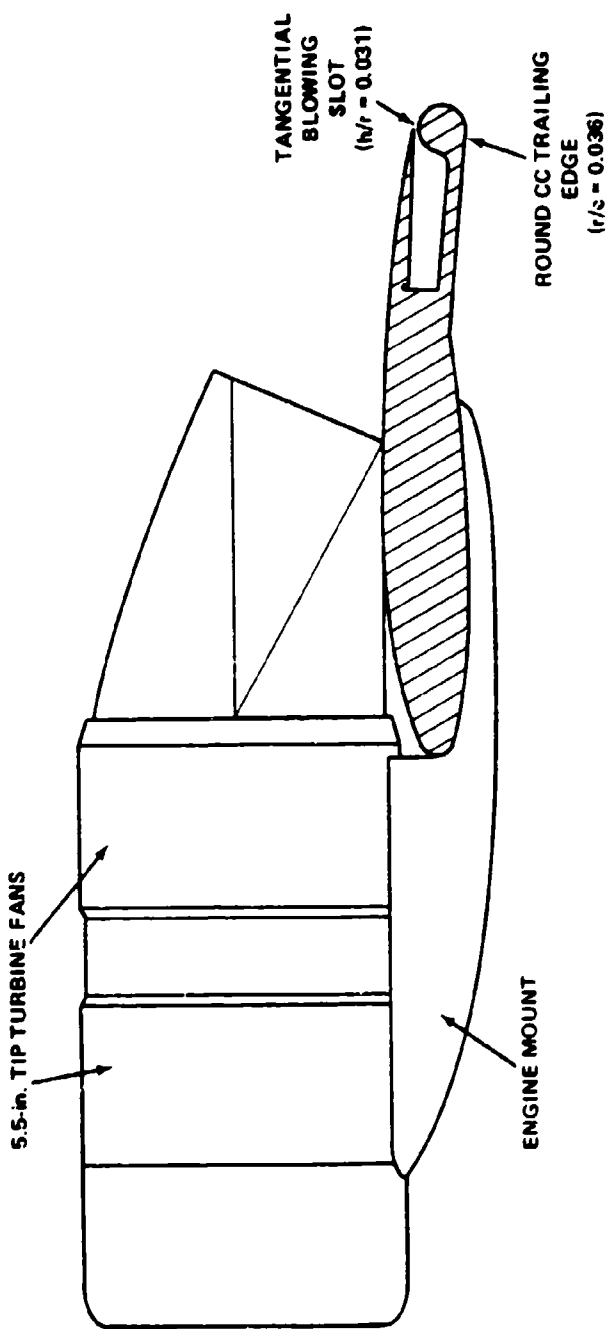


Figure 3b - Simulated turbofan Engine Mounting

Figure 3 (Continued)

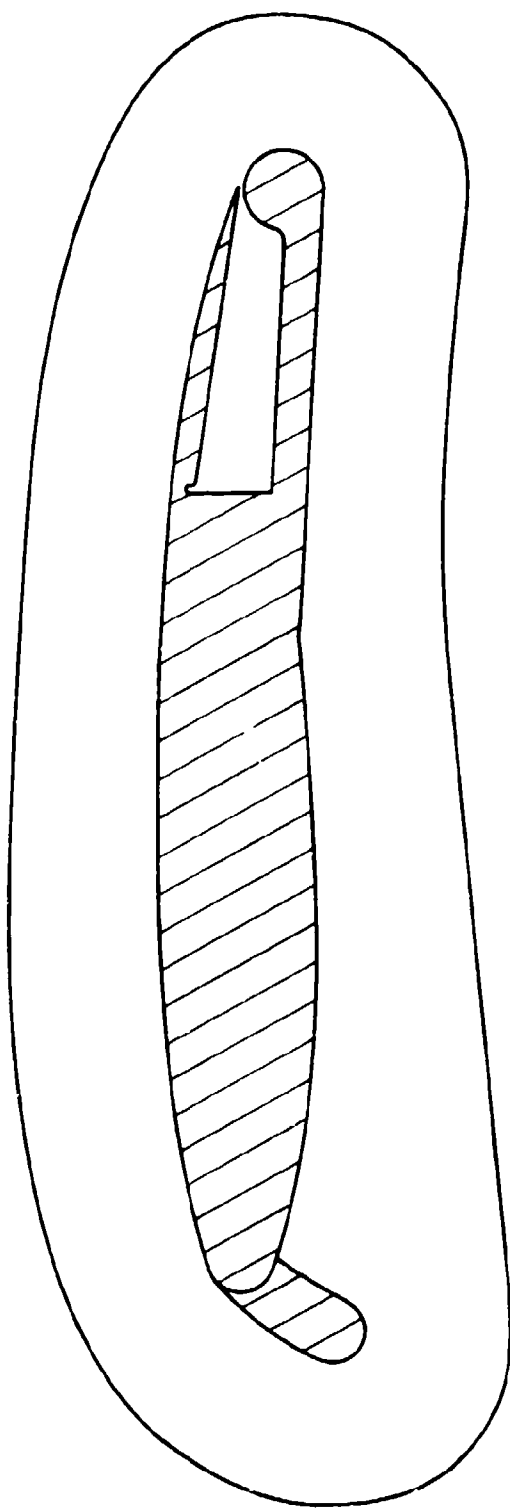


Figure 3c - Root Fence

Figure 4 - Turbofan Simulator Nozzle Geometry

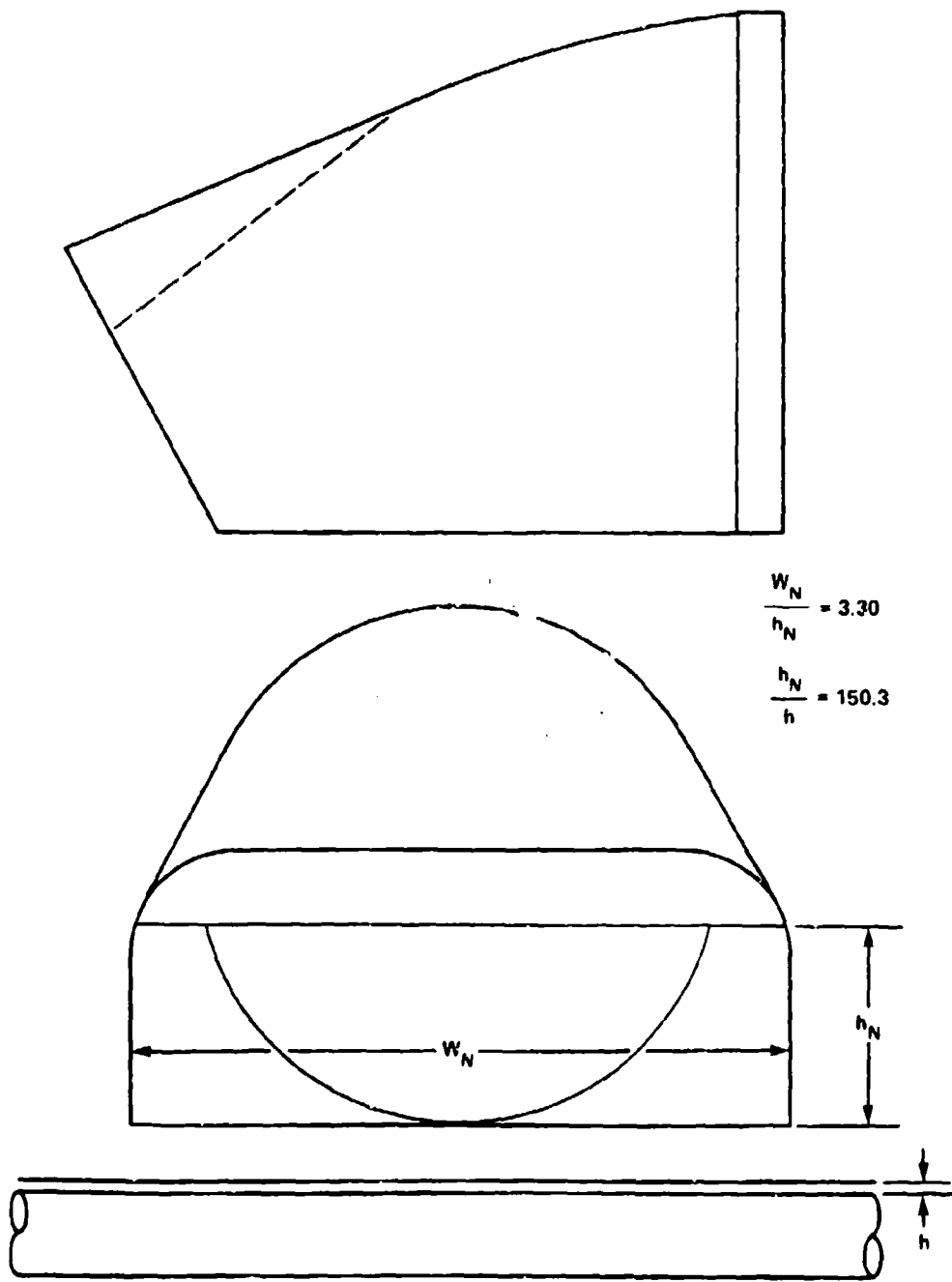


Figure 4a - Nozzle With an Internal Flap

Figure 4 - (Concluded)

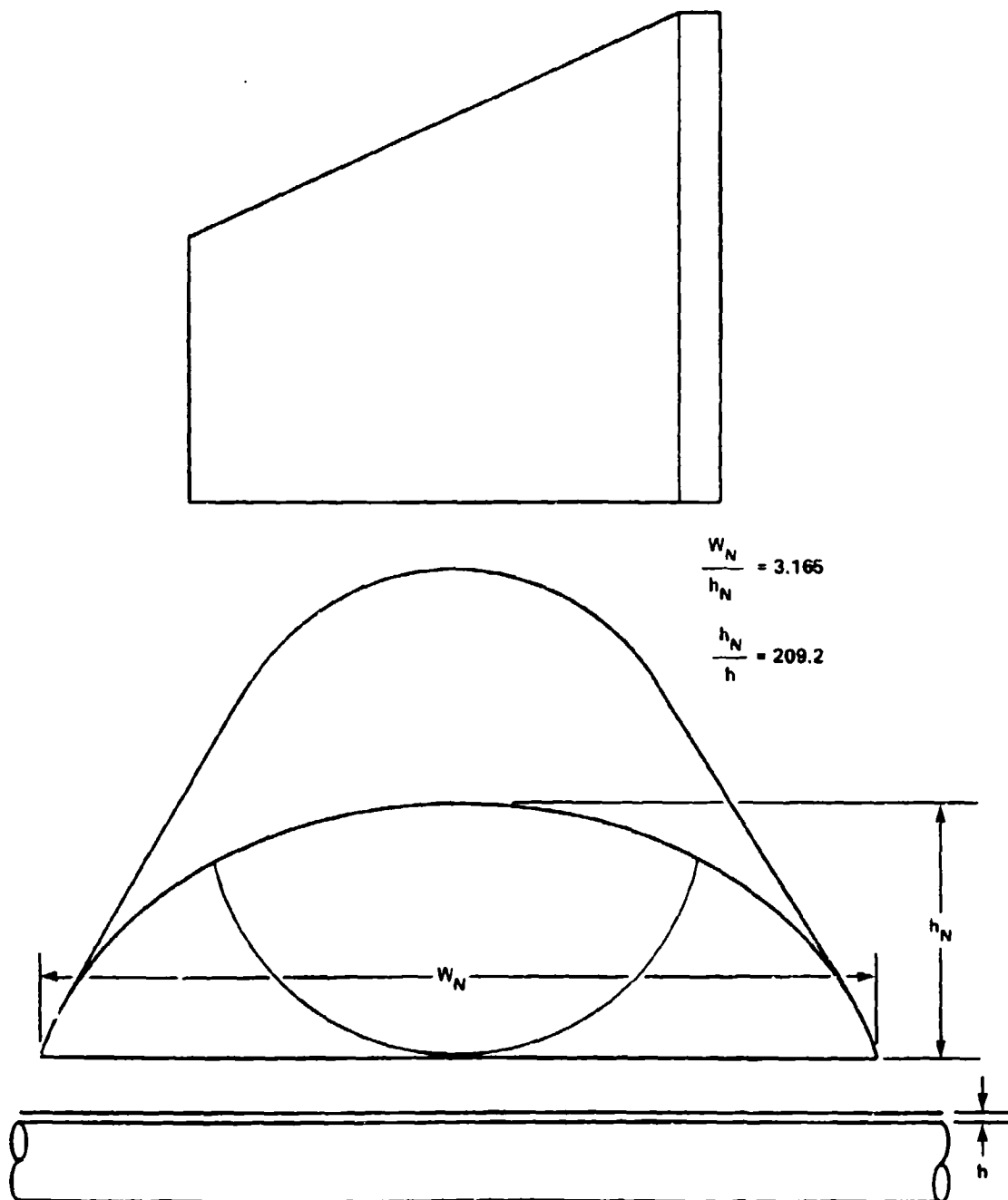
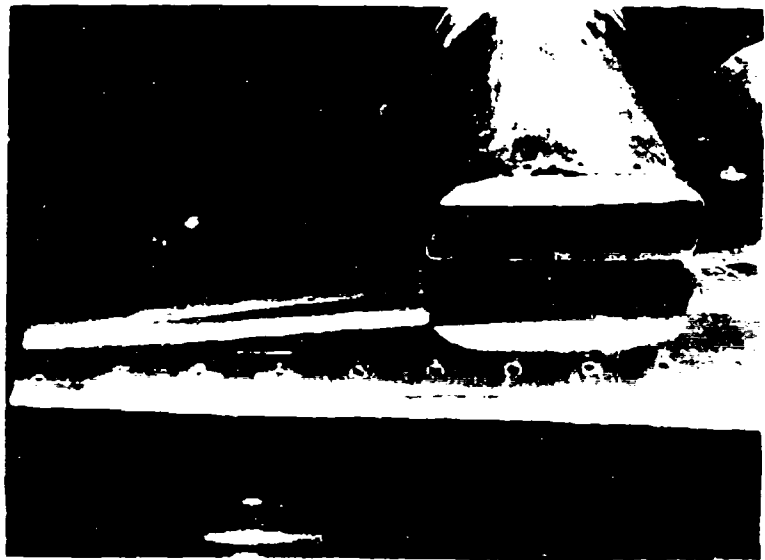


Figure 4b - D Shaped Nozzle



Aft View of Engine Nozzle and CCW Trailing Edge



Front View of Engine, Fuselage, Wing,  
and Krueger Leading Edge Flap

Figure 5 - Model Installation on Splitter Plate in DTRSPC  
5- by 10-Foot North Wind Tunnel

Figure 6 - Optional Fences

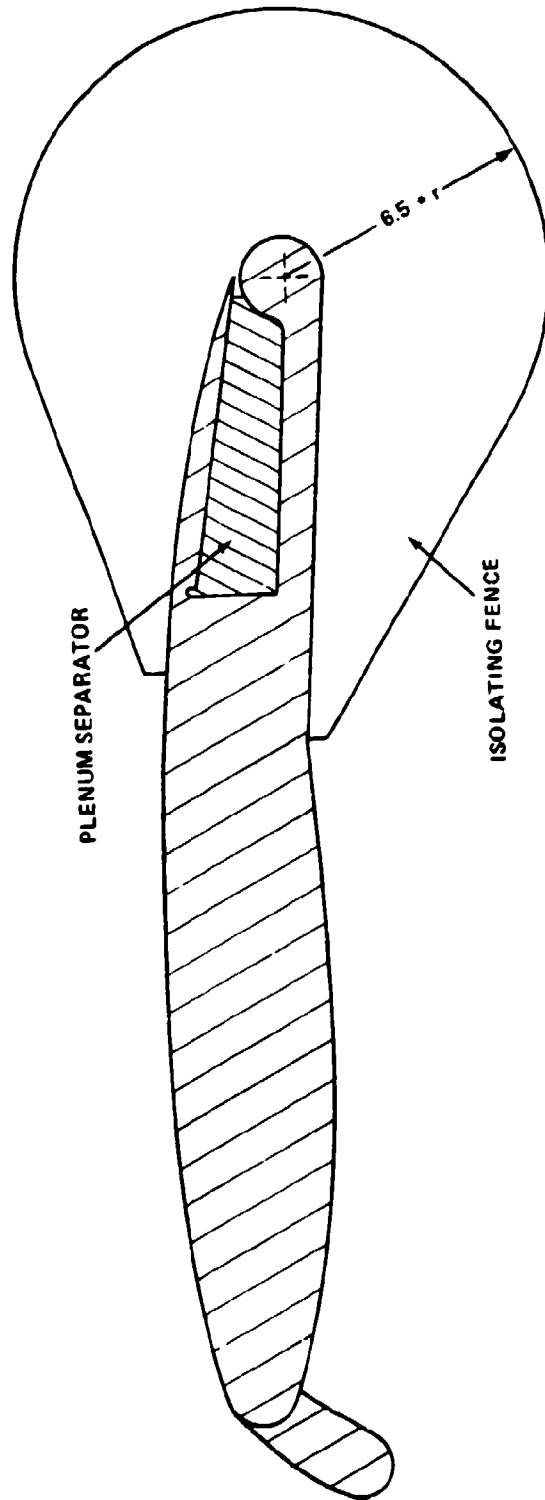


Figure 6a - Fence Isolating the Propulsive Jet at the Plenum Separator

Figure 6 (Continued)

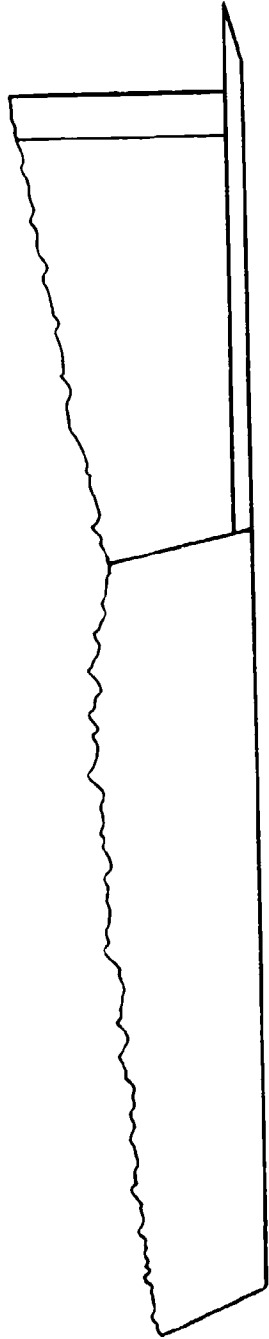


Figure 6b - Large King Tip Fence

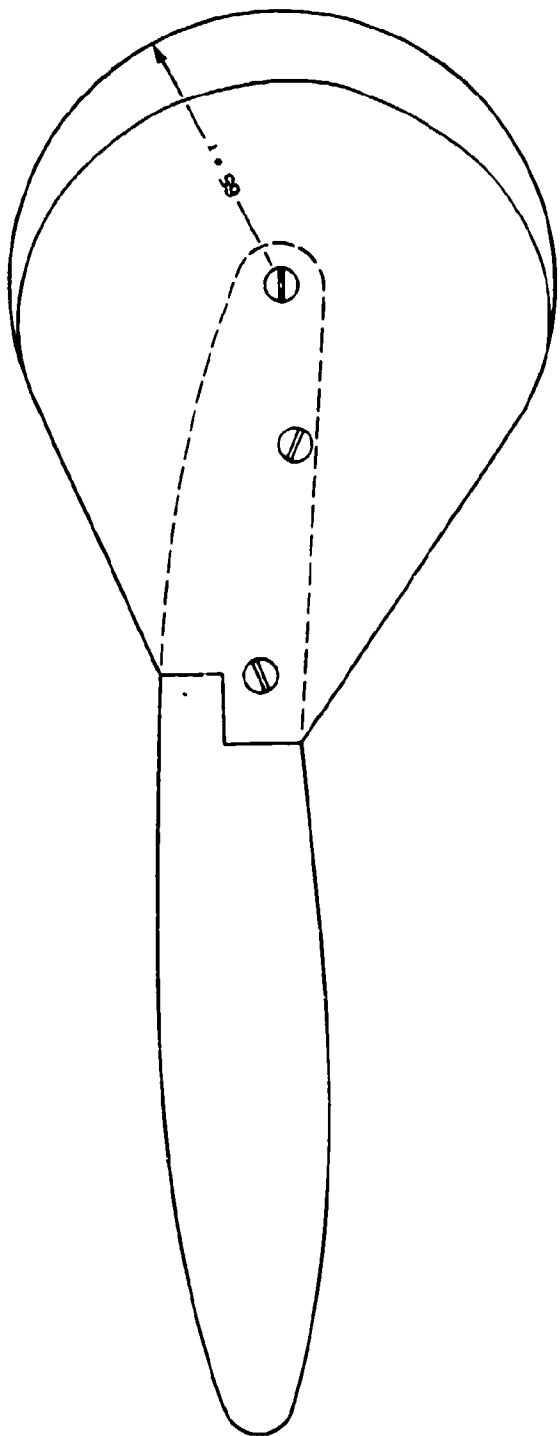


Figure 6 (Continued)

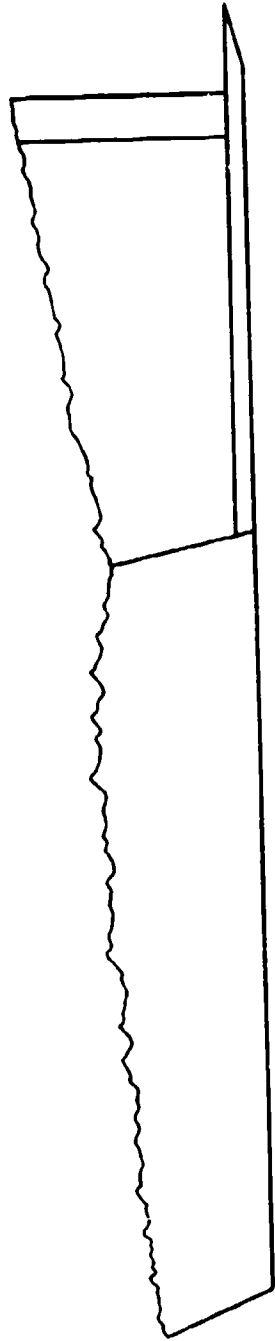


Figure 6c - Small Wing Tip Fence

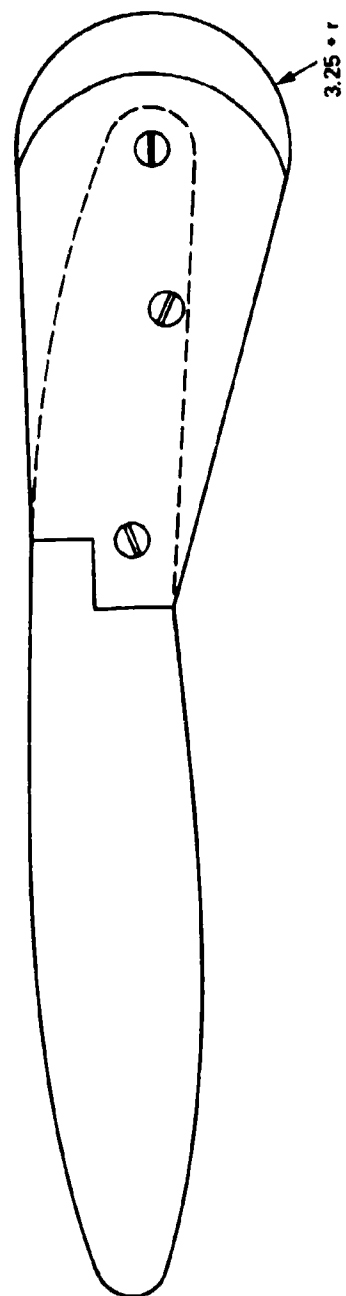


Figure 7 - Tip Devices

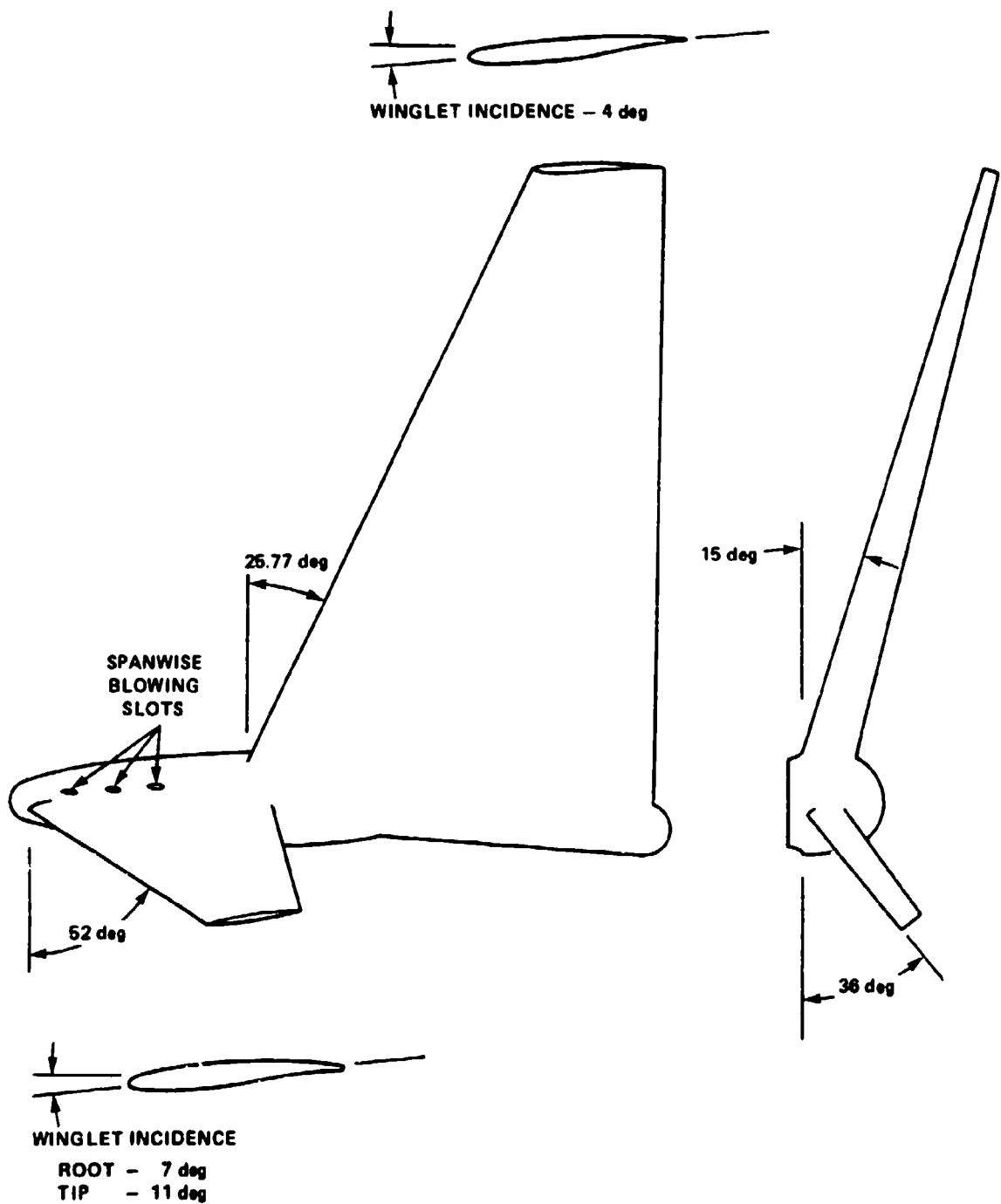


Figure 7a - Winglet with Small Lower Surface and Large Upper Surface

Figure 7 (Continued)

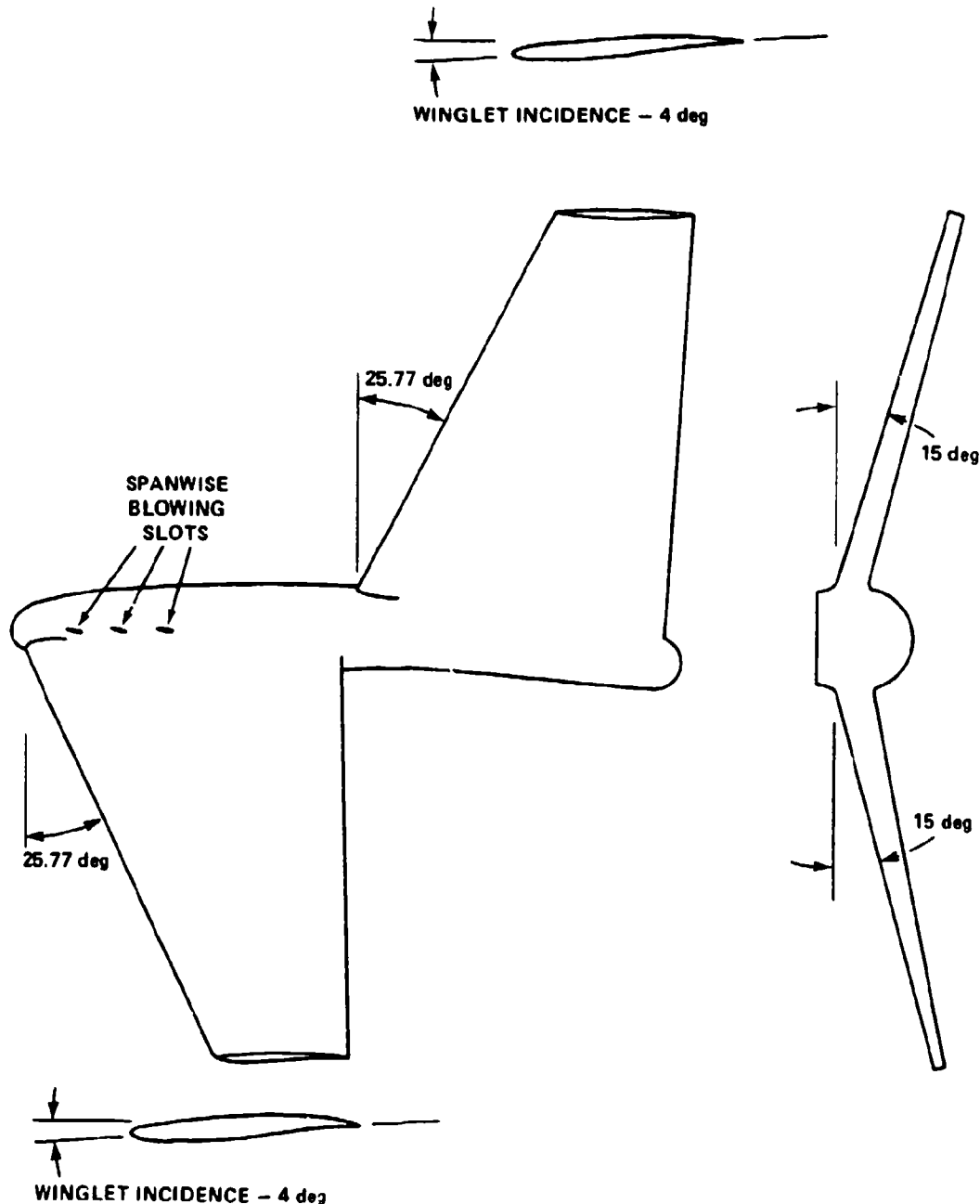


Figure 7b - Winglet with Equal Upper and Lower Surface Areas

Figure 7 (Continued)

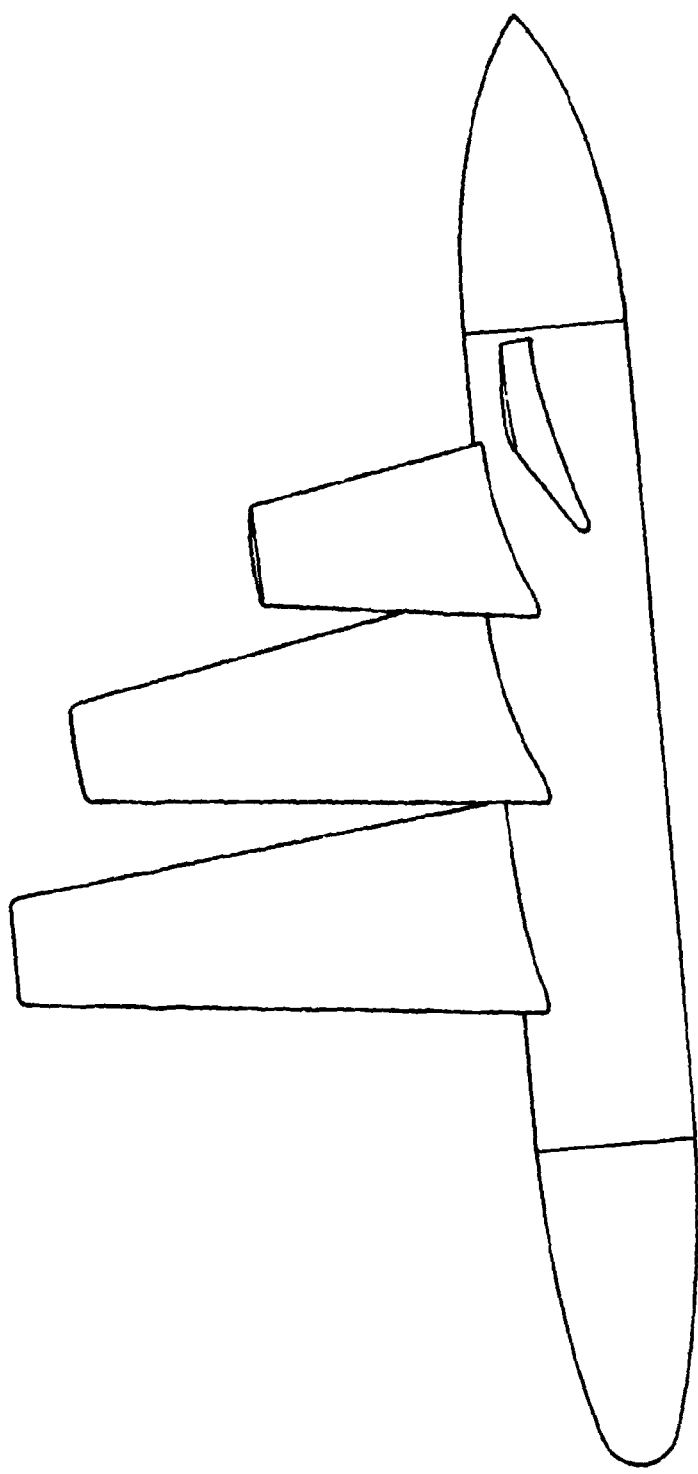


Figure 7c - Tip Sails

Figure 7 (Continued)

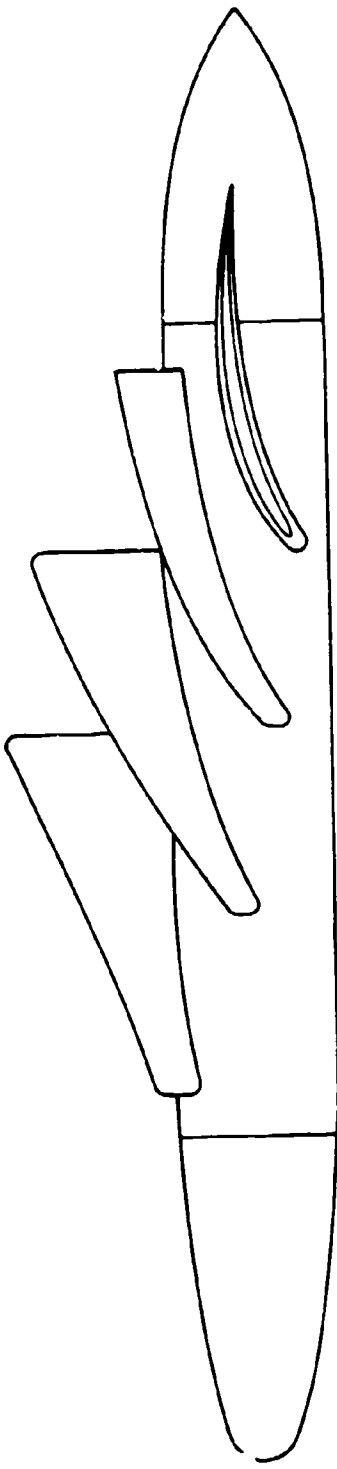
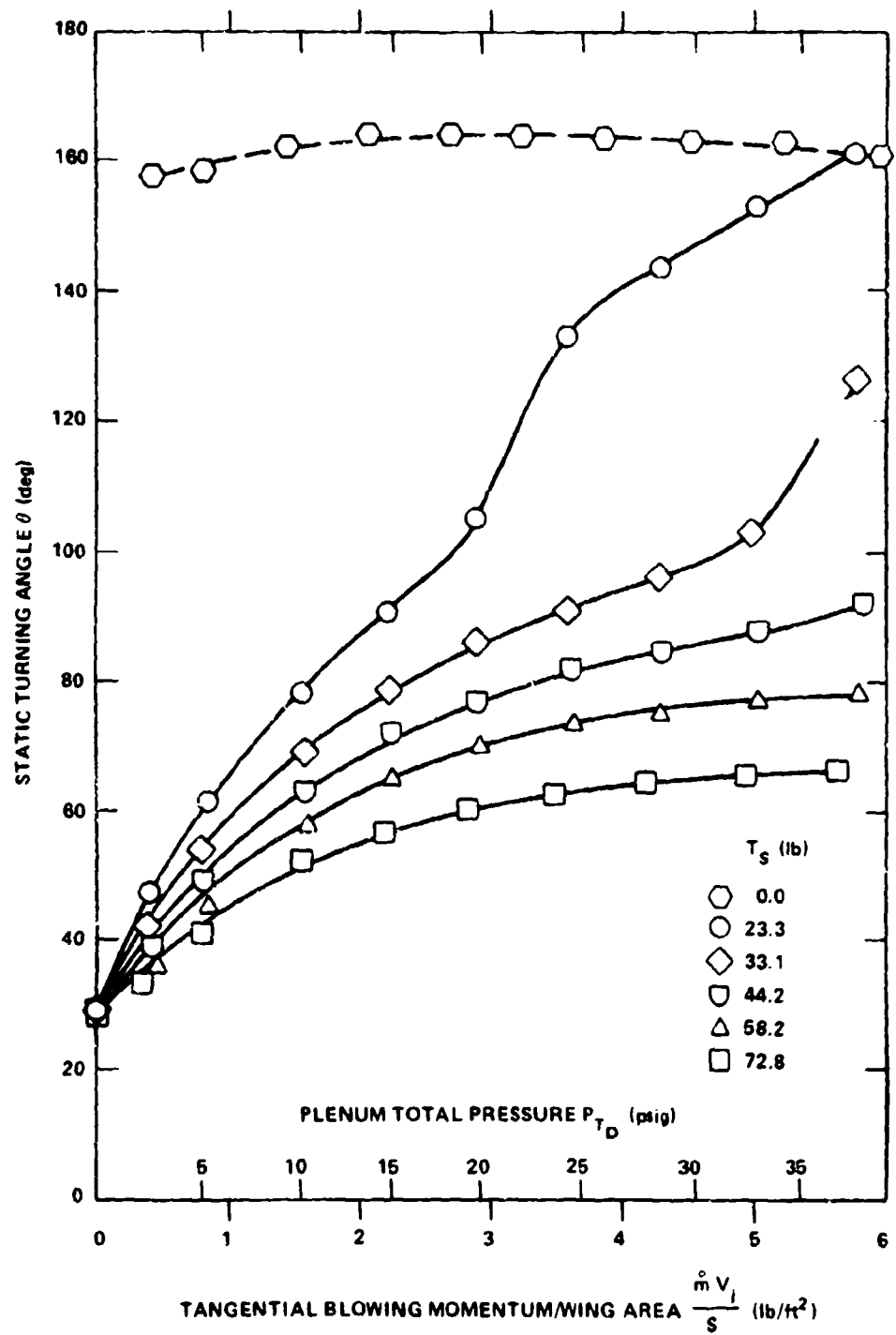


Figure 7d - Cascades

**Figure 8 - Static Turning Employing the Nozzle with an Internal Flap and Partial Span Tangential Blowing ( $\alpha_B = 0$  deg)**



**Figure 8a - Static Thrust Turning**

Figure 8 (Continued)

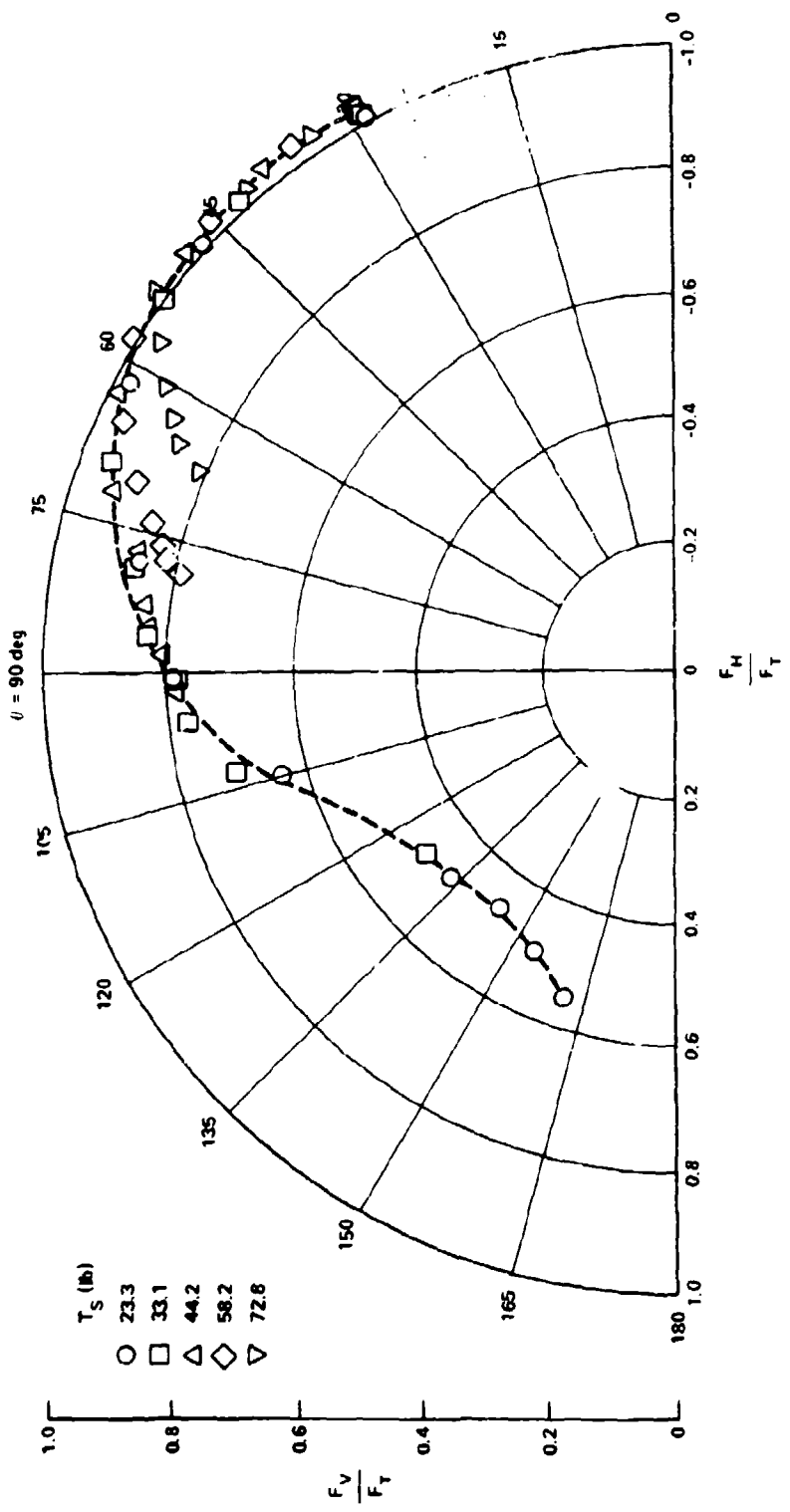


Figure 8b - Static Turning Efficiency

Figure 9 - Effect of Isolating the Propulsive Jet  
 with a Partial Chord Wing fence  
 (Nozzle with an Internal Flap, Partial Span  
 Tangential Blowing and  $\alpha_g = 0$  deg)

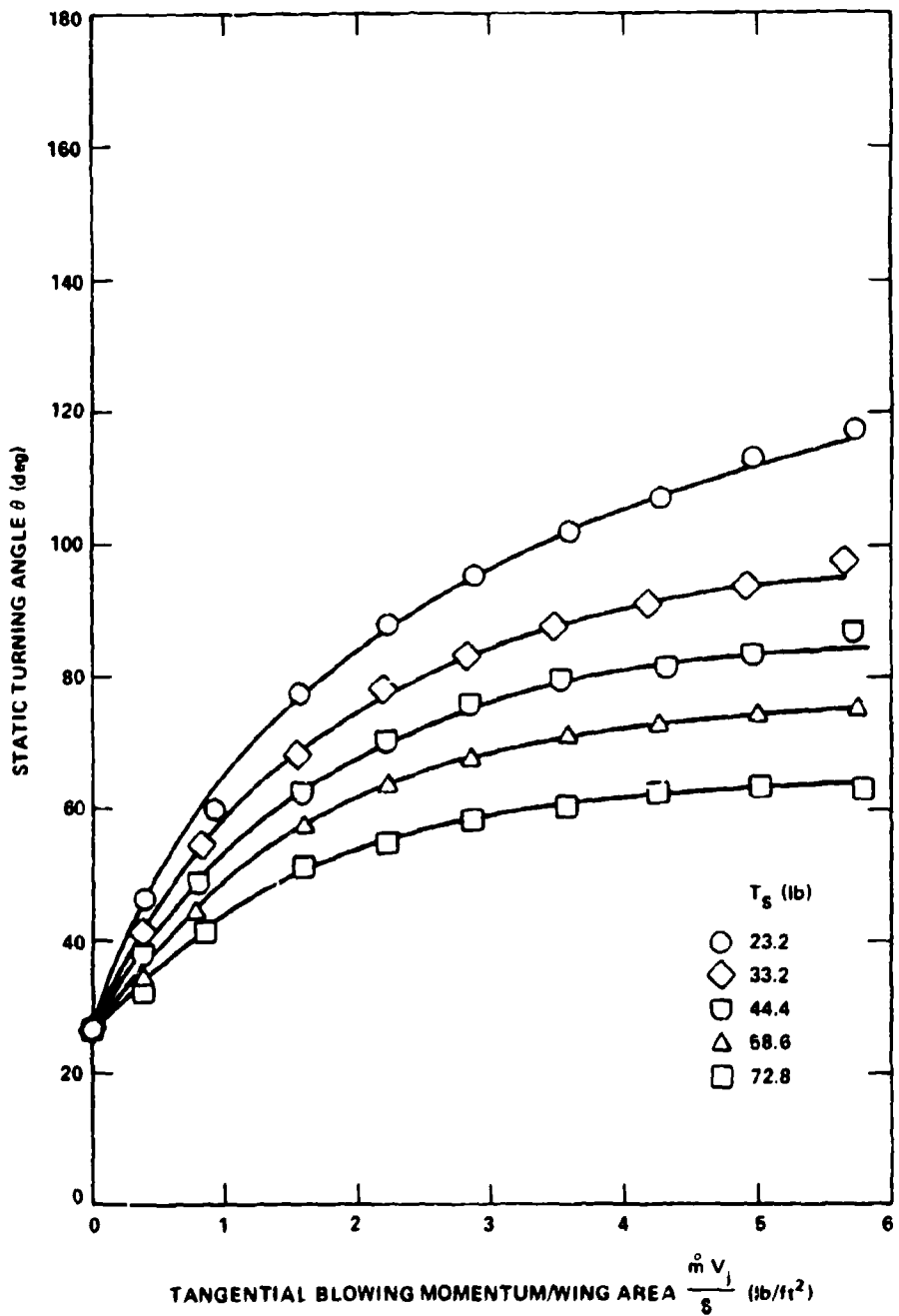


Figure 9a - Static Thrust Turning

Figure 9 (Continued)

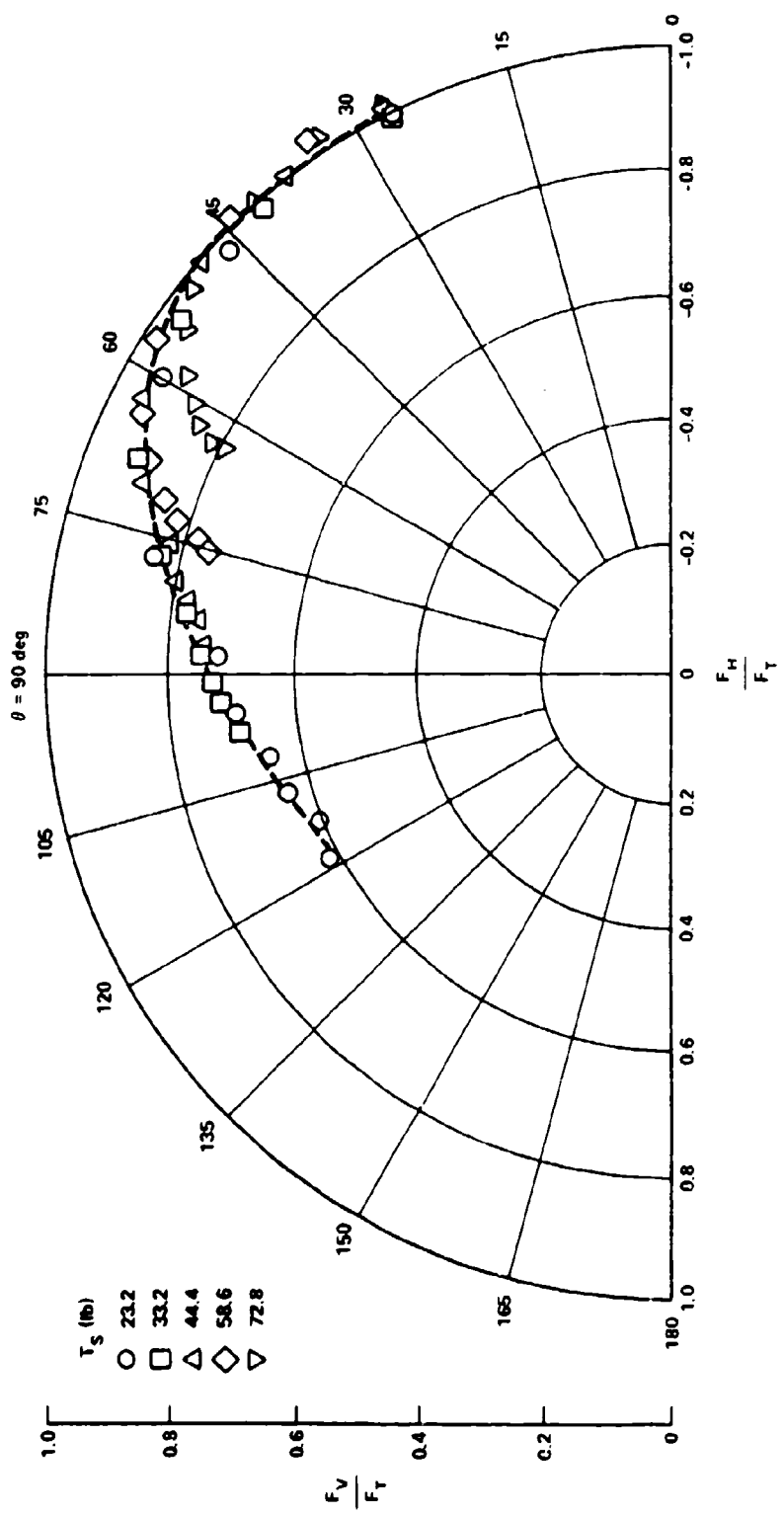


Figure 9b - Static Turning Efficiency

Figure 10 - Static Turning Employing the D-Nozzle  
and Partial Span Tangential Blowing  
( $\alpha_g = 0$  deg)

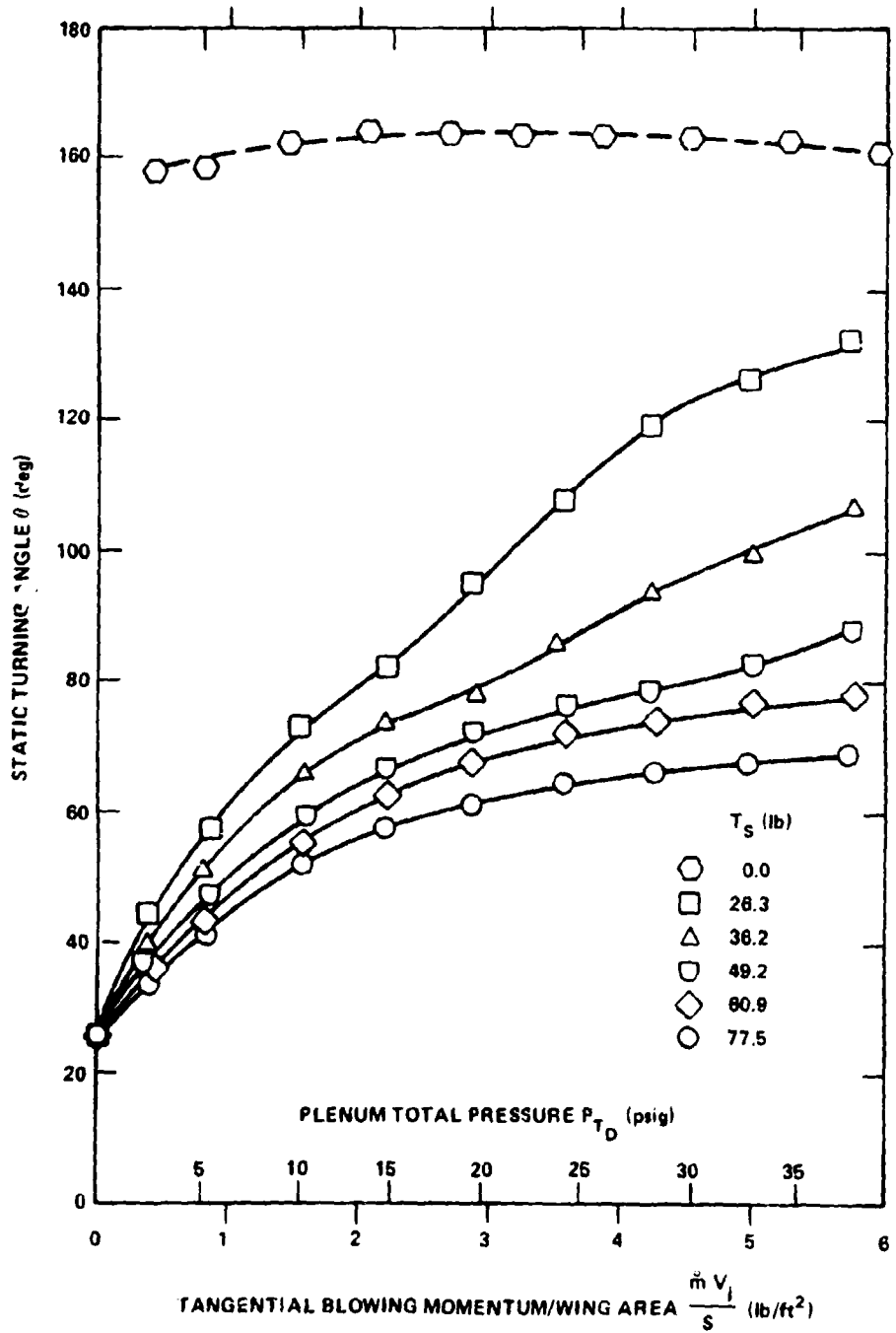


Figure 10a - Static Thrust Turning

Figure 10 (Continued)

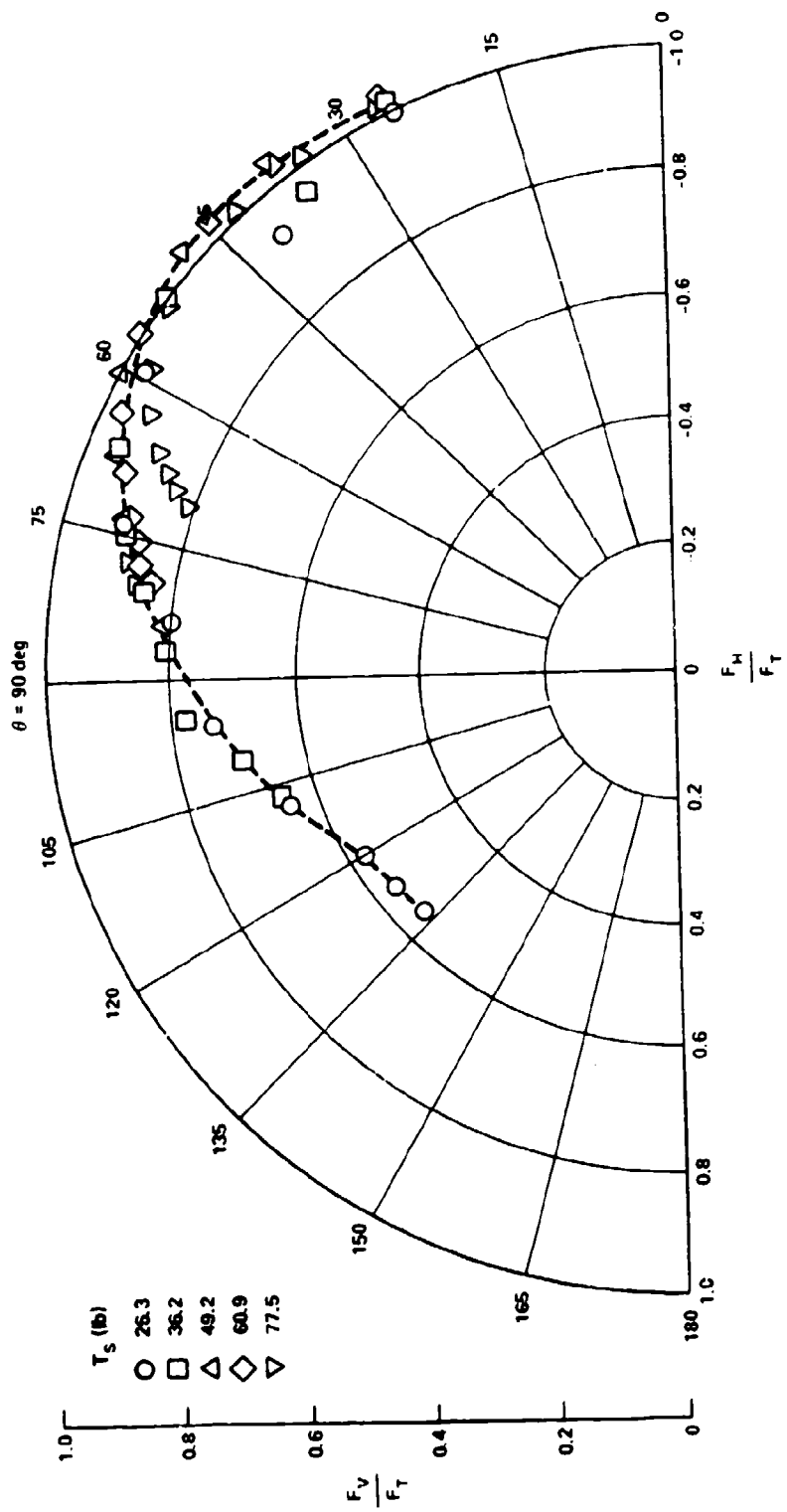


Figure 10b - Static Turning Efficiency

Figure 11 - Static Turning Employing the D-Nozzle  
and Full Span Tangential Blowing  
( $\alpha_g = 0$  deg)

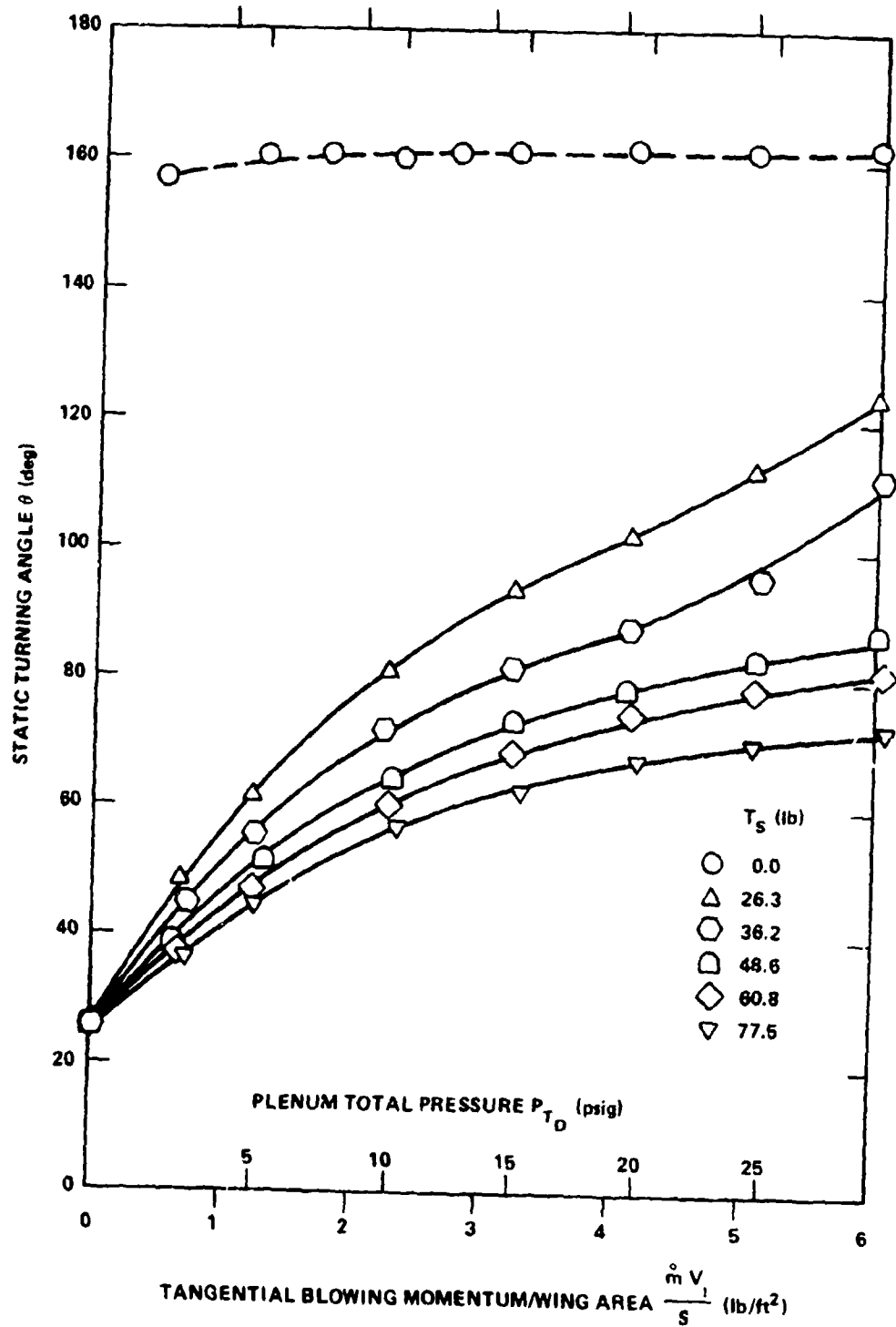


Figure 11a - Static Thrust Turning

Figure 11 (Continued)

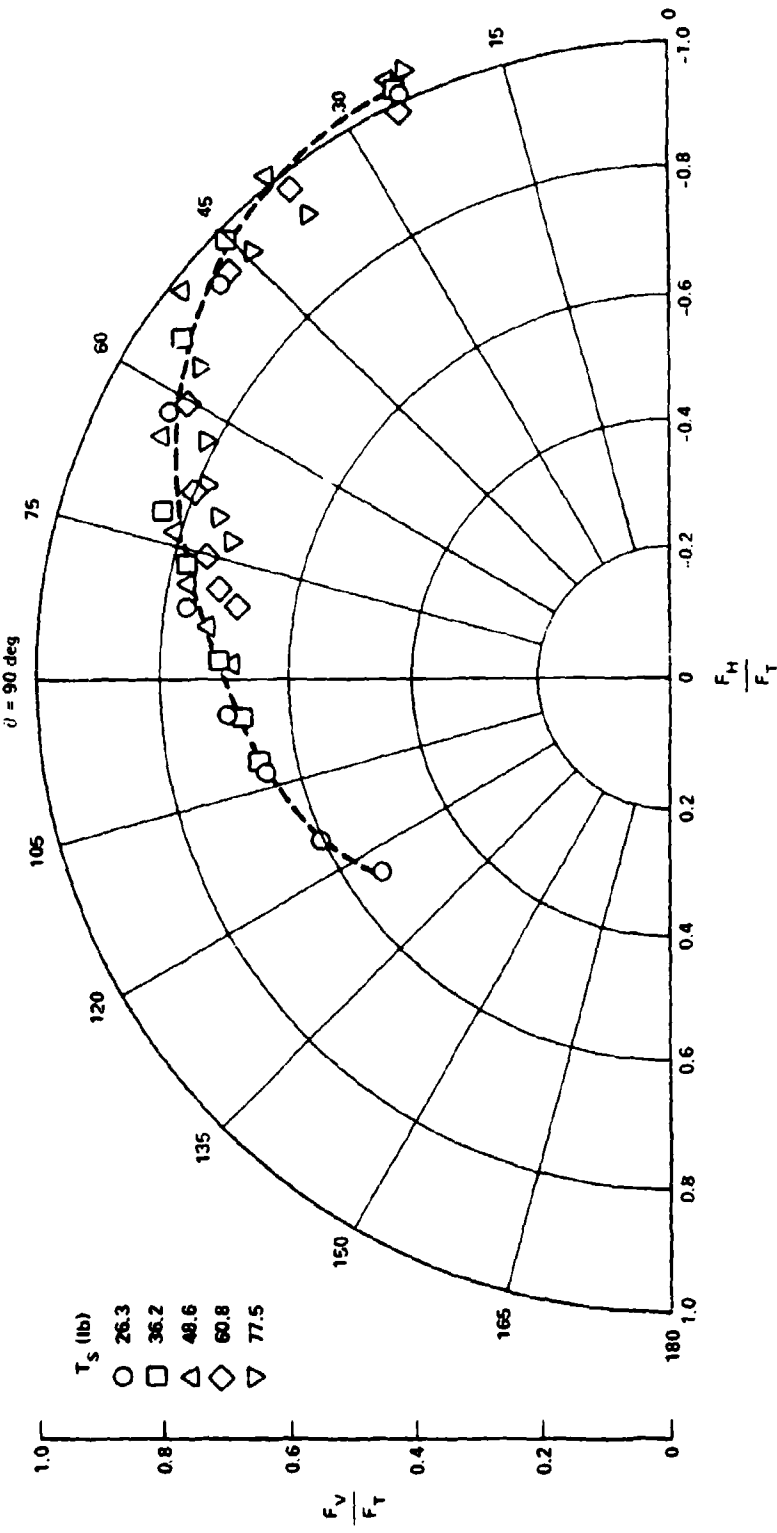


Figure 11b - Static Turning Efficiency

Figure 12 - Flow Visualization of Static Turning Employing  
the v-Nozzle and Full Span Tangential Blowing  
( $T_s = 24.5$  lb and  $\psi_g = 0$  deg)



Figure 12a -  $P_{T_D} = 0$  psig



Figure 12b -  $P_{T_D} = 1.0$  psig

Figure 12. (Cont'd.)



Figure 12c -  $P_{\lambda_{12}} = 2 \times 10^{-6}$



Figure 12d -  $P_{\lambda_{12}} = 10^{-6}$

RECEIVING PATH BLANK-NOT FLUDED

Figure 13 - Effect of Variation in Partial Span Tangential Blowing  
on the Longitudinal Aerodynamics Associated with Thrust Turning,  
(D-nozzle and  $\alpha_g = 0$  deg)

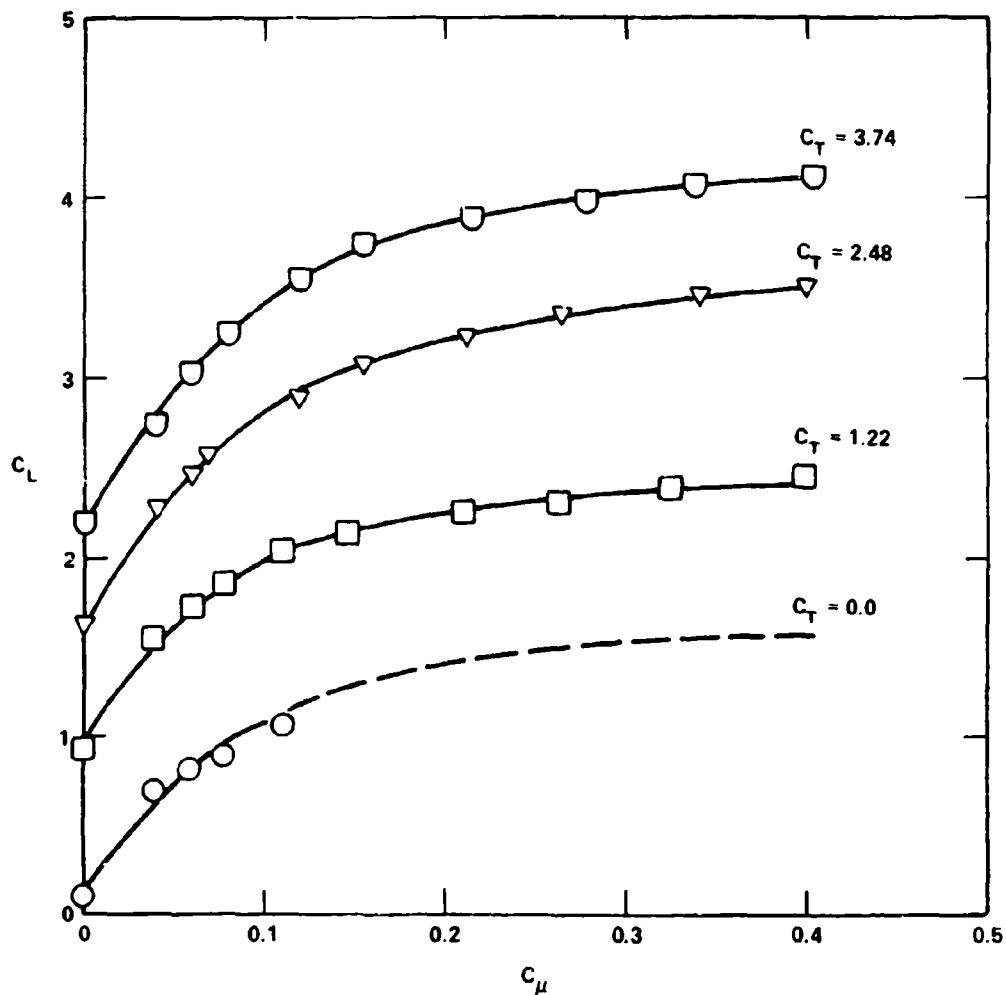


Figure 13a - Lift Coefficient

Figure 13 (Continued)

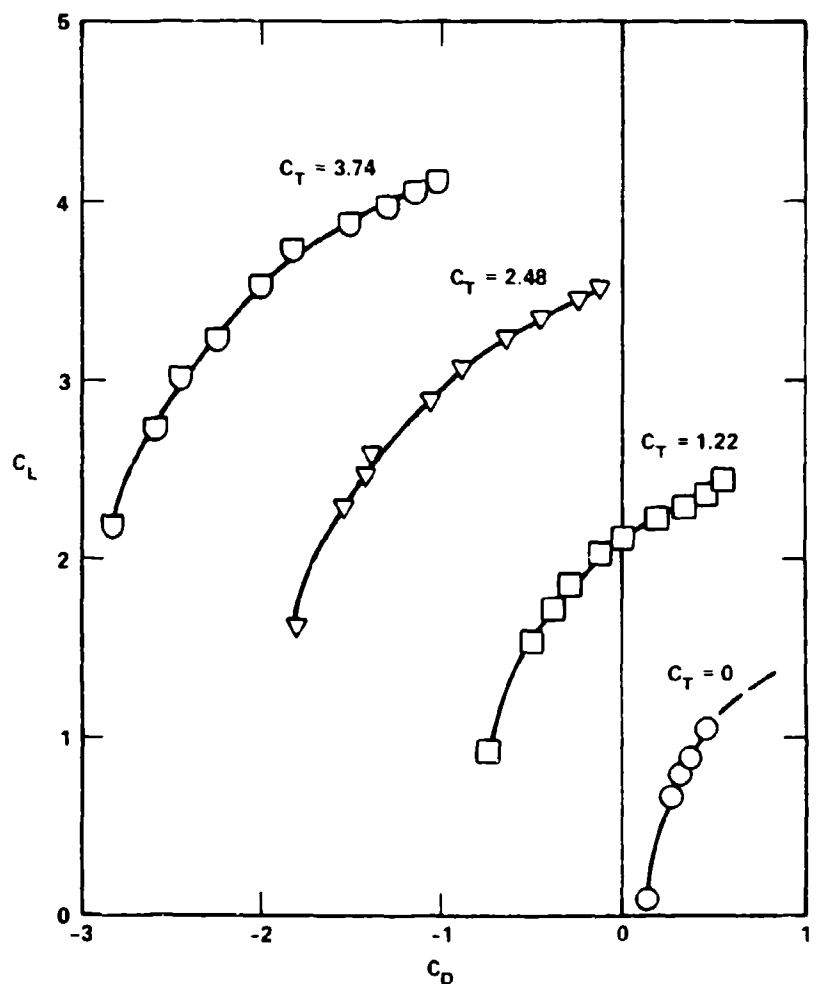


Figure 13b - Drag Polar

Figure 13 (Continued)

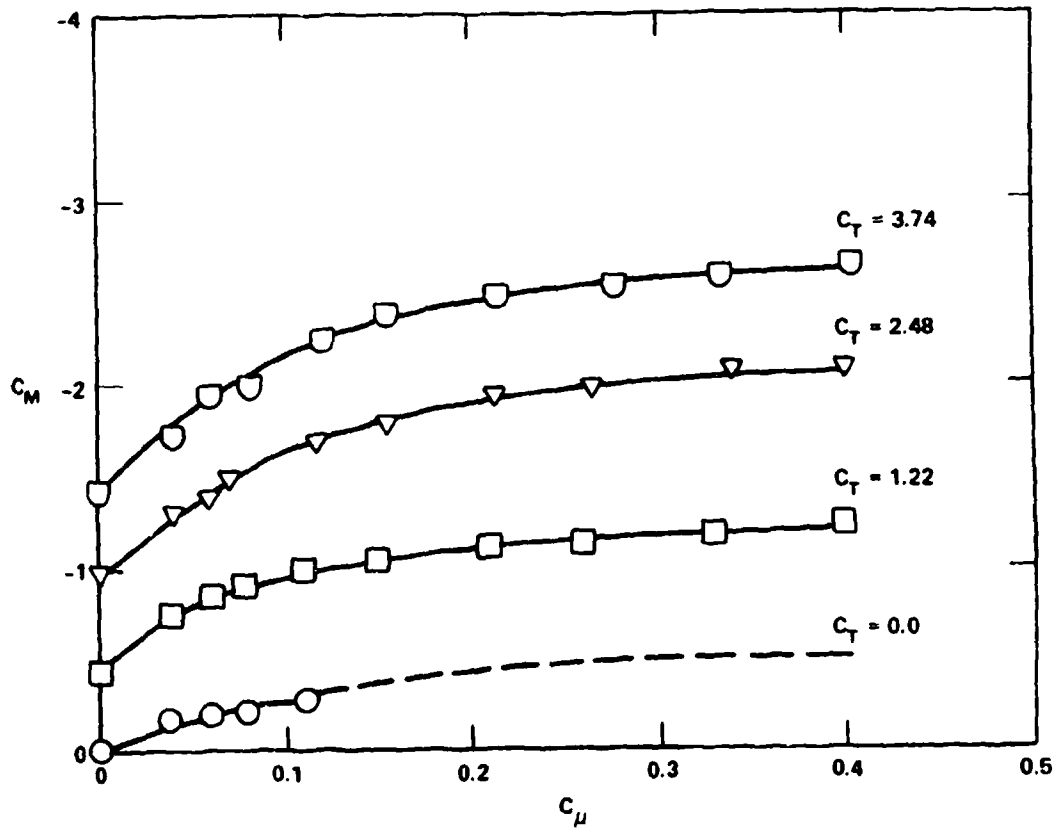


Figure 13c - Pitching Moment Coefficient

Figure 14 - Effect of Variation in Angle of Attack  
on the Longitudinal Aerodynamics Associated  
with Thrust Turning  
(D-nozzle and partial span tangential blowing)

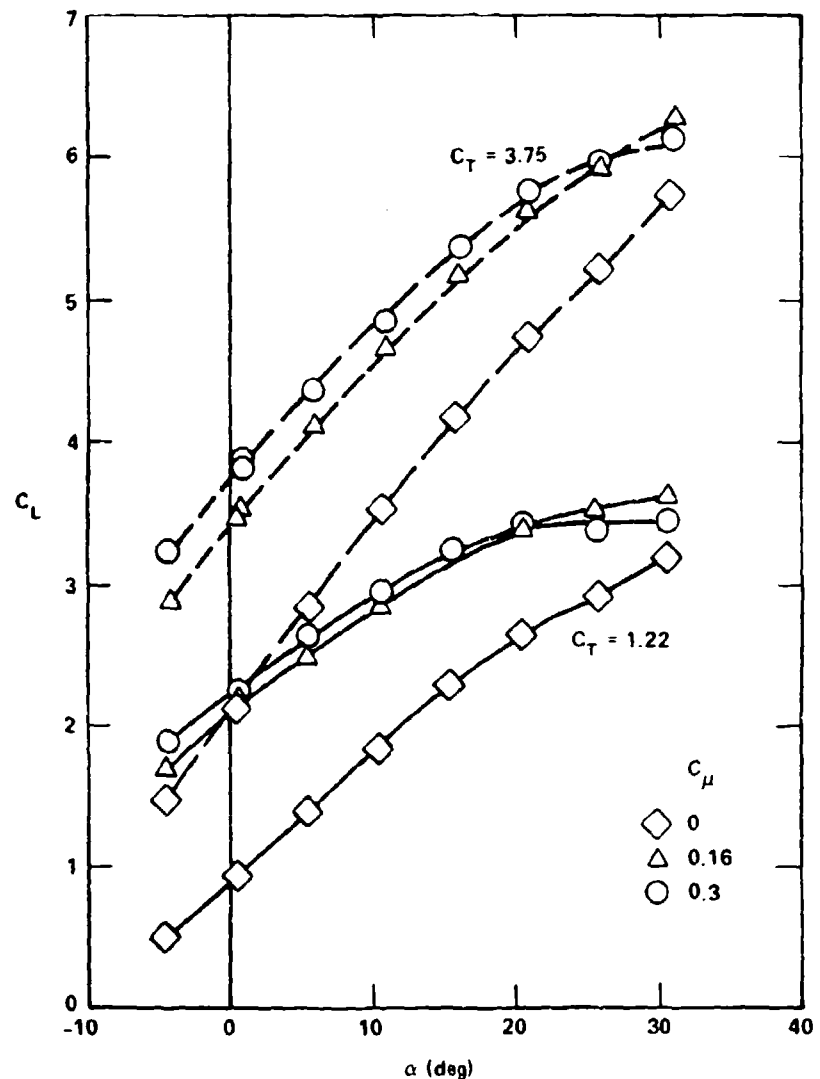


Figure 14a - Lift Coefficient

Figure 14 (Continued)

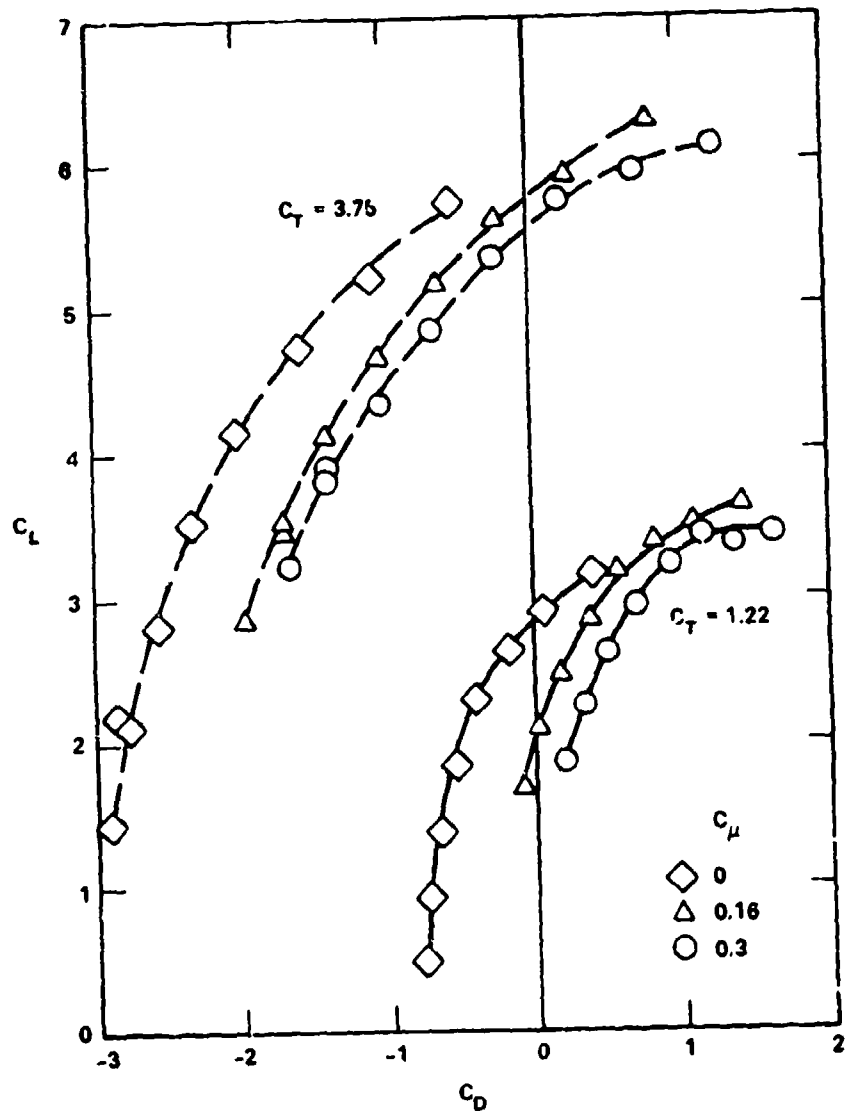


Figure 14b - Drag Polar

Figure 14 (Continued)

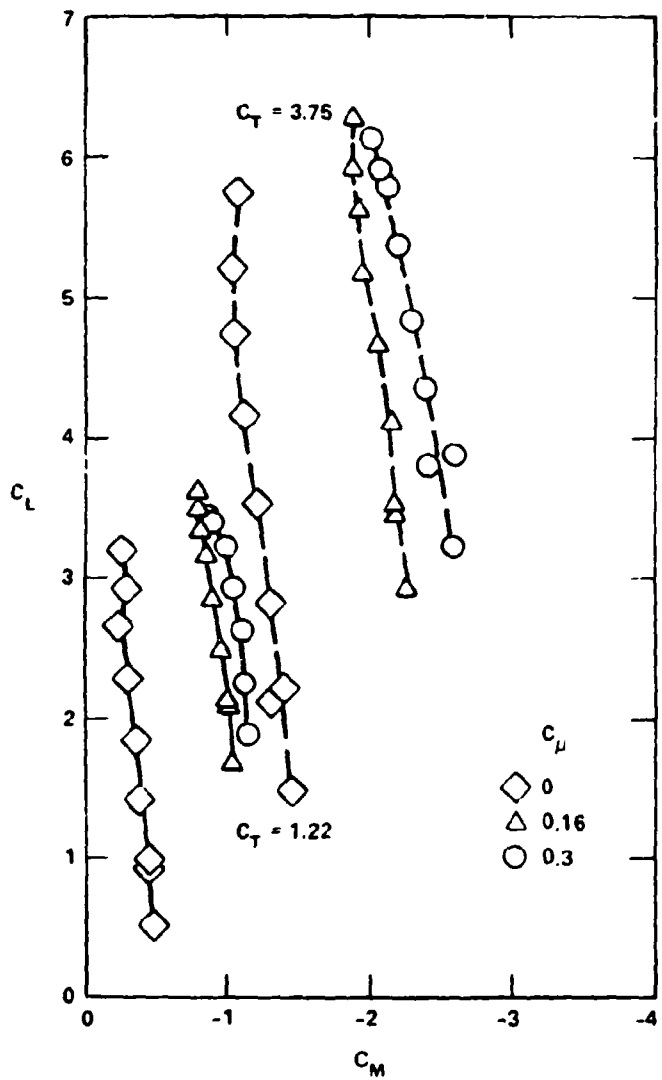


Figure 14c - Pitching Moment Coefficient

Figure 15 - Effect of Variation in Full Span Tangential Blowing  
on the Longitudinal Aerodynamics  
(D-nozzle and  $\alpha_g = 0$  deg)

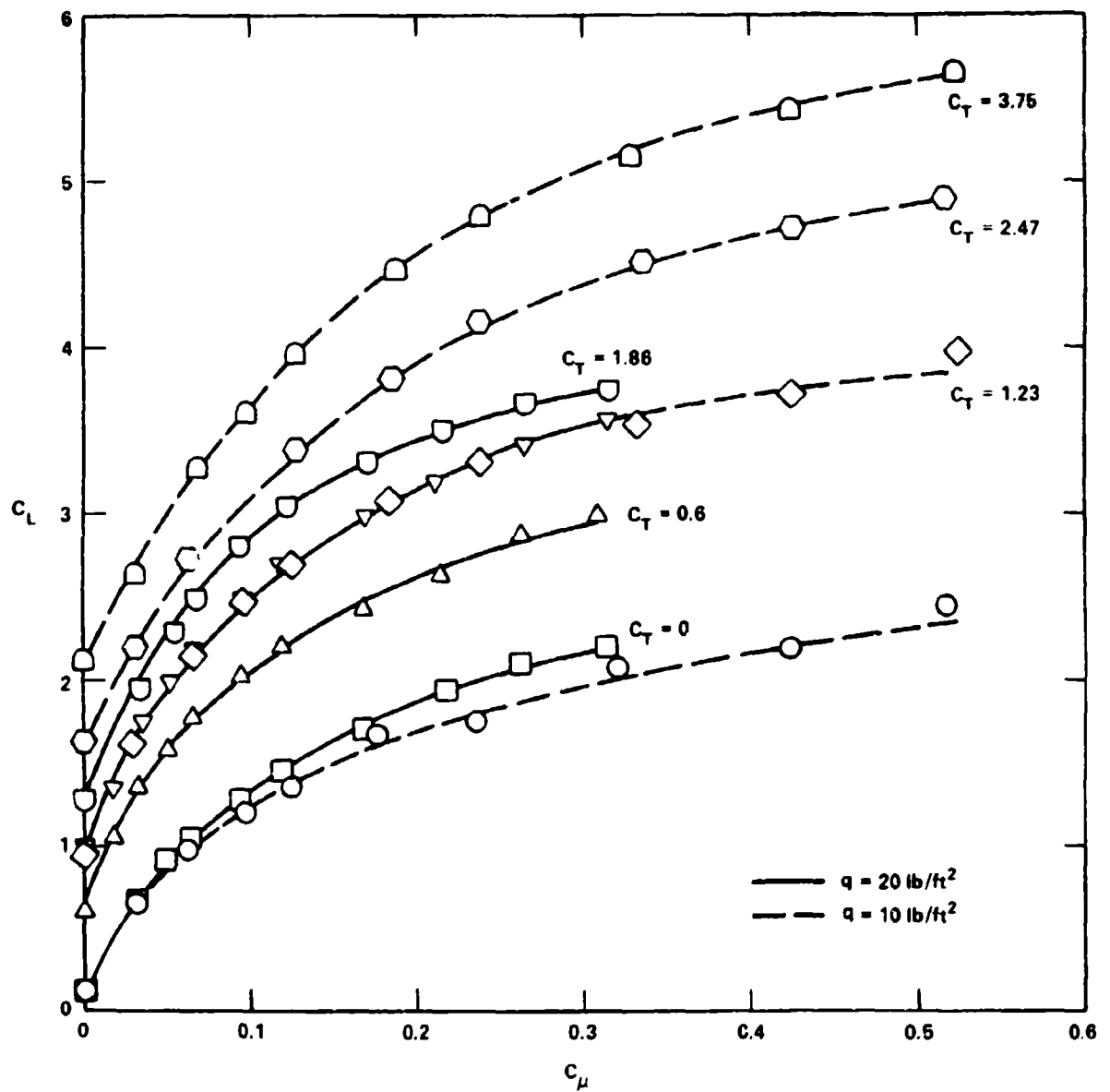


Figure 15a - Lift Coefficient

Figure 15 (Continued)

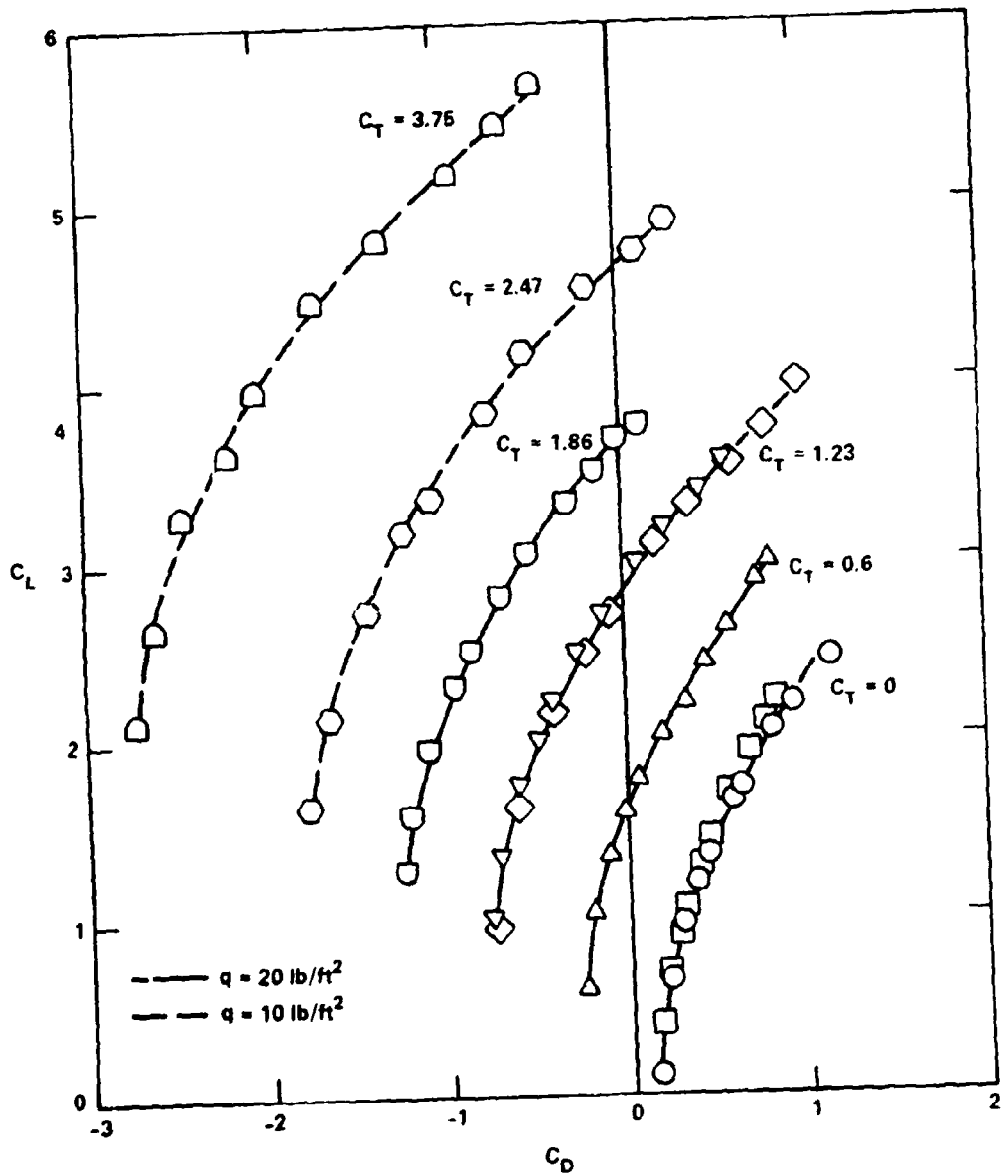


Figure 15b - Drag Polar

Figure 15 (Continued)

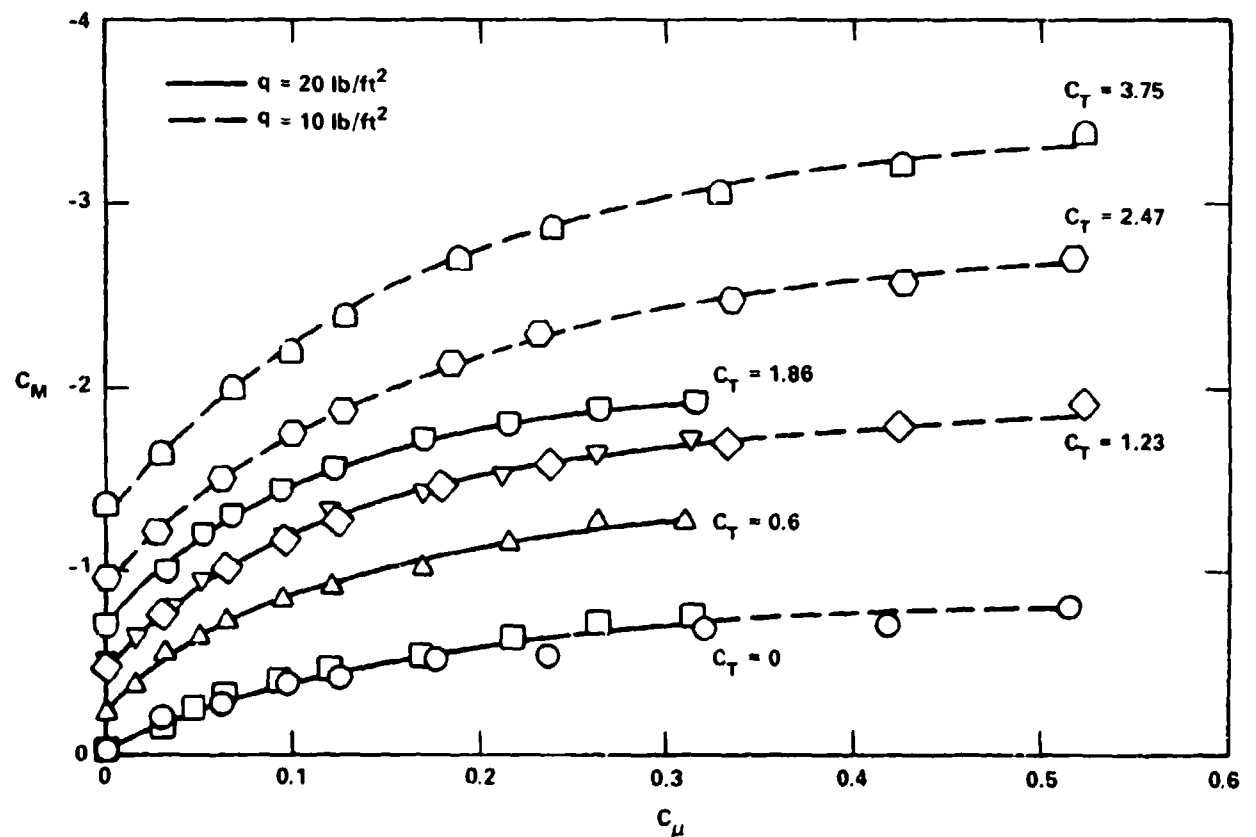


Figure 15c - Pitching Moment Coefficient

Figure 16 - Effect of Variation in Angle of Attack  
on the Longitudinal Aerodynamics  
(D-nozzle and full span tangential blowing)

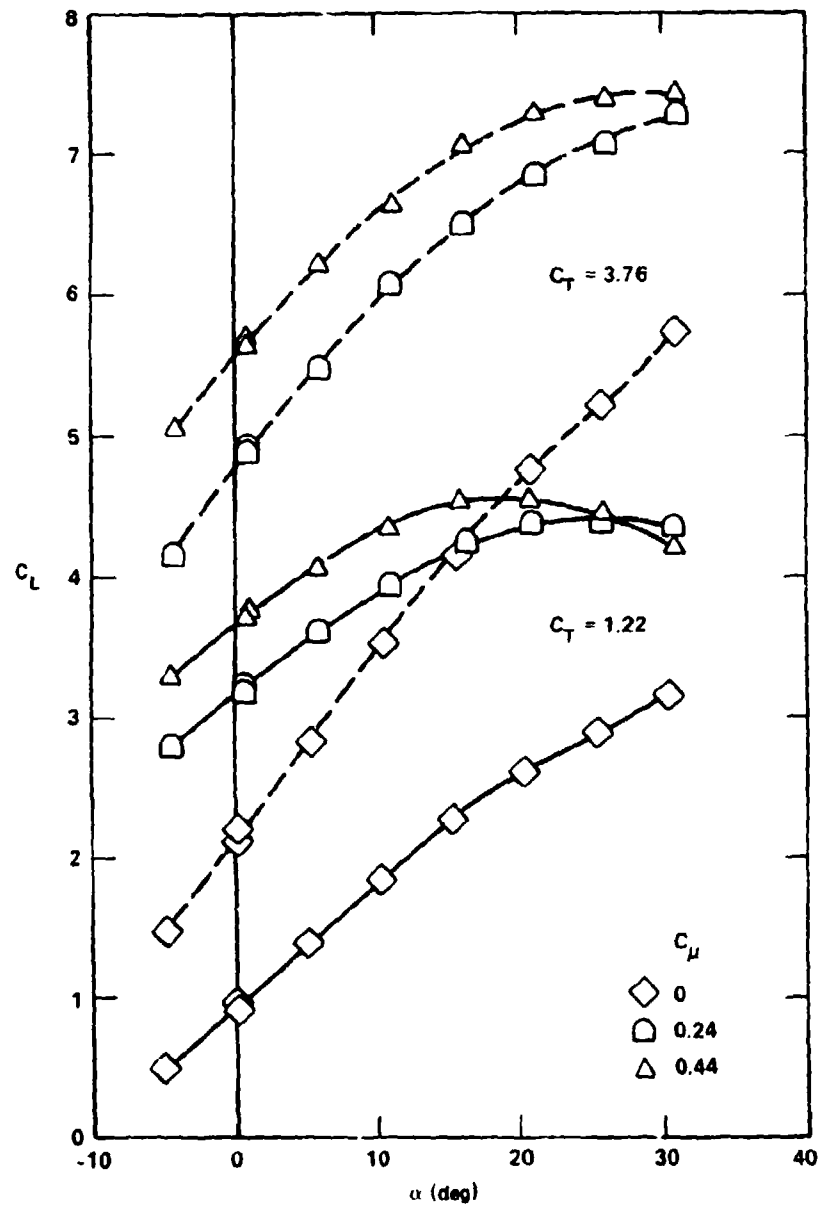


Figure 16a - Lift Coefficient

Figure 16 (Continued)

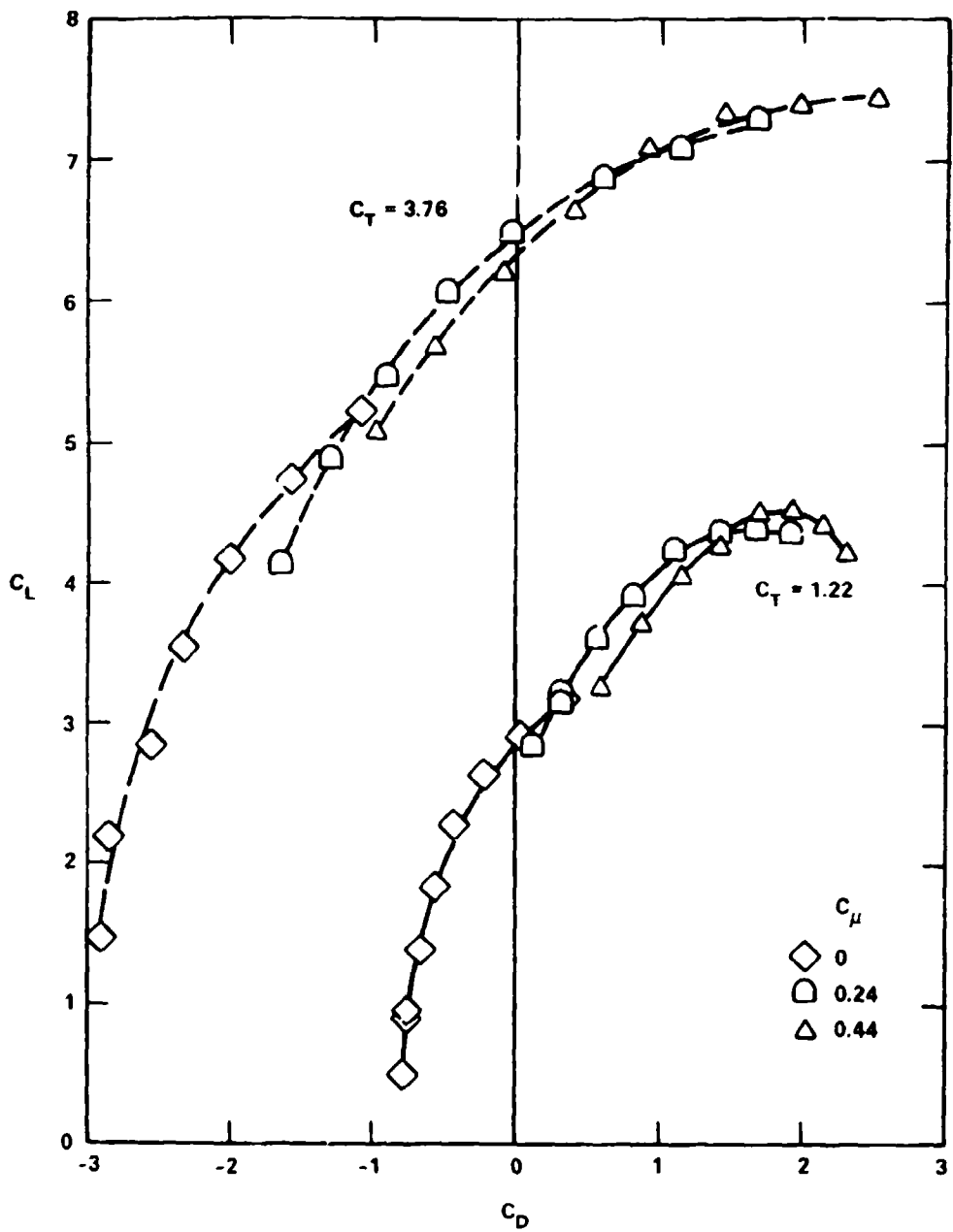


Figure 16b - Drag Polar

Figure 16 (Continued)

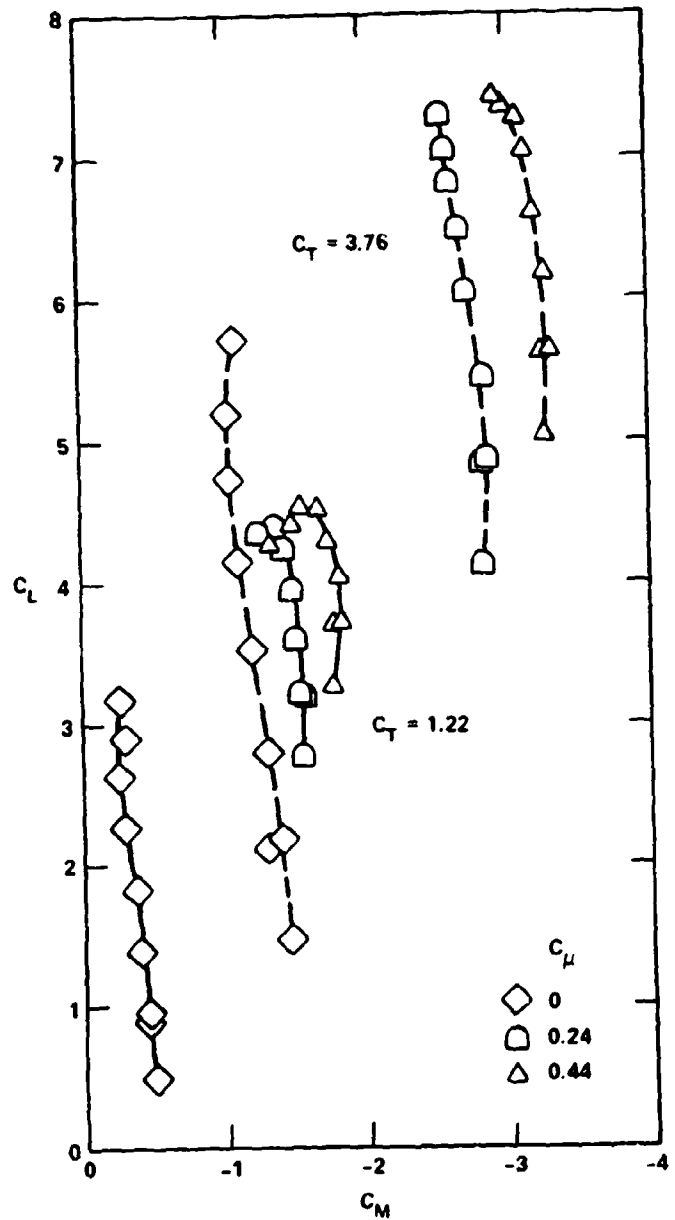


Figure 16c ~ Pitching Moment Coefficient

Figure 17 - Configuration Buildup (D-Nozzle)

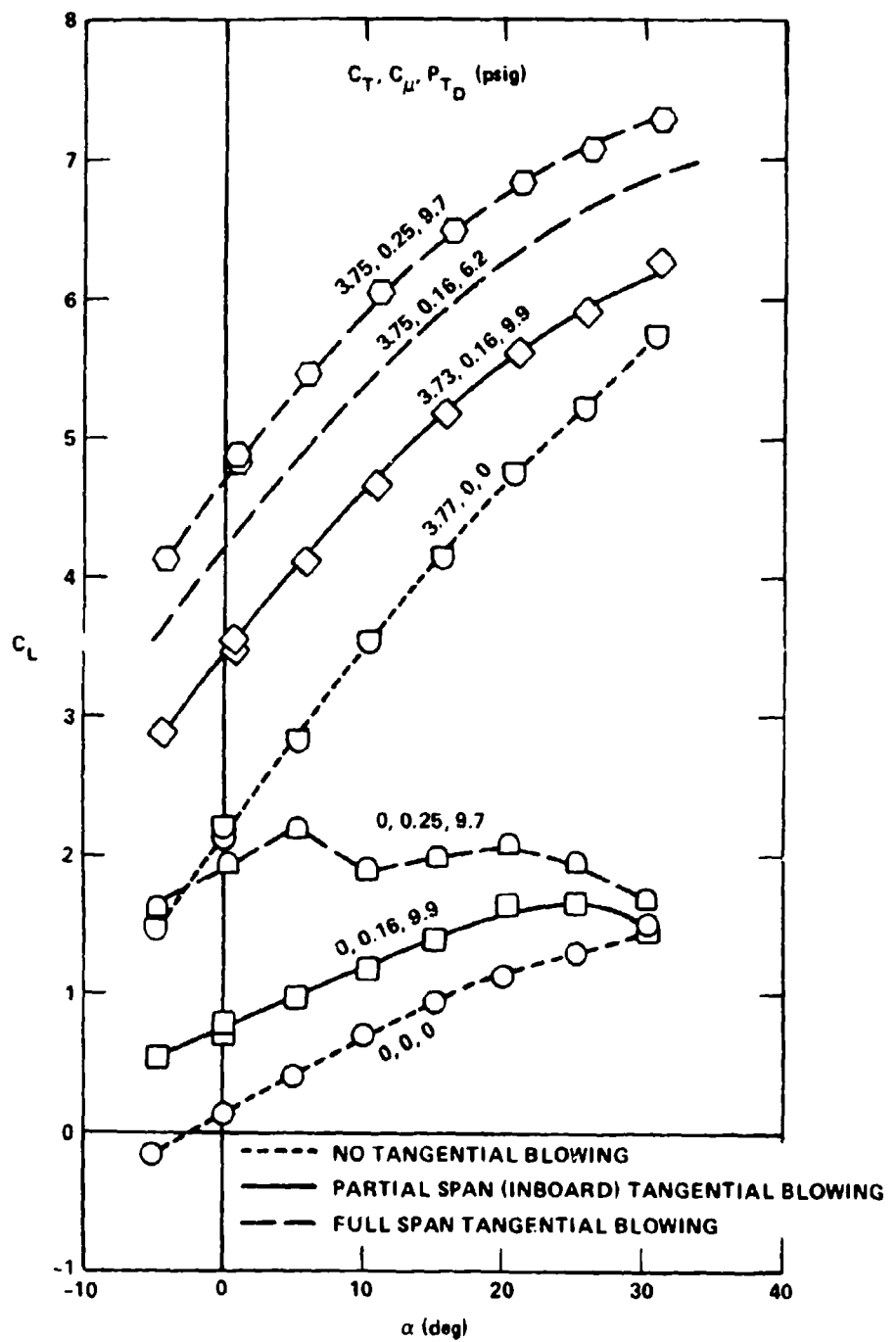


Figure 17a - Lift Coefficient

Figure 17 (Continued)

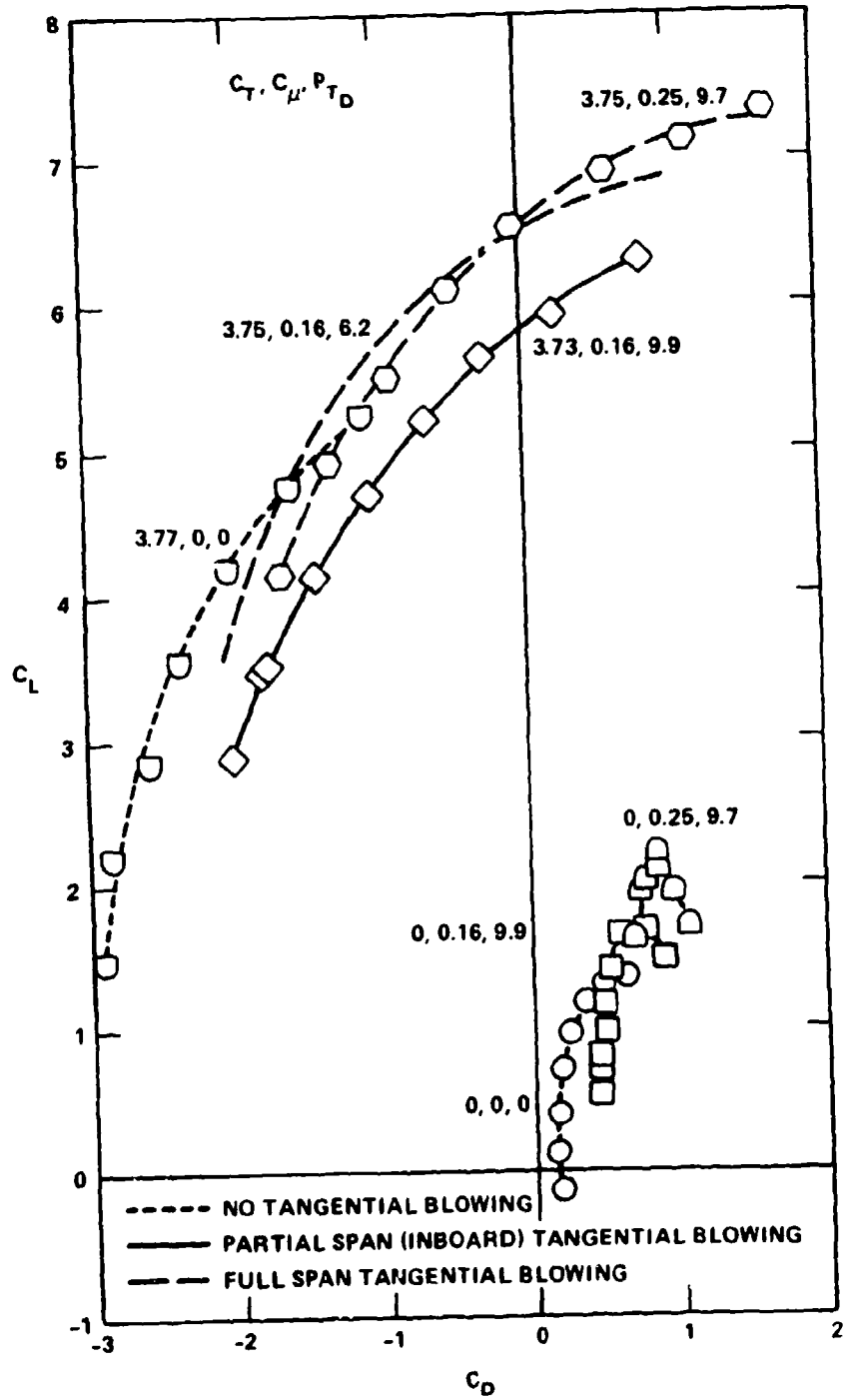


Figure 17b - Drag Polar

Figure 17 (Continued)

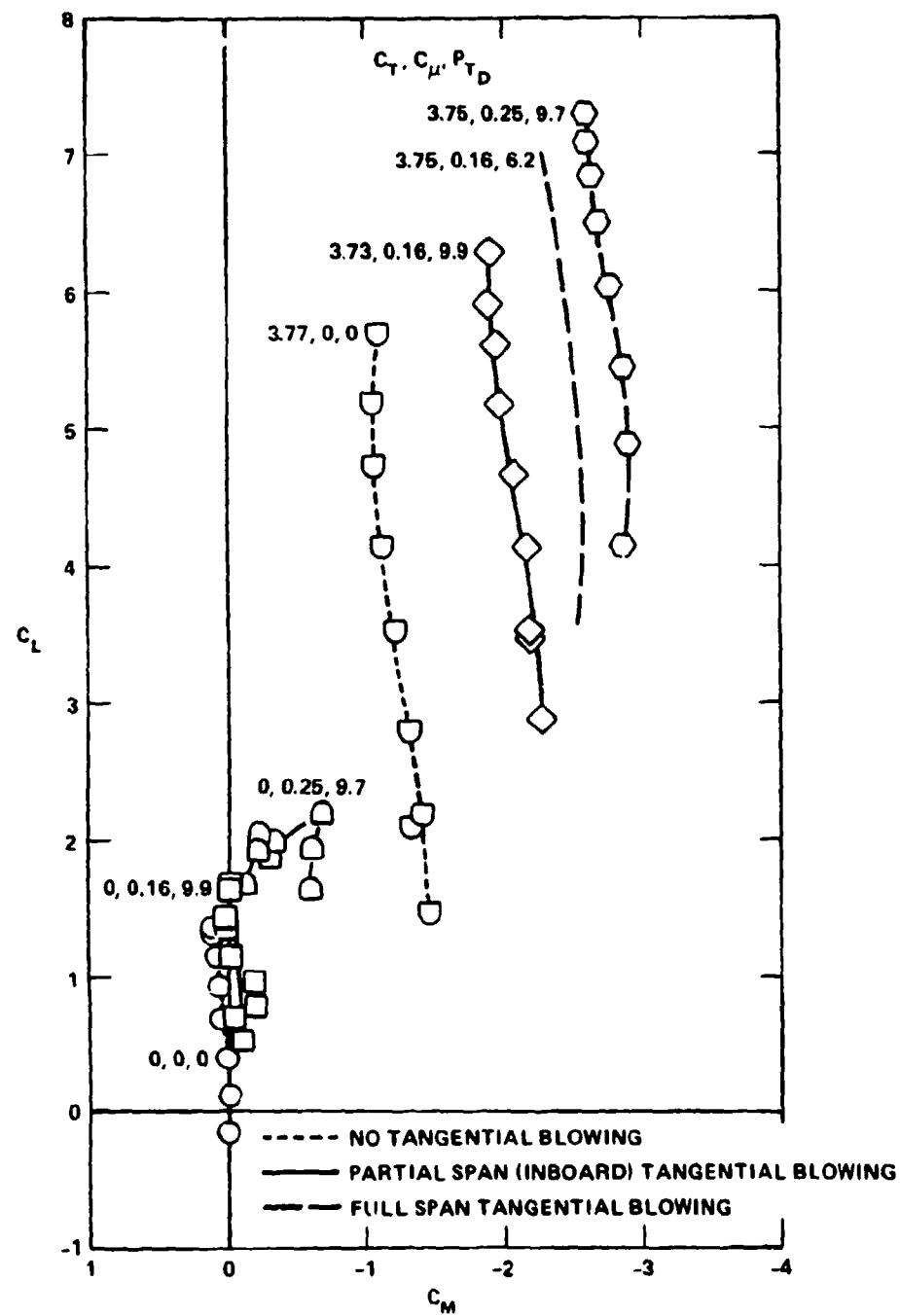


Figure 17c - Pitching Moment Coefficient

Figure 18 - Flow visualization of Inflight turning Employing  
the D-Nozzle and Full Span Tangential Blowing  
( $T_S = 24.5$  lb,  $q = 10$  lb/ft $^2$  and  $\alpha_g = 0$  deg)



Figure 18a -  $P_{T_D} = 0$  psig

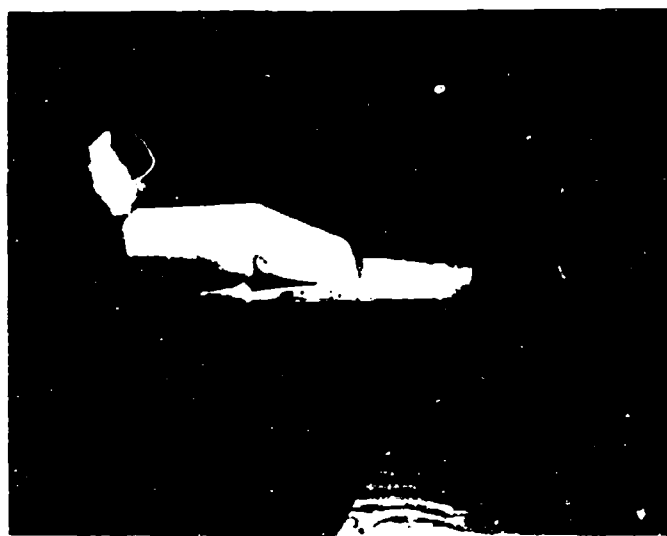


Figure 18b -  $P_{T_D} = 10$  psig

Figure 18 (continued)

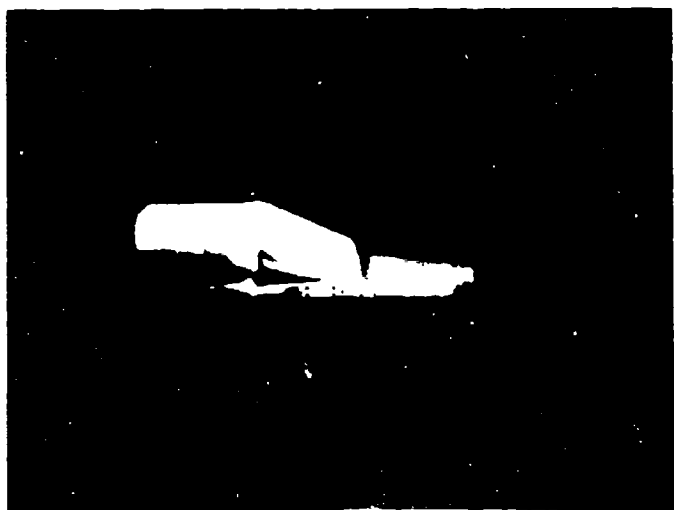


Figure 18c -  $P_{\text{exp}} = 15 \text{ psi}$

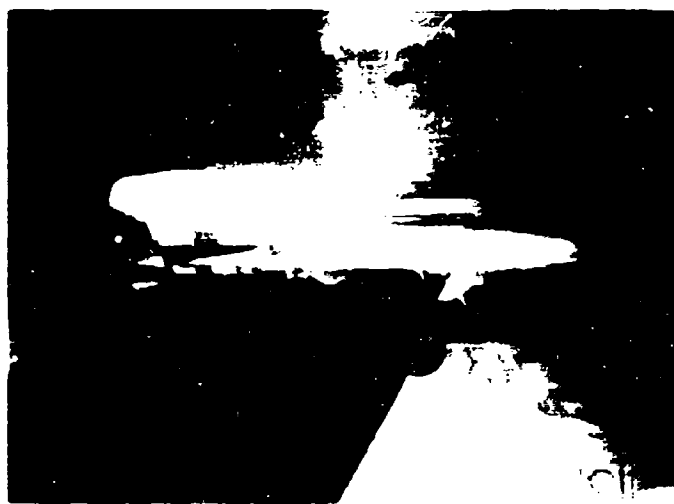


Figure 18d -  $P_{\text{exp}} = 30 \text{ psi}$

Figure 19 - Partial Chord Tip Fence Influence on Lift and Drag  
(D-Nozzle and Full Span Tangential Blowing)

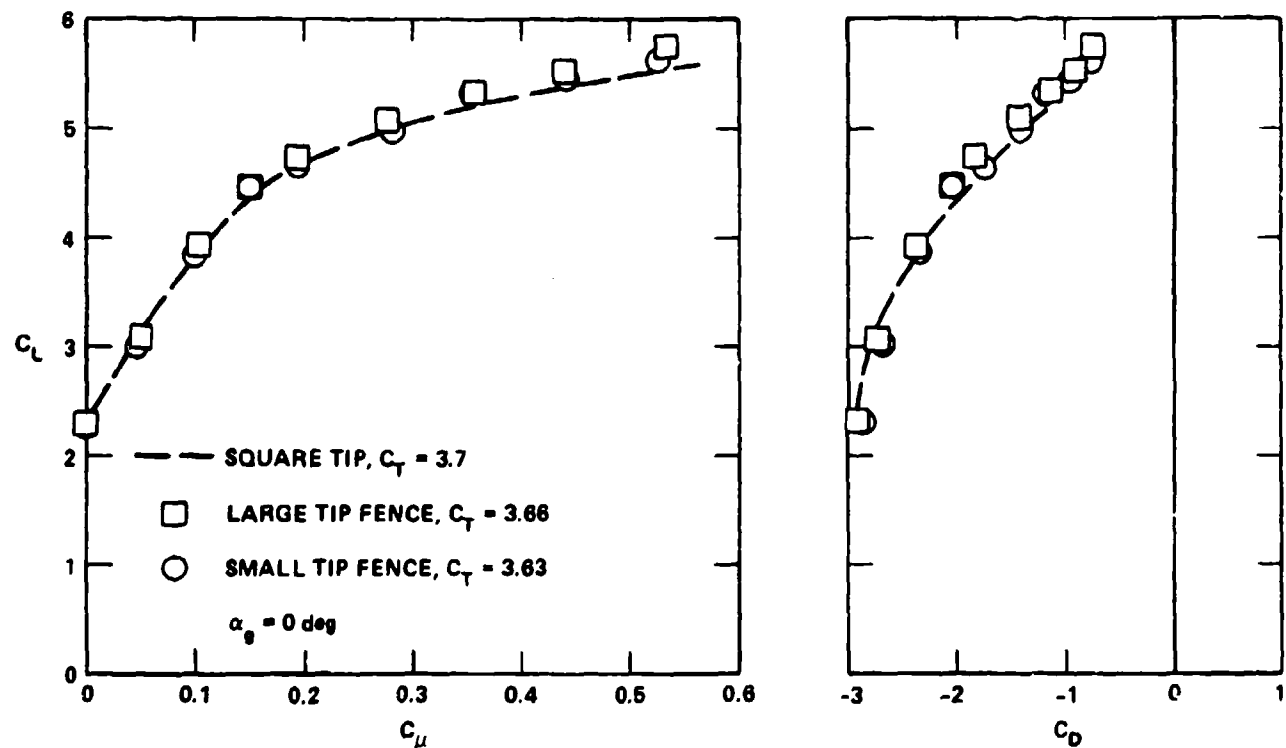


Figure 19a - Effect of Blowing Variation

Figure 19 (Continued)

- — SQUARE TIP,  $C_T = 3.68$  AND  $C_\mu = 0.71$
- LARGE TIP FENCE,  $C_T = 3.68$  AND  $C_\mu = 0.71$
- SMALL TIP FENCE,  $C_T = 3.63$  AND  $C_\mu = 0.70$

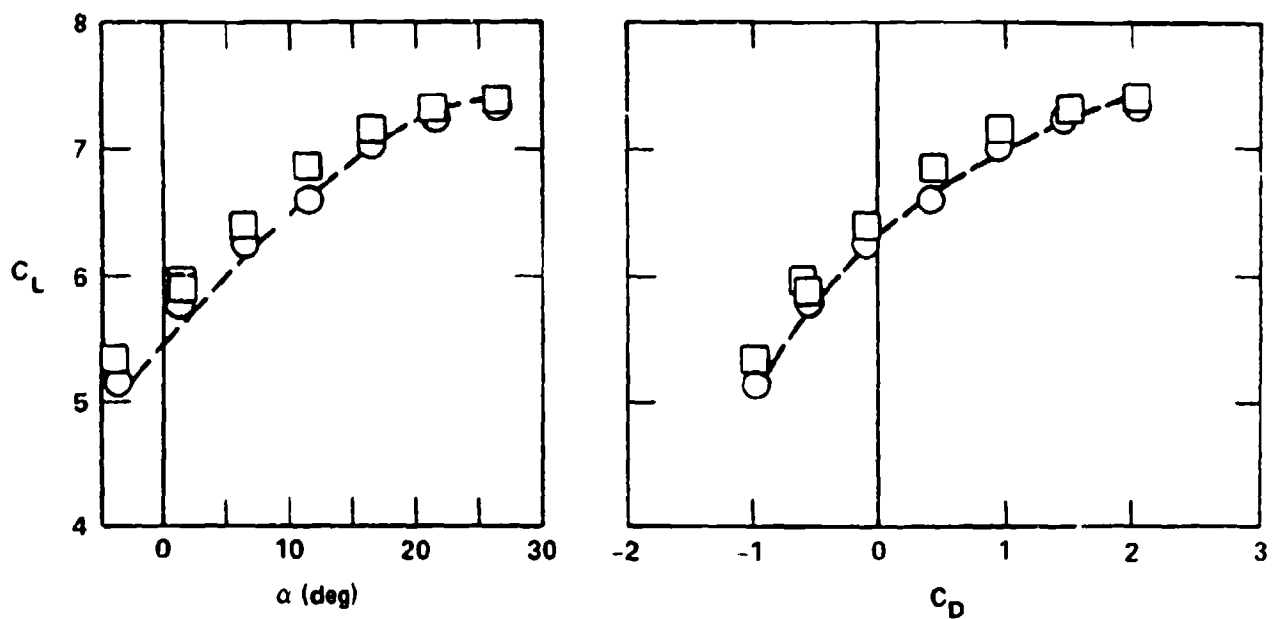


Figure 19b - Effect of Angle of Attack Variation

Figure 20 - Tip Sails and Cascades Influence on Lift and Drag  
 (D-Nozzle and Full Span Tangential Blowing)

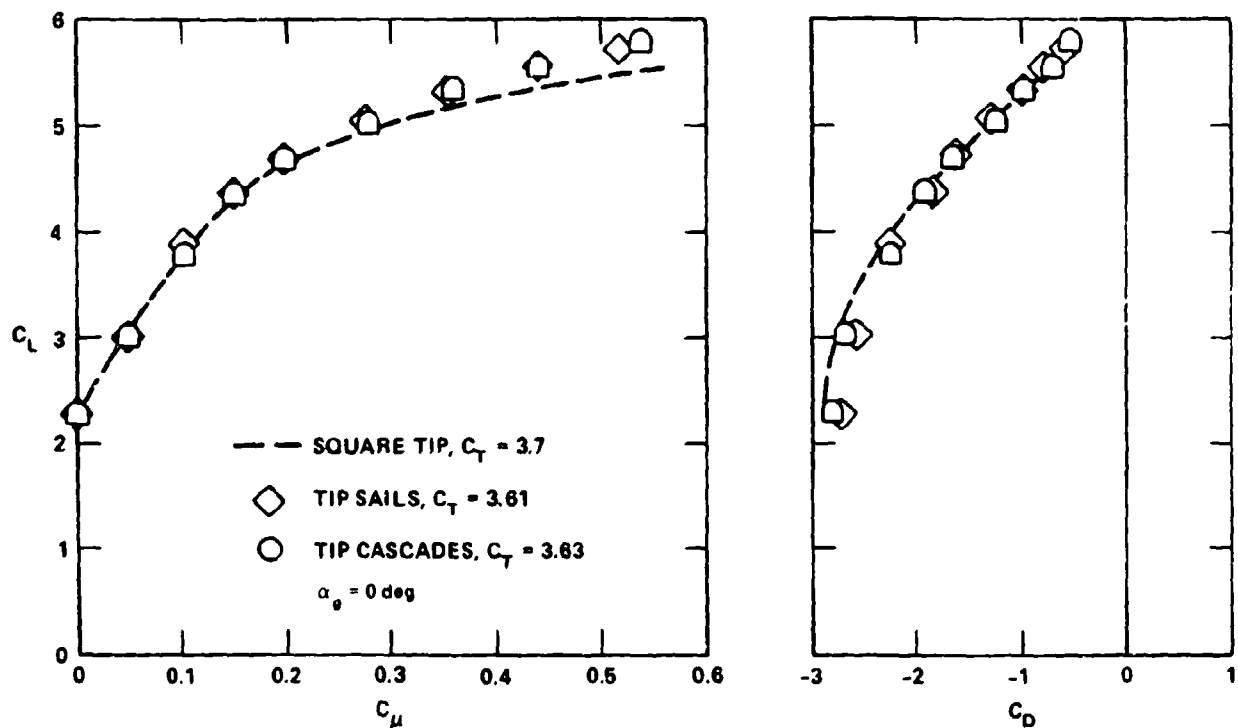


Figure 20a - Effect of Blowing Variation

Figure 20 (Continued)

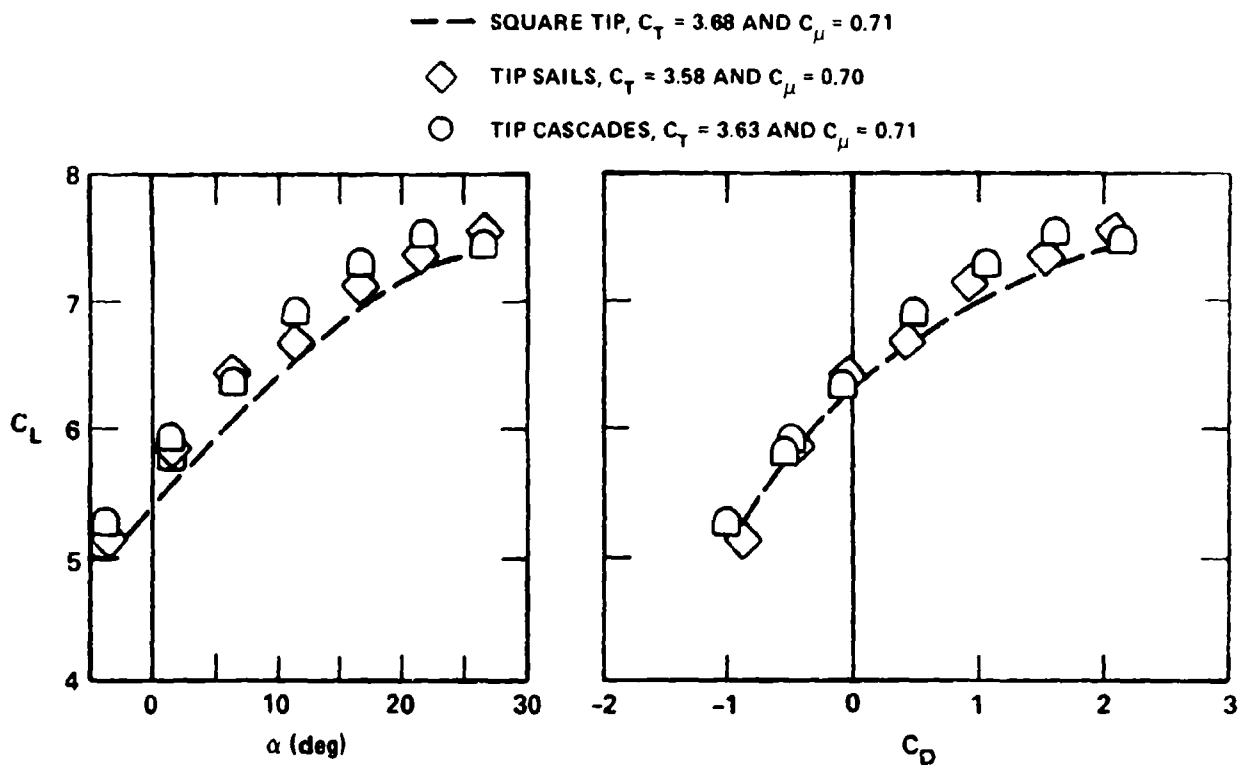


Figure 20b - Effect of Angle of Attack Variation

Figure 21 - Winglet Influence on Lift and Drag  
(D-Nozzle and Full Span Tangential Blowing)

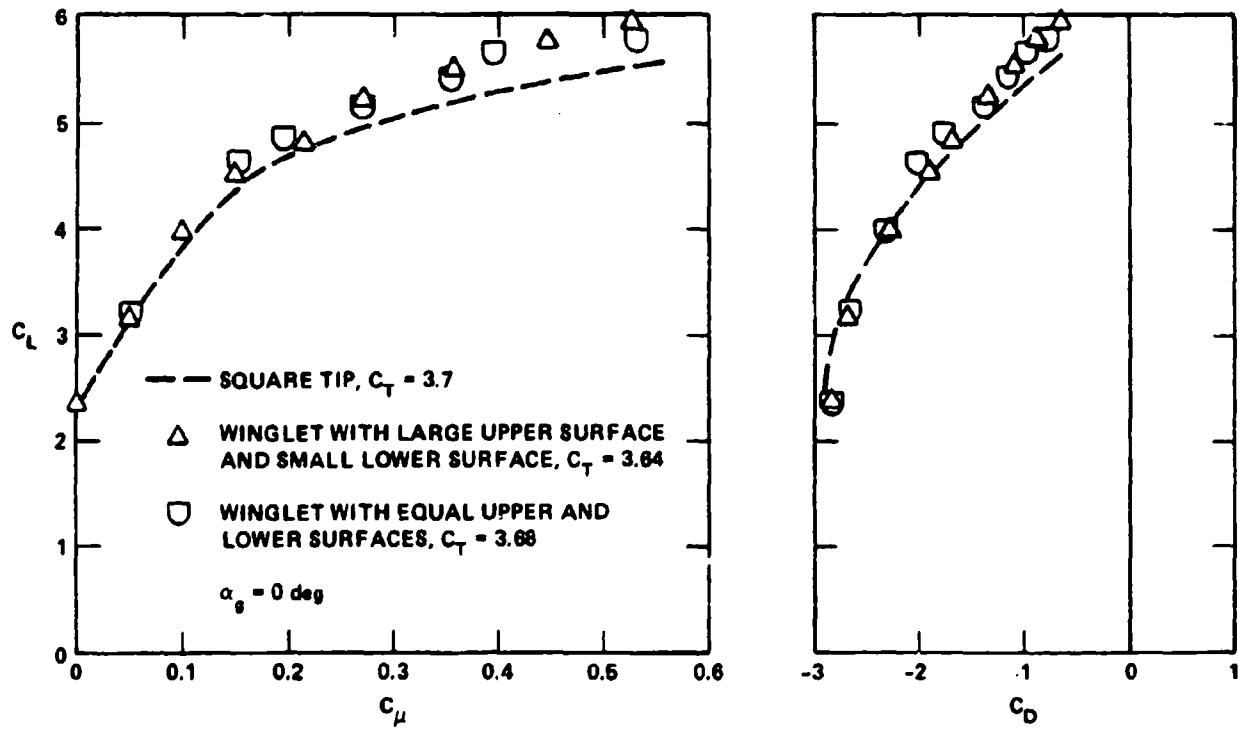


Figure 21a - Effect of Blowing Variation

Figure 21 (Continued)

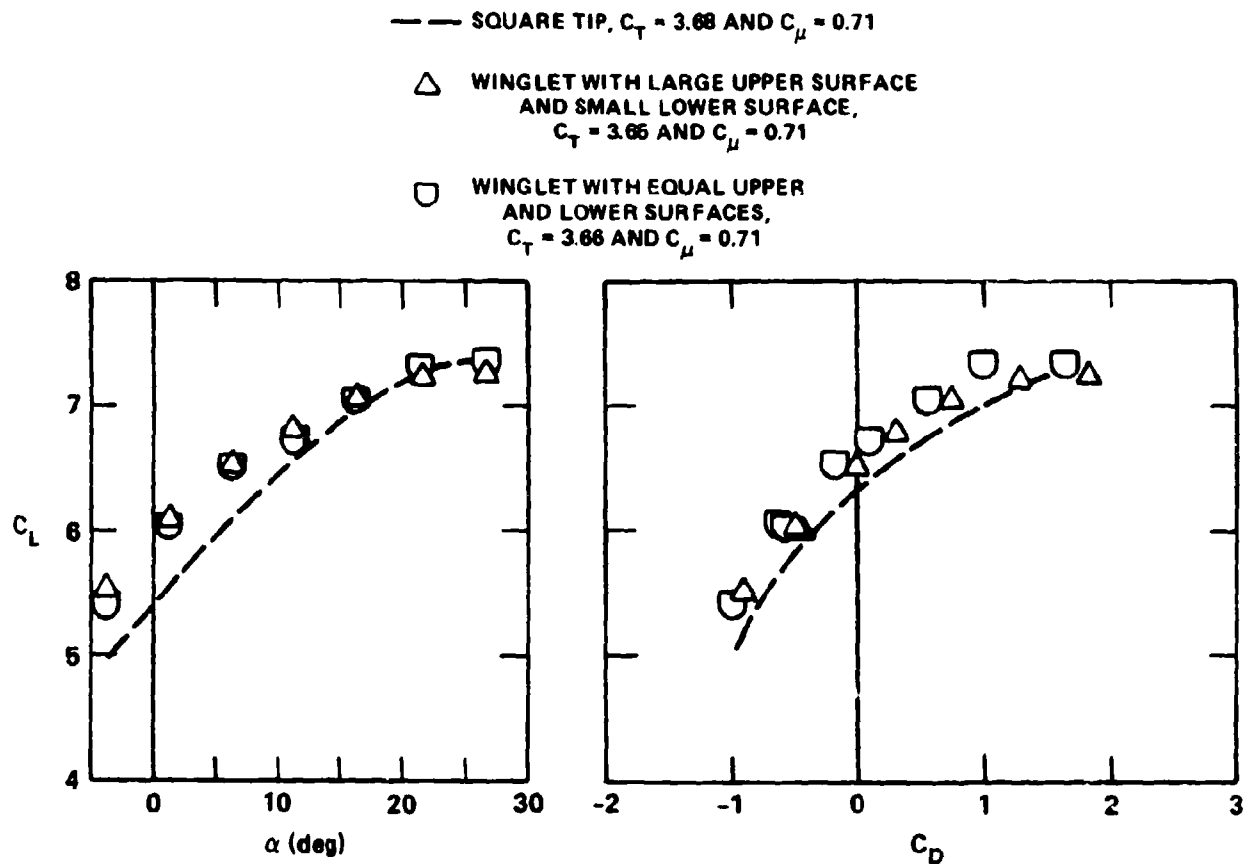


Figure 21b - Effect of Angle of Attack Variation

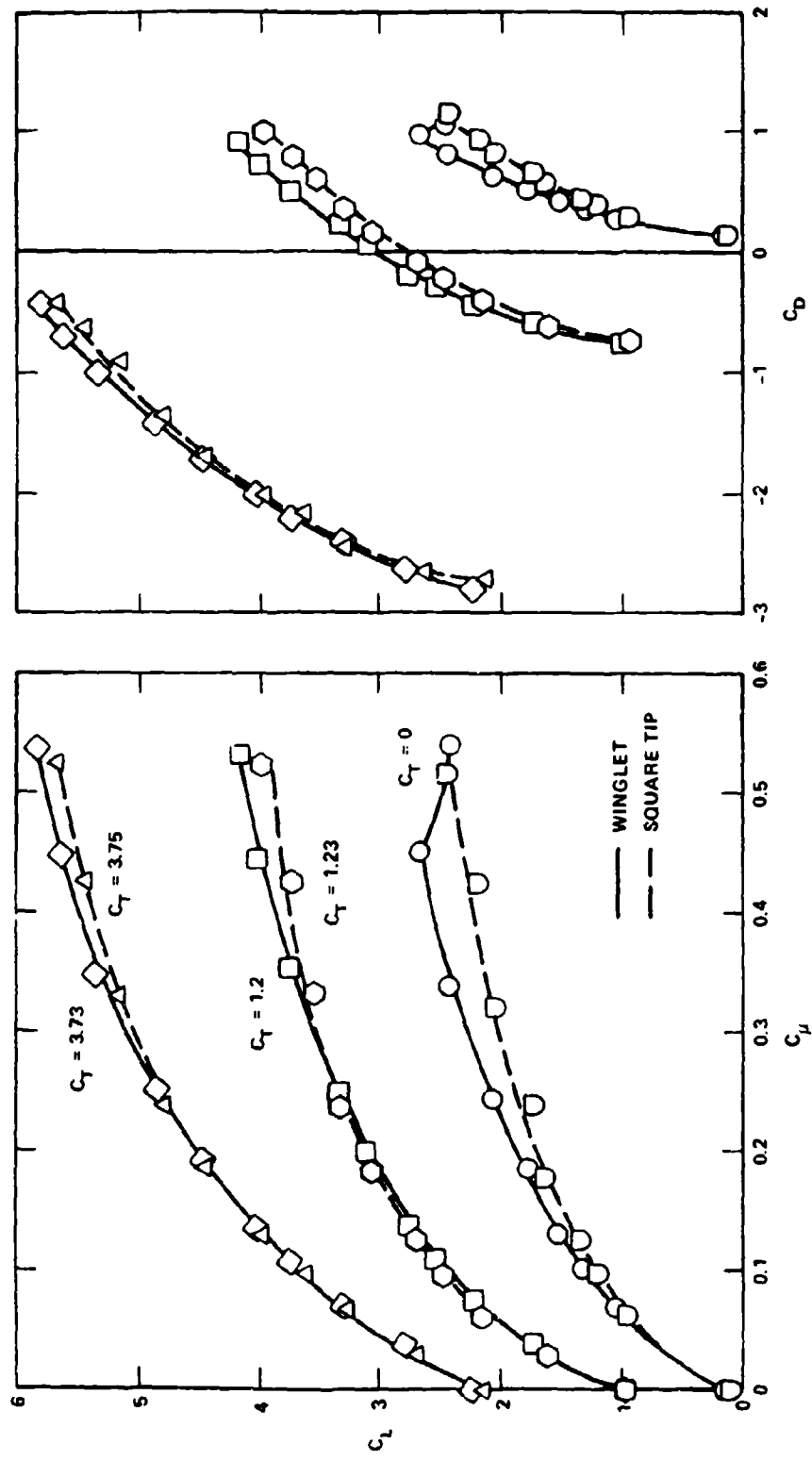


Figure 22 - Effect of Upper Surface Winglet and Variation in Full Span Tangential Blowing on Lift and Drag  
 (--) Nozzle and  $\alpha_g = 0$  deg)

Figure 23 - Effect of Upper Surface Winglet and Variation  
in Angle of Attack on Lift and Drag  
(D-nozzle and full span tangential blowing)

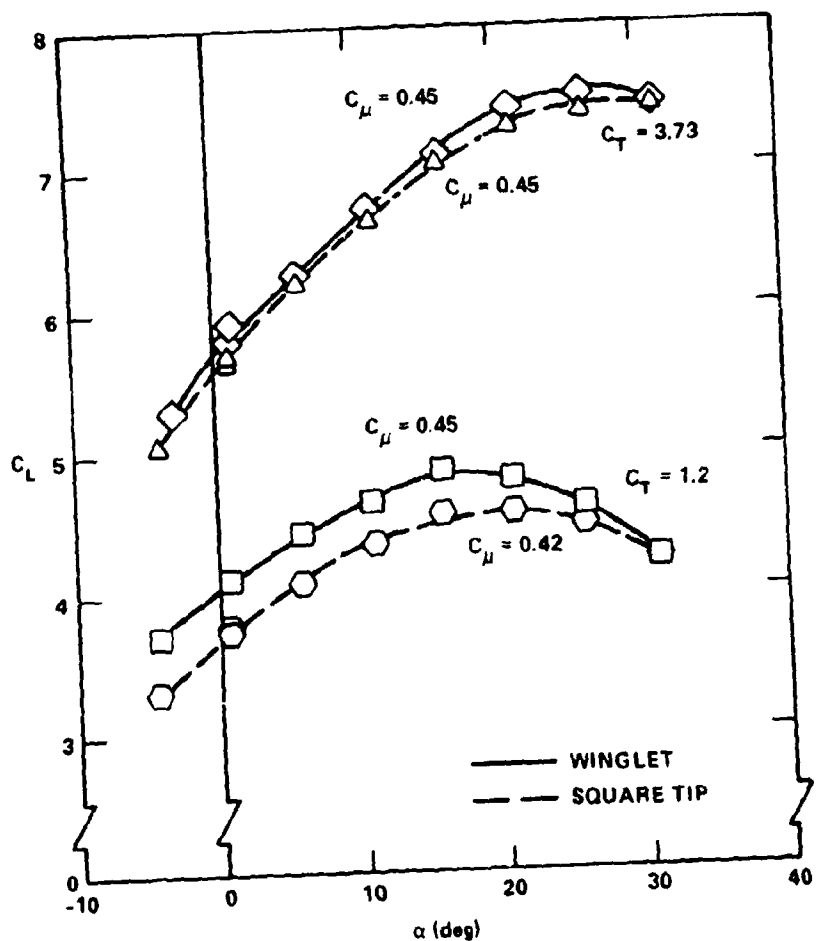


Figure 23a - Lift Coefficient

Figure 23 (Continued)

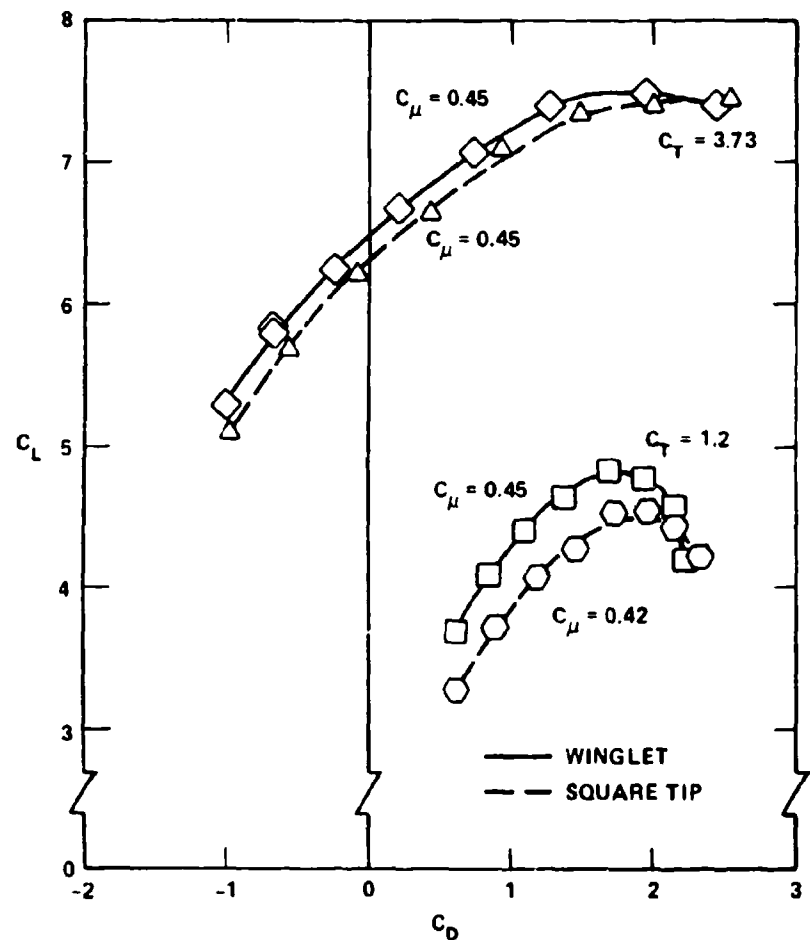


Figure 23b - Drag Polar

Figure 24 - Simulated Thrust Reversing During Landing Ground Roll  
 (D-nozzle,  $P_{T_D} = 20$  psig, and  $\alpha_g = 5$  deg)

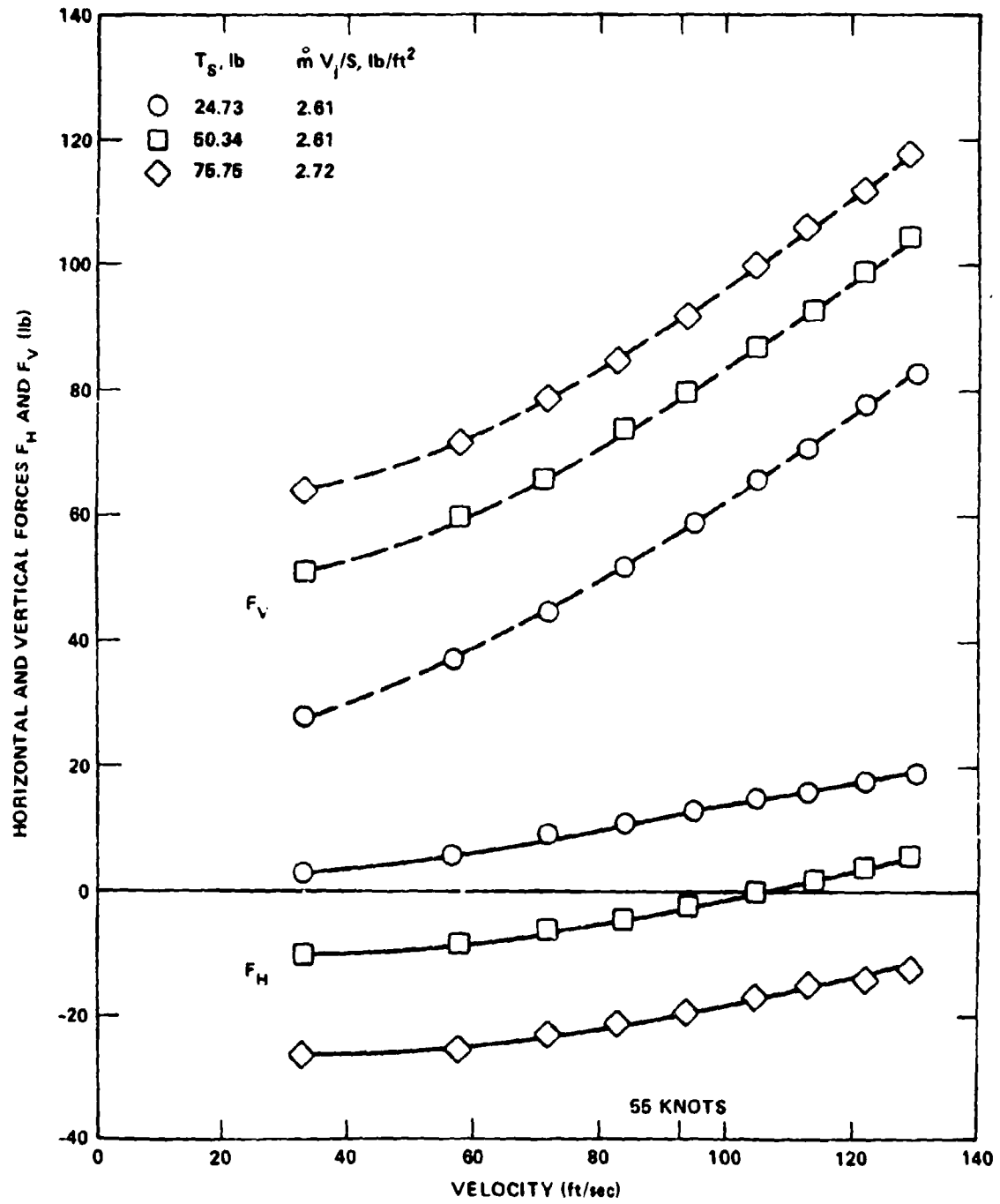


Figure 24a - Partial Span Tangential Blowing

Figure 24 (Continued)

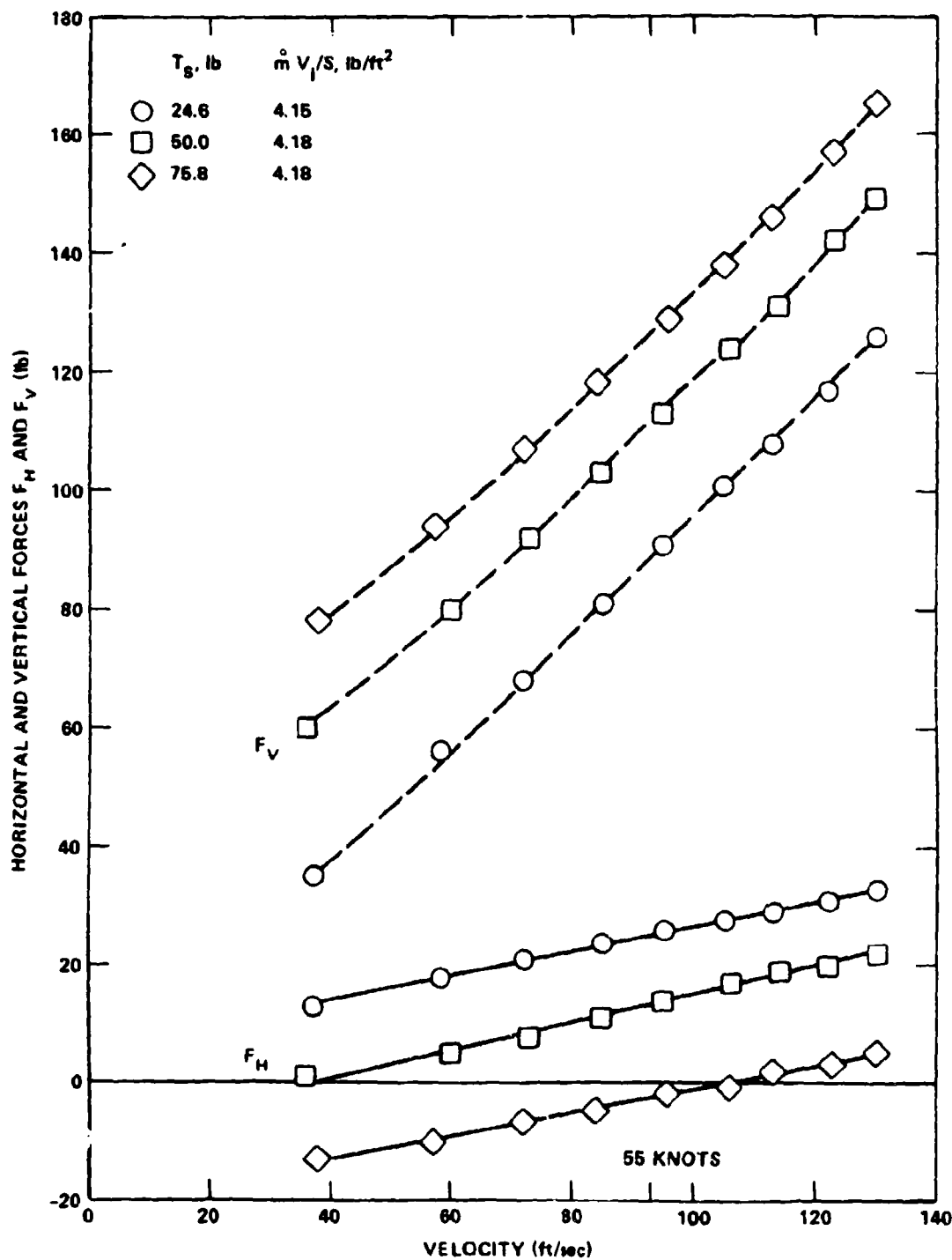


Figure 24b - Full Span Tangential Blowing

Figure 25 - Effect of Percent of Span Employing Tangential Blowing  
on Simulated Thrust Reversing  
(D-Nozzle and  $\alpha_g = 5$  deg)

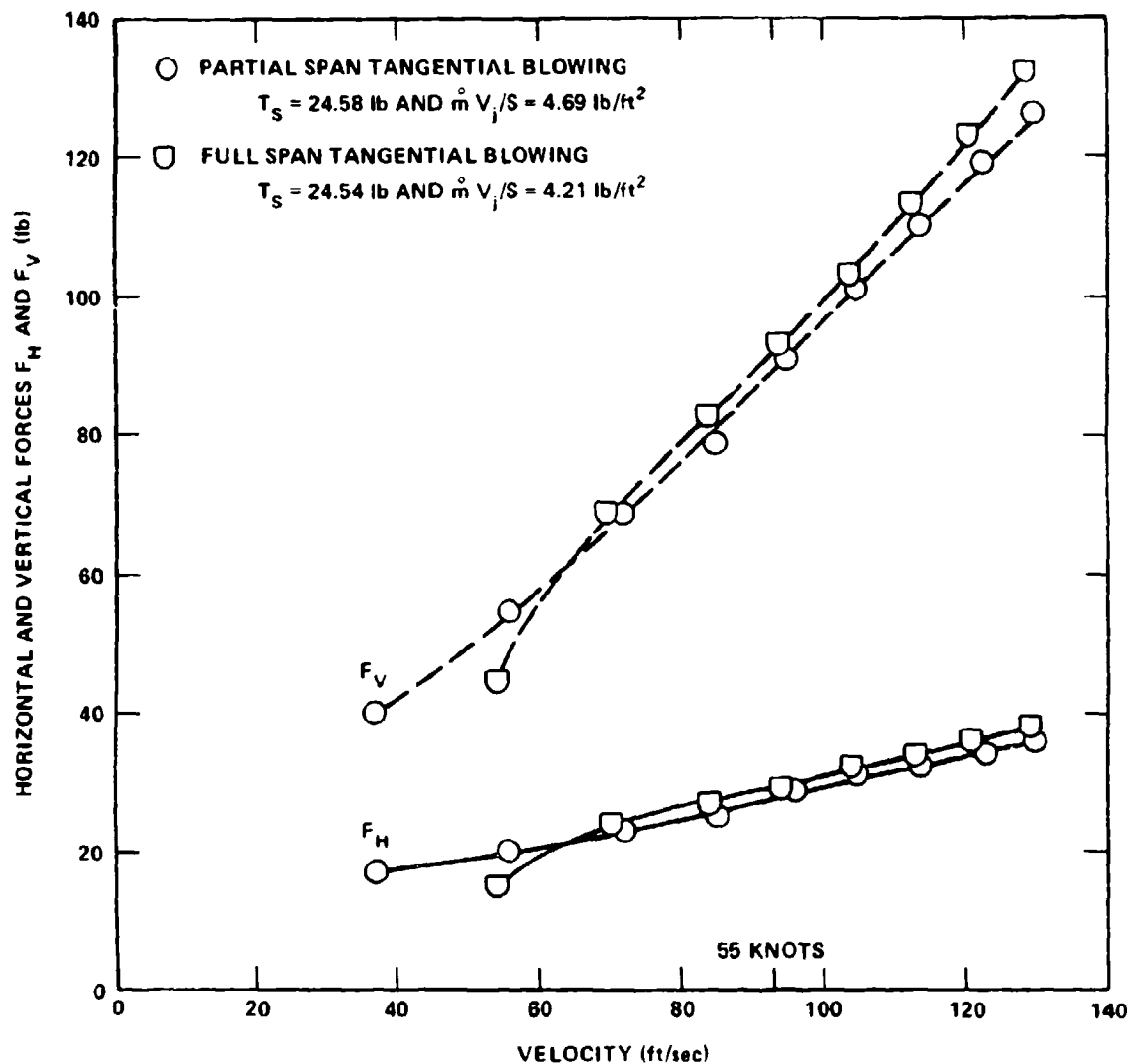


Figure 25a - Low Thrust

Figure 25 (Continued)

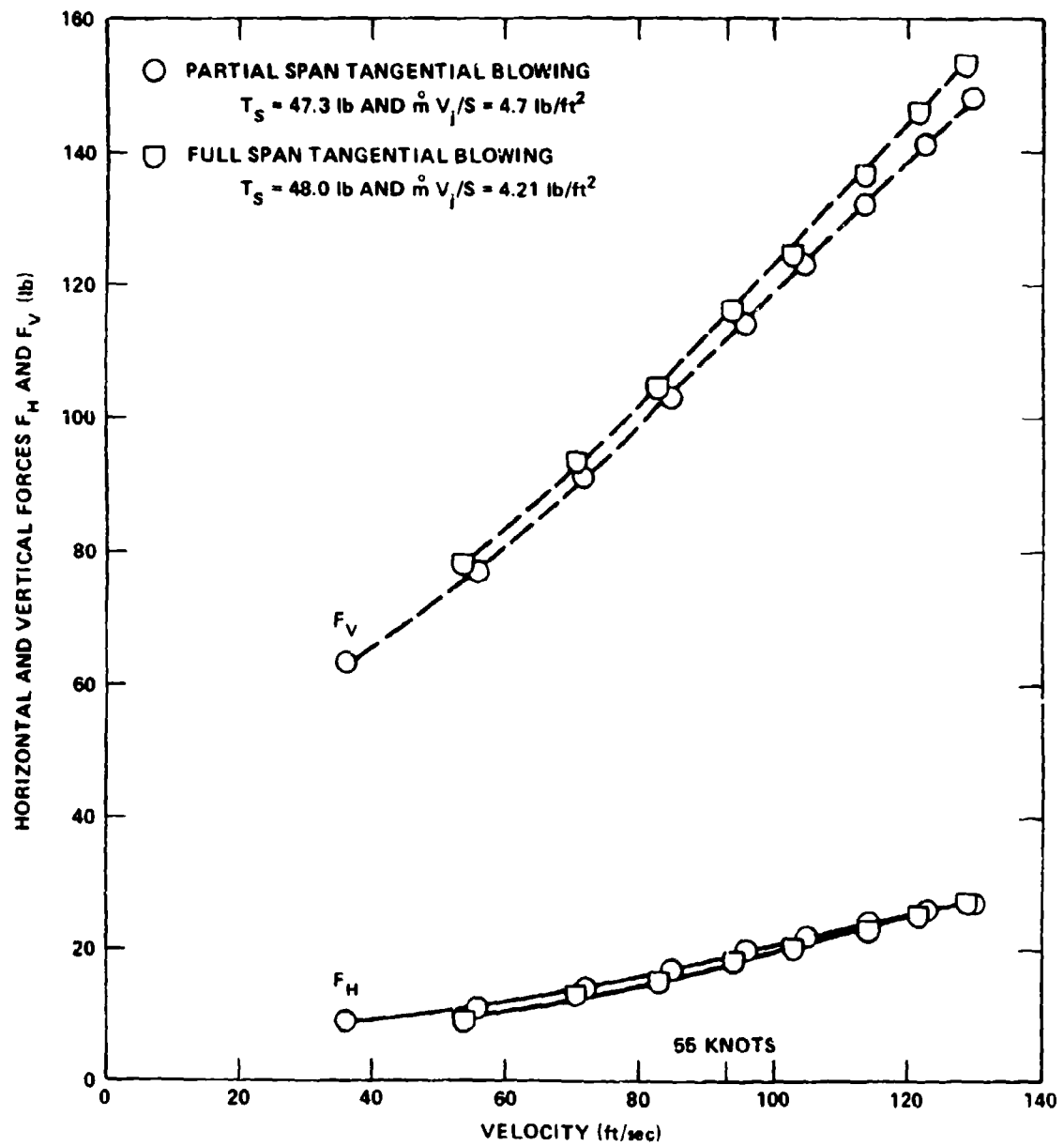


Figure 25b - Medium Thrust

Figure 26 - Simulated Thrust Reversing Employing the Nozzle  
with an Internal Flap and Partial Span Tangential Blowing  
( $\alpha_g = 5$  deg)

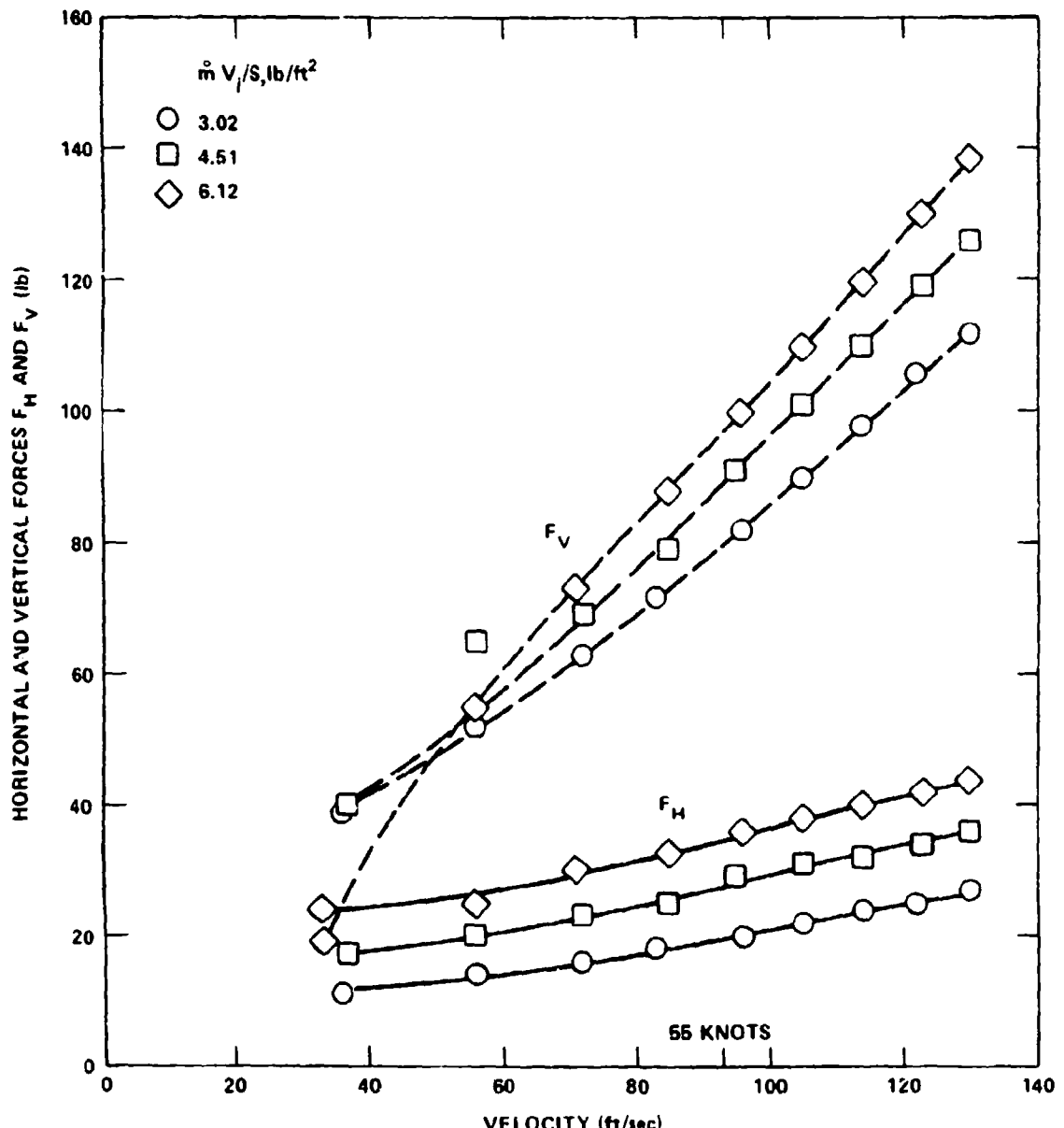


Figure 26a -  $T_S = 24.6$  lb

Figure 26 (Continued)

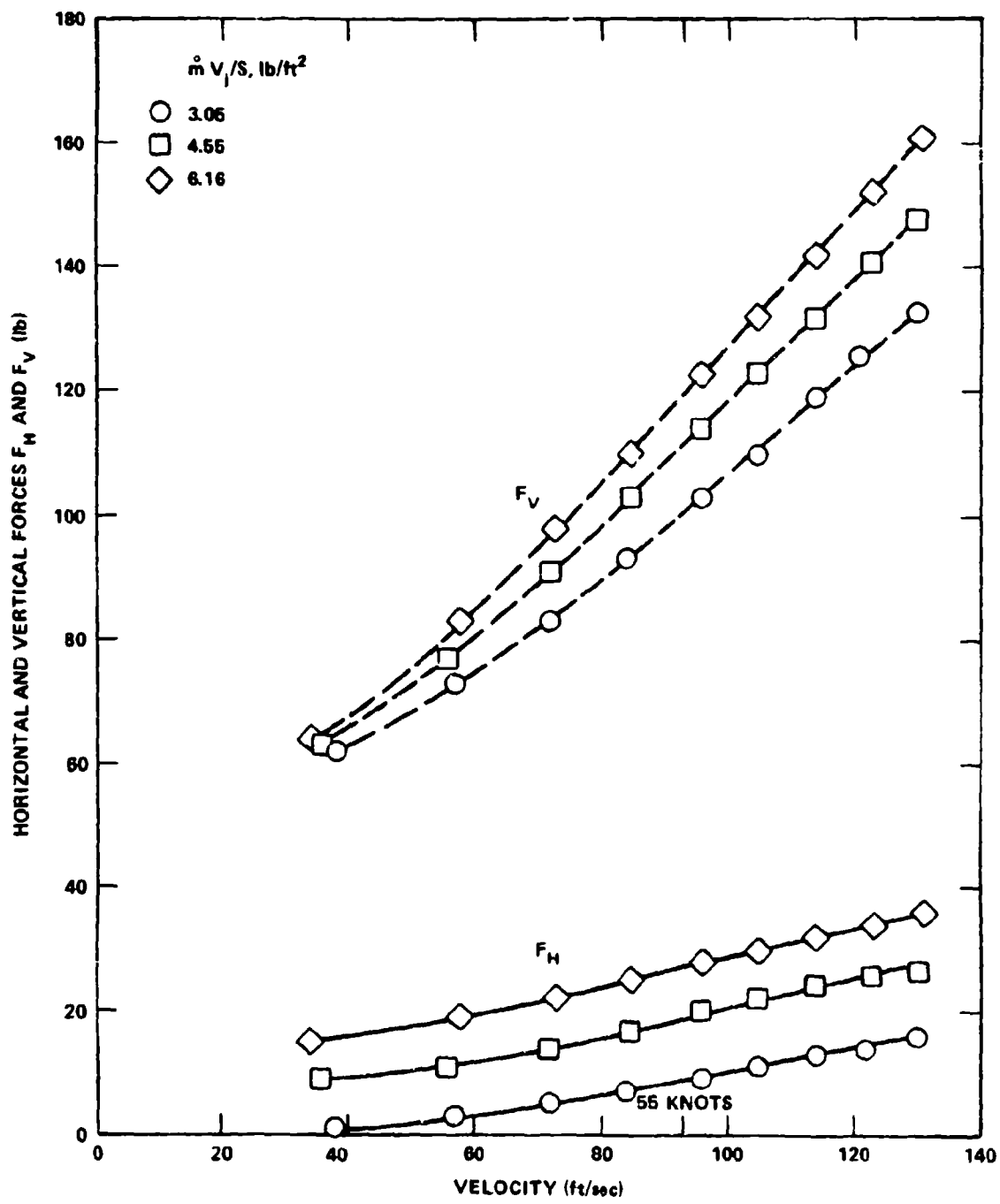


Figure 26b -  $T_S = 47.4$  lb

DTNSRDC ISSUES THREE TYPES OF REPORTS

1. DTNSRDC REPORTS, A FORMAL SERIES, CONTAIN INFORMATION OF PERMANENT TECHNICAL VALUE. THEY CARRY A CONSECUTIVE NUMERICAL IDENTIFICATION REGARDLESS OF THEIR CLASSIFICATION OR THE ORIGINATING DEPARTMENT.
2. DEPARTMENTAL REPORTS, A SEMIFORMAL SERIES, CONTAIN INFORMATION OF A PRELIMINARY, TEMPORARY, OR PROPRIETARY NATURE OR OF LIMITED INTEREST OR SIGNIFICANCE. THEY CARRY A DEPARTMENTAL ALPHANUMERICAL IDENTIFICATION.
3. TECHNICAL MEMORANDA, AN INFORMAL SERIES, CONTAIN TECHNICAL DOCUMENTATION OF LIMITED USE AND INTEREST. THEY ARE PRIMARILY WORKING PAPERS INTENDED FOR INTERNAL USE. THEY CARRY AN IDENTIFYING NUMBER WHICH INDICATES THEIR TYPE AND THE NUMERICAL CODE OF THE ORIGINATING DEPARTMENT. ANY DISTRIBUTION OUTSIDE DTNSRDC MUST BE APPROVED BY THE HEAD OF THE ORIGINATING DEPARTMENT ON A CASE BY CASE BASIS.